Development of VHH- and Antibody- based Imaging and Diagnostic Tools

by

Zeyang Li

Bachelor of Science in Biochemistry

University of Wisconsin-Madison, WI, 2011

Submitted to the Department of Chemistry

In Partial Fulfilment of the requirement for the

Degree of Doctor of Philosophy

at the

Massachusetts Institute of Technology

June 2018

Signature redacted

Signature of Author.....

Department of Chemistry
21 May 2018

Signature redacted

Certified by.....

Hidde Ploegh
Senior Investigator
Program in Cellular and Molecular Medicine
At Boston Children's Hospital

Signature redacted

Accepted by.....

Robert W. Field
Haslam and Dewey Professor of Chemistry
Chairman, Departmental Committee for Graduate students

This doctoral thesis has been examined by a committee of the Department of Chemistry as follows:

Signature redacted

Barbara Imperiali
Class of 1922 Professor of Biology and Chemistry
MacVicar Faculty Fellow
Thesis Committee Chair

Signature redacted

Hidde Ploegh
Senior Investigator
Program in Cellular and Molecular Medicine
At Boston Children's Hospital
Thesis Supervisor

Signature redacted

Bradley L. Pentelute
Pfizer-Laubach Career Development Professor of Chemistry

Abstract

The immune system distinguishes self from non-self to combat pathogenic incursions. Evasion tactics deployed by viruses, microbes, or malignant cells may impede an adequate response. In such cases, therapeutic interventions aid in the elimination of pathogens and the restoration of physiological homeostasis. A major road block in the development of such therapies is the reliance on imperfect detection methods to identify site(s) of infection, or to monitor immune cell recruitment to sites of infection or inflammation *in vivo*. The goal of this thesis is overcome at least some of these limitations by utilizing novel tools that have been developed and refined in the laboratory to facilitate *in vitro* and *in vivo* characterization of specific immune subsets. We then track their recruitment to sites of active immune responses, such as infection or tumor progression sites. These tools consist of two components: one that confers specificity for immune cells and the other offers a site for labeling in a controlled manner. Single-domain antibodies (VHHs) from camelids are amongst the smallest (15 KDa) proteins that can recognize a diverse set of targets with excellent specificity. Chemoenzymatic labeling of molecules using sortase allows site-specific attachment of a single label of interest to the target protein containing the sortase recognition sequence LPXTG. VHHs specific for immune cell determinants labeled with sortase technology facilitate non-invasive and efficient monitoring of cells that infiltrate immunological niches *in vivo* in a manner not possible until now.

This thesis presents the development of novel methods to allow *in vitro* and in vivo detection and imaging of specific immune subsets and their recruitment to sites of an active immune response. This thesis aims to (1) use DNA oligomers as a scaffold to push the limits of fluorescence labelling yield (2) create small and efficient biosensors for the rapid capture of specific lymphocyte subsets from peripheral blood samples using VHHs and graphene oxide nanosheets (3) develop radioisotope-labeled VHHs to track immune cell subsets to elucidate the roles of innate and adaptive immune components in the course of infection.

Chapter 1 describes a new method for protein labeling via site-specific modification of proteins using a DNA scaffold. To avoid self-quenching of multiple fluorophores localized in close proximity, Holliday junctions were used to label proteins site-specifically with fluorophores. Holliday junctions enable the introduction of multiple fluorophores with reasonably precise spacing to improve fluorescence yield for both single domain and full-sized antibodies, without deleterious effects on antigen binding.

Chapter 2 presents a biosensor generated for characterization of leukocytes from whole blood using a graphene oxide surface coated with single domain antibody fragments. This format allows quick and efficient capture of distinct white blood cell subpopulations from small samples of whole blood in a format that does not require any specialized equipment such as cell sorters or microfluidic devices.

Chapter 3 documents a non-invasive immune-PET imaging method for tracing CD8+ T cells in the course of influenza A infection to better elucidate their protective mechanism(s) and immunopathological effects.

Acknowledgements

I am most grateful to my Ph.D. advisor, Professor Hidde Ploegh for his initial faith, ongoing patience and exceptional guidance. Coming to MIT to work with Hidde is one of the greatest decisions I have made. I joined his group towards the end of my first semester, anxious about my scientific abilities and my knowledge in immunology. Hidde gave me the much-needed opportunity and supervision to complete my doctoral training. I am grateful to Hidde not only for this chance but also for his extraordinary scientific insights and inspirational discussions that come with his magnificent mentorship. He has been unbelievably kind and patient with me, giving me the opportunity to find solutions, to explore, to fail, to trouble shoot and ultimately to learn and discover. My graduate research experience with Hidde will continue to shape who I am as a scientist in the future.

I would also like thank my committee members, Prof. Dr. Barbara Imperiali and Prof. Dr. Brad L. Pentelute, for their most incisive critiques on my work through my graduate training. Nothing in this thesis would be possible without the support from my committee members.

I want to thank my first mentor in the lab, Christopher S. Theile, who has trained me on organic synthesis and also been a great friend over the years. Another inspiring part about Ploegh group is how the entire laboratory strive to be supportive and collaborative with each other. It has been a great journey and a lot of fun to work with everyone in the Ploegh lab. I have shared the excitement for science and worked together with Prof. Dr. Guan-yu Chen, Dr. Tao Fang, Dr. Ross Cheloha, Prof. Dr. Matthias Truttmann, Dr. Andrew Woodham, Ms. Novalia Pishesha, Ms. Yushu Joy Xie, Ms. Djenet Bousbaine, Dr. Jingjing Ling, Mr. Jason Nguyen, Ms. Jana Volaric, Mr. Paul W. Rothlauf, Dr. Angelina M. Bilate, Dr. Ana Avalos, Dr. Joao Duate, Dr. Leo Hanke, Prof. Dr. Florian I. Schmidt, and Prof. Dr. Takeshi Maruyama. I cherished discussing, arguing, troubleshooting, and brainstorming with them. I also want to thank our lab manager, Mr. Robert Miller, who has been a wonderful friend and provided me with tremendous support.

MIT is a wonderful place for collaborations. My thesis was made possible by outstanding collaborators from the labs of Prof. Dr. Angela Belcher, Prof. Dr. Frederick Alt, and Prof. Dr. Gerry Fink. All the wonderful people that I worked with provided valuable feedback and tremendous support throughout the research.

Graduate school can be stressful sometime and my family has been the rock that made everything possible. I am the first and the only one in my family to graduate with a science degree. Thank you, to my Mom and Dad, for providing me with the freedom to chase my dream. I would also like to thank my fiancé Michael, who has been a great supporter of my graduate school endeavors, my life and career. My world is more is more beautiful with you in it.

At last, thanks to all my friends and family, who had the courage to ask me
'how's your thesis coming along?'

Table of Contents

List of Figures

List of Tables

Scope of Thesis

This thesis aims to develop novel methods to allow in vitro and in vivo detection and imaging of specific immune subsets and their recruitment to sites of active immune response.

Chapter 1 describes a new method for protein labeling via site-specific modification of proteins using a DNA scaffold. Site-specific modification of proteins with fluorophores can render a protein fluorescent without compromising its function. To avoid self-quenching of multiple fluorophores installed in close proximity, we used Holliday junctions to label proteins site-specifically. Holliday junctions enable modification with multiple fluorophores at reasonably precise spacing. We designed a Holliday junction with three of its four arms modified with a fluorophore of choice and the remaining arm equipped with a dibenzocyclooctyne substituent to render it reactive with an azide-modified, fluorescent single domain antibody fragment or an intact immunoglobulin, produced in a sortase-catalyzed reaction. We conclude that fluorescent Holliday junctions improve fluorescence yields for both single domain and full-sized antibodies, without deleterious effects on antigen binding.

Chapter 2 presents a biosensor generated for characterization of leukocytes from whole blood using graphene oxide surface coated with single domain antibody fragments. Peripheral blood can provide valuable information on an individual's immune status. Cell-based assays typically target leukocytes and their products. Characterization of leukocytes from whole blood requires their separation from the far more numerous red blood cells Current methods to classify leukocytes, such as recovery on antibody-coated beads or fluorescence-activated cell sorting require long sample preparation times and relatively large sample volumes. A simple method that enables the characterization of cells from a small peripheral whole blood sample could overcome limitations of current analytical techniques. We describe the development of a simple graphene oxide surface coated with single domain antibody fragments. This format allows quick and efficient capture of distinct WBC subpopulations from small samples of whole

blood in a geometry that does not require any specialized equipment such as cell sorters or microfluidic devices.

Chapter 3 demonstrates a non-invasive immune-PET imaging method for tracing $CD8^+$ T cells in the course of influenza A infection. Immuno-positron emission tomography (immuno-PET) is a non-invasive imaging method that enables tracking of immune cells in live animals. Here we used a nanobody that recognizes CD8 and labeled it with ^{89}Zr to image $CD8^+$ T cells in the course of an infection with influenza A virus (IAV). Numbers of $CD8^+$ T cells were elevated in the mediastinal lymph node (MLN) as early as 4 days post-infection (dpi), and as early as 6 dpi in the lung. Over the course of the infection, we show that $CD8^+$ T cells are initially distributed diffusely throughout and then accumulate in specific regions of the lung, distributions that correlate with morbidity. We also show a difference in the distribution and migration pattern of $CD8^+$ T cells obtained from control or IAV infected mice adoptively transferred into infected versus control animals. Immuno-PET thus allows non-invasive dynamic monitoring of the immune response to infectious agents in living animals at unprecedented resolution.

Chapter 1. Holliday Junctions Generate Super-Bright Antibodies and Antibody Fragments in Sortase-Catalyzed Reactions

The work presented in this chapter is a part of the following manuscript and is reproduced here with permission from the authors.

Zeyang Li, Christopher S. Theile, Guan-Yu Chen, Angelina M. Bilate, Joao N. Duarte, Ana M. Avalos, Tao Fang, Roberto Barberena, Shuji Sato, Hidde L. Ploegh*

Angew Chem Int Ed Engl. **2015** Sep 28;54(40):11706-10. doi: 10.1002/anie.201505277

1.1 Introduction

Fluorescent versions of various biomolecules[1] are important tools to study their structure and function. To enable detection by flow cytometry and fluorescence microscopy, [2] proteins are commonly labeled with chromophores having excitation and emission wavelengths longer than those of their endogenous aromatic amino acids, Trp, Tyr or Phe. The intensity of the emitted fluorescent signal limits detection and quantification of commercially available fluorophores, whether attached covalently or non-covalently. Brightness of fluorescein- or rhodamine-labeled proteins does not necessarily increase proportionally with the extent of labeling.[3] In fact, fluorescence yield often decreases, because fluorophores self-quench when present in high local concentrations. [4] Moreover, chemical labeling techniques are not particularly specific, because they can modify any accessible free lysine or cysteine side chain.[5] Introduction of non-canonical amino acids, or careful placement of the cysteine or lysine residues targeted for modification onto the scaffold also circumvents specificity issues in labeling. The presence of multiple fluorophores installed more or less randomly complicates detailed characterization of the target of interest and may also compromise its function.[6] Finally, the use of genetic fusions with a fluorescent protein is a viable alternative, but the presence of the fluorescent protein may again affect the function of its fusion partner.[7-8]

Site-specific labeling methods for the installation of fluorescent probes on proteins include formylglycine-generating enzyme (FGE), used to append an aldehyde tag onto a specific pentapeptide sequence, which may then react with aminooxy-linked fluorophores,[3, 9] or biotin ligase, which may be used to attach biotin or biotin derivatives onto a 11-residue recognition sequence.[10] Tag-mediated labelling utilizing self-labelling proteins as the SNAP-, CLIP-, or the Halo-tag may be used to attach exogenously supplied fluorophores.[11] Intein-mediated protein ligation (IPL) creates a C-terminal thioester that can be ligated to a short fluorescently labeled peptide.[12] Sortase-mediated modifications have also been used for site-specific labeling.[3, 13-18]

Regardless, self-quenching interferes with fluorescence yields when multiple fluorophores are installed in close proximity. The challenge therefore remains to increase signal intensity compared to that of a single fluorophore, and to do so site-specifically.

1.2 Result

Here we describe the use of Holliday junctions as semi-rigid DNA-based structures to enable attachment of multiple fluorescent probes onto a ~15 kDa single chain antibody fragment (VHH) to overcome self-quenching and improve signal strength (**Figure 1.1**). Because each of the 4 oligonucleotides that participate in the formation of the Holliday junction is unique and is synthesized separately, each arm can be fixed with respect to length and the substituent of choice. The structure of the protein-DNA conjugate allows positioning of the fluorophores at a distance sufficient to avoid quenching. We demonstrate an almost linear increase in fluorescence intensity by gel electrophoresis of the substrate-DNA conjugate in comparison with singly labeled substrate. We confirmed the fluorescence intensity augmentation of a DNA-labeled single domain antibody fragment (VHH7) specific for Class II MHC products by cytofluorimetry. VHH7's antigen binding capacity was not affected by installation of the Holliday Junction. This technology is applicable to any protein of interest and extends the utility of sortase-mediated ligations.

Holliday junctions are highly negatively charged polyelectrolytes that can undergo a two-state-like isomerization transition in the presence of metal ions such as Mg^{2+}[3]. This metal ion-induced transition may place fluorophores installed at the extremities in close proximity of one another, a transition minimized in the presence of low concentrations of metal ions, as used under to standard extracellular labeling conditions. The cruciform planar structure is more stable in the absence of high [Mg^{2+}].[19-20] At low [Mg^{2+}], Holliday junctions are cruciform, the angle between two

adjacent

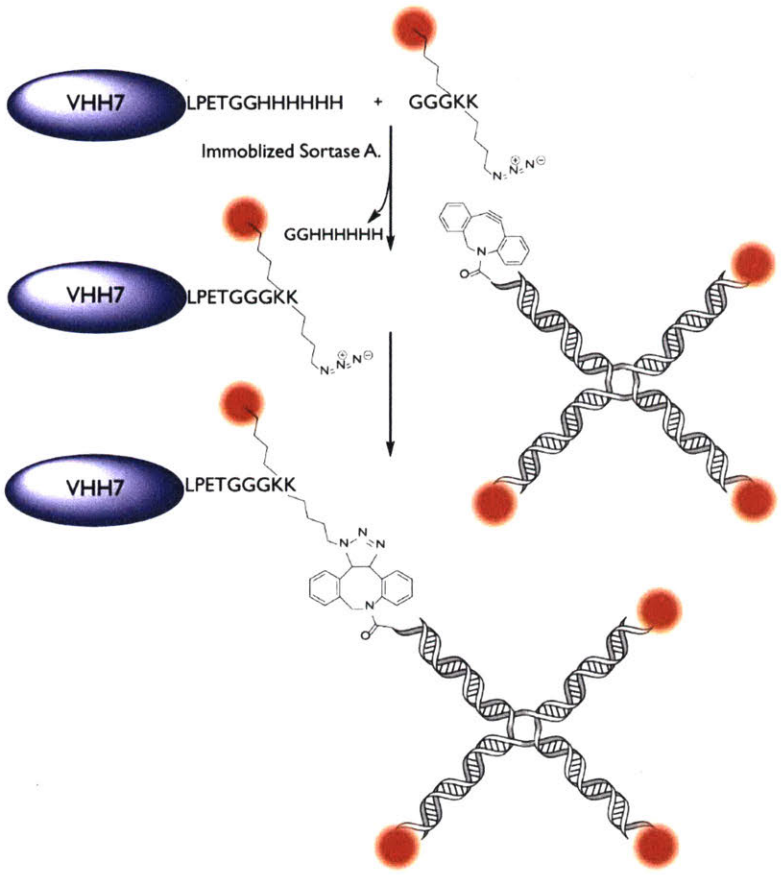

Figure 1.1 The single domain antibody fragment, VHH7, is equipped with a C-terminal LPETG motif to enable sortase recognition. A short peptide containing an N-terminal GGG sequence serves as the nucleophile in the sortase-mediated ligation step to install an azide group and a fluorescent moiety onto the VHH. Meanwhile, three sets of ssDNA of unique sequence are reacted with N-hydroxysuccinimide (NHS)-activated TAMRA and a fourth strand is reacted with NHS-activated DBCO. The sequence of each DNA strand allows assembly of a Holliday junction. After overnight incubation with the VHH, the DBCO and azide react in a copper-free "click" cycloaddition to yield the desired product.

helical arms being ~90° [21], and therefore provides a rigid scaffold to attach fluorophores in a manner that avoids self-quenching. Four strands of appropriately complementary 50bp single stranded DNA were used to create a Holliday junction (**Figure 1.2**). This separates the points of fluorophore attachment by an estimated distance of 24 nm. We modified the sequence[22] for each branch with an AT-rich stretch to avoid quenching by G residues near the 5' point of fluorophore attachment. The 5' end of each DNA strand was modified to contain an amine handle, which was then reacted with an N-hydroxysuccinimide (NHS)-activated carboxytetra-methylrhodamine (TAMRA) or NHS-activated dibenzocyclooctyne (DBCO).

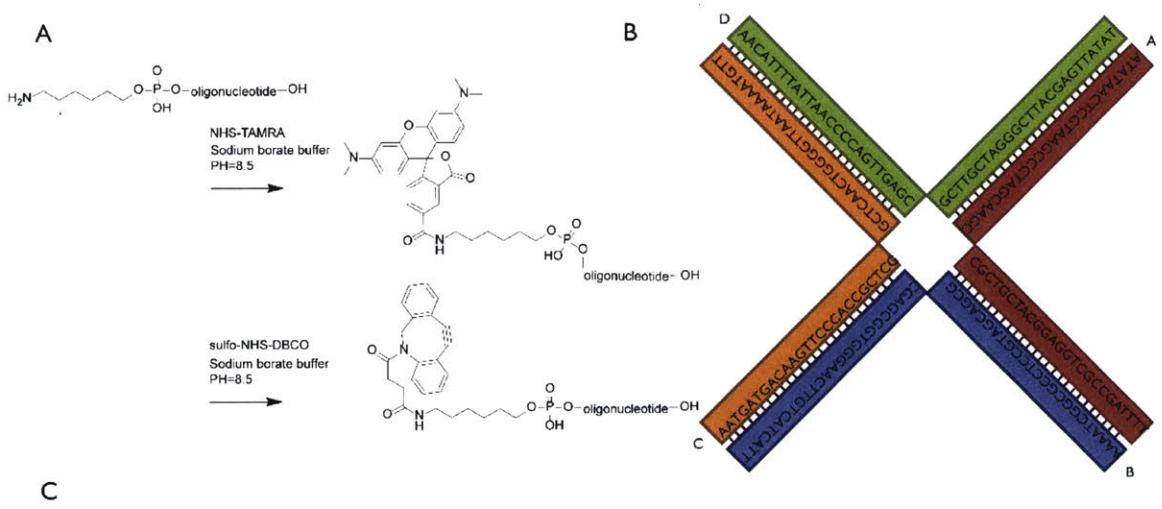

BRANCH	SEQUENCE
A	ATA TAA CTC GTA AGC CCT AGC AAG CCG CTG CTA CGG AGG TCG CCG ATT TT
B	AAA ATC GGC GAC CTC CGT AGC AGC GCG AGC GGT GGG AAC TTG TCA TCA TT
C	AAT GAT GAC AAG TTC CCA CCG CTC GGC TCA ACT GGG GTT AAT AAA ATG TT
D	AAC ATT TTA TTA ACC CCA GTT GAG CGC TTG CTA GGG CTT ACG AGT TAT AT

Figure 1.2 All four oligos were synthesized with Amino Modifier C6 for standard 5' labeling. Oligonucleotide C was used for DBCO coupling and the others (A,B,D) were used for fluorophore labeling. (A) Modification of oligo nucleotide with NHS activated moiety. (B)Structure of assembled Holliday junction (C) The DNA sequence of Branch A-D.

After assembly into a Holliday junction, each dye and the DBCO handle will thus be positioned away from each other. Separately we installed a short peptide containing a fourth TAMRA dye and an azide functionality at the protein's C-terminus, using a sortase-mediated ligation. The Holliday junction and protein were then joined via these "click" handles to yield a product with four fluorophores attached to VHH7, the protein of interest. We attached one to four fluorophores on the four branches of the Holliday junction to compare the signal intensity by *in situ* gel scanning after electrophoretic separation. The observed signal intensity proportionally increased and confirmed that Förster resonance energy transfer between the TAMRA probes is prevented by the spacing of the fluorophores (**Figure 1.3A**). We measured the fluorescent intensity using ImageQuant and found a ~3.7-fold increase in signal strength for the $(TAMRA)_4$

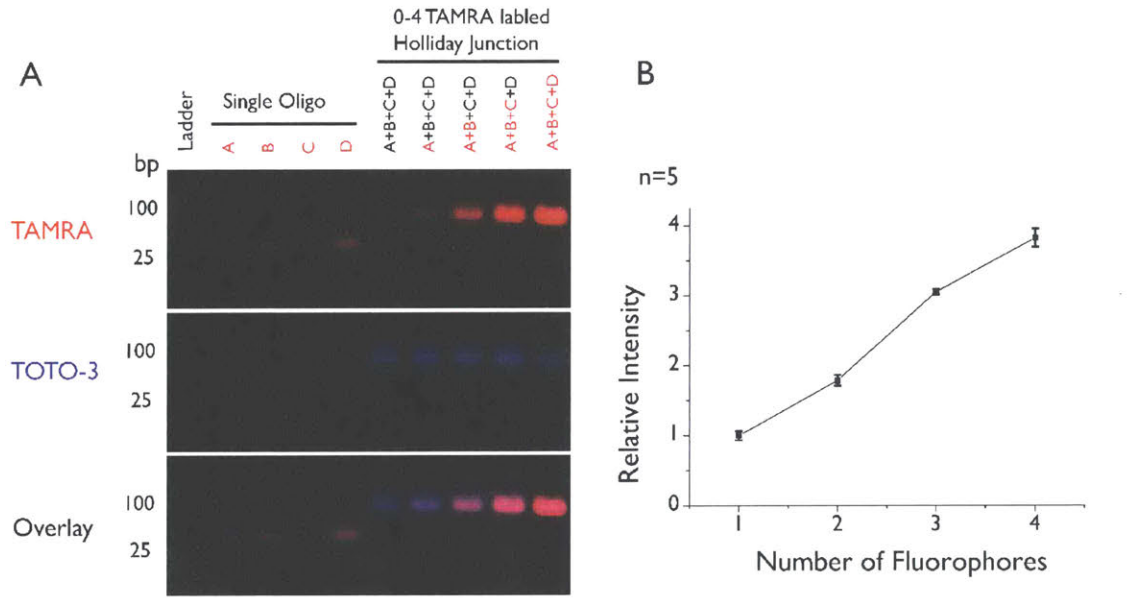

Figure 1.3 (A) Fluorescent scanning (580 nm emission) shows the increase in fluorescence upon addition of each successive TAMRA moiety to the Holliday Junction. The middle section of the gel shows a fluorescence scan of the gel stained with TOTO-3 dye to demonstrate even loading of the various DNA oligomers. (B) The fluorescence intensity of the singly labeled Holliday junction was set to 1.0 and the intensities of the other adducts were expressed relative to this value to assess 3.8-fold increase upon attachment of additional fluorophores.

labeled probe in comparison to TAMRA mono-labeling (**Figure 1.3B**) in good agreement with expectations.

To demonstrate the utility of the multiple fluorophore probes we labeled VHH7, [23] modified to contain a C-terminal LPETGGHHHHHH motif for both purification and for sortase-mediated ligations. Sortase A from *S. aureus* recognizes the LPXTG motif, cleaves between the T and G with simultaneous formation of an active thioester intermediate, which is then resolved by a poly-glycine nucleophile. We used a nucleophile of the sequence GGGK(TAMRA)K(azide) (**Figure 1.4**). We used a mutant sortase with increased activity and that is not dependent on Ca^{2+} independence[3]. We achieved full conversion of VHH7 to the desired product with a single TAMRA dye and an azide handle for a "click" ligation. The Holliday Junction was produced by labeling the 5' end of the three strands with a TAMRA dye. The fourth strand was labeled at the 5' position with a dibenzocyclooctyl (DBCO) handle for a copper-free strain-promoted cycloaddition. The four individual strands were then hybridized to obtain the Holliday structure. Upon incubation at 4 °C overnight with the GGGK(TAMRA)K(azide)-modified VHH7, the two "click" handles reacted to form the protein-DNA hybrid. As observed in the DNA-only Holliday junctions, the DNA-protein hybrid likewise demonstrates the expected increase in fluorescence intensity compared to the single fluorophore labeled protein (VHH7-TAMRA) (**Figure 1.5**).

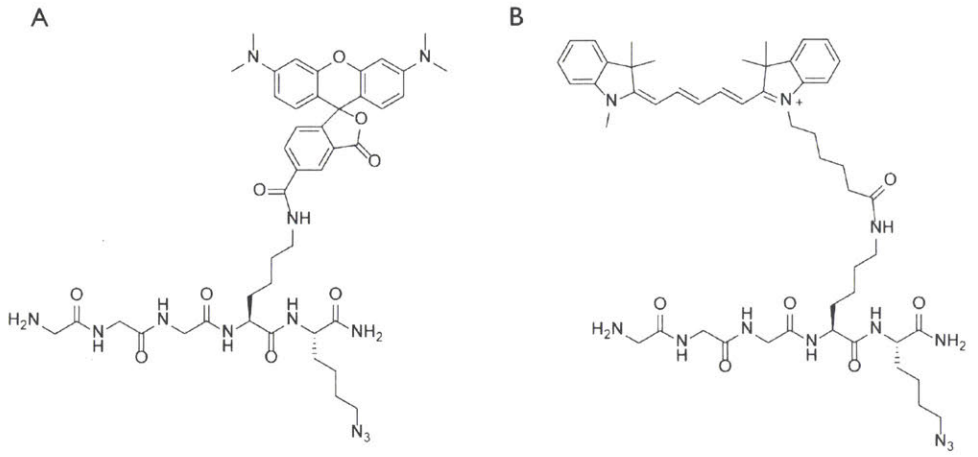

Figure 1.4. (A) GGGK(TAMRA)K(azide) (B)GGGK(Cy5)K(azide)

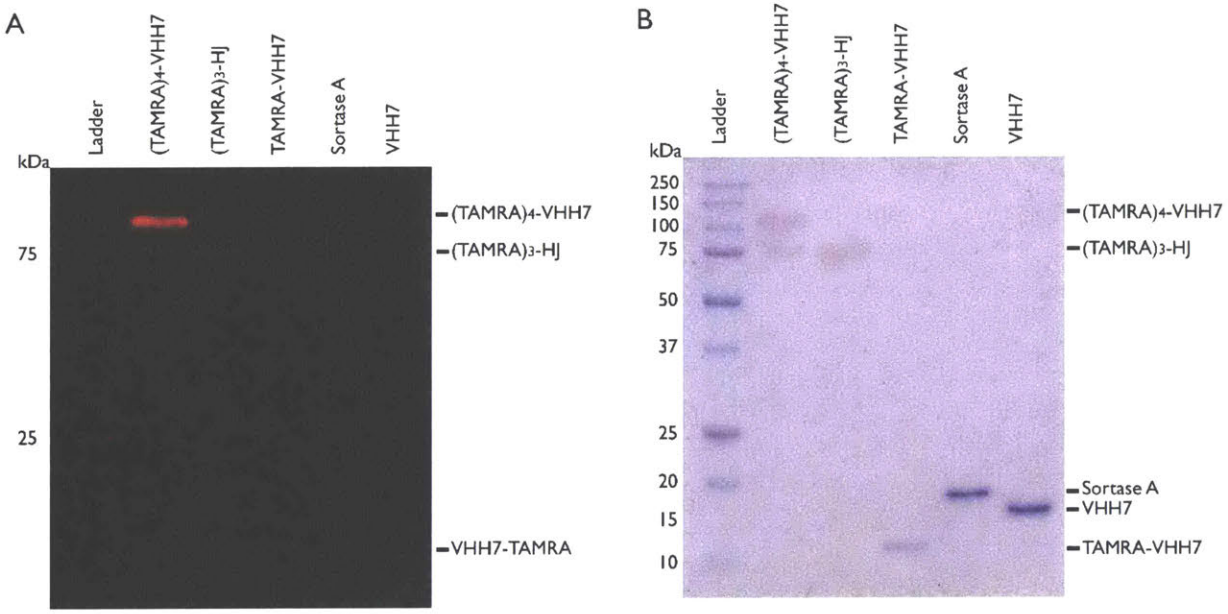

Figure 1.5. Fluorescent scanning (580 nm emission) (shown in A) and the corresponding Coomassie-stained gel (shown in B). Equal amounts of mono TAMRA-labeled VHH7 and $(TAMRA)_4$-labeled VHH7 were loaded on the gel. The $(TAMRA)_4$-labeled VHH7 shows the expected increase in fluorescence intensity.

Holliday junction-modified VHH7 was used in flow cytometry to analyze splenocytes from homozygous Class II MHC-EGFP knock in mice, in which all Class II MHC-expressing cells (e.g. B cells and dendritic cells) display an intact Class II MHC β-chain, fused at its C-terminus with EGFP. Upon addition of either VHH7-TAMRA or the VHH7-Holliday junction, the Class II MHC-EGFP positive fraction shifts to yield the expected double positive population. At all concentrations tested we observed a ~4-fold increase in fluorescence (**Figure 1.6C**) for the VHH7-Holliday junction adduct, compared to singly labeled VHH7 (**Figure 1.6B**). Therefore, binding of VHH7 is not affected by appending the Holliday junction at a position distal from the antigen binding site (**Figure 1.6A**). We also examined performance of labeled VHH7 in confocal microscopy. Class II MHC-EGFP$^+$ B cells were incubated for 30 minutes at 4 °C with either VHH7 containing a single TAMRA or with $(TAMRA)_4$-labeled VHH7 and then examined at ambient temperature at identical instrument settings. Singly labeled VHH7-TAMRA yielded a faint signal, but $(TAMRA)_4$-labeled VHH7 produced a much improved image, showing co-localization for surface and internalized Class II MHC-EGFP (**Figure 1.7**). This example illustrates the utility of this labeling method, especially for imaging of proteins that may be expressed only at low levels.

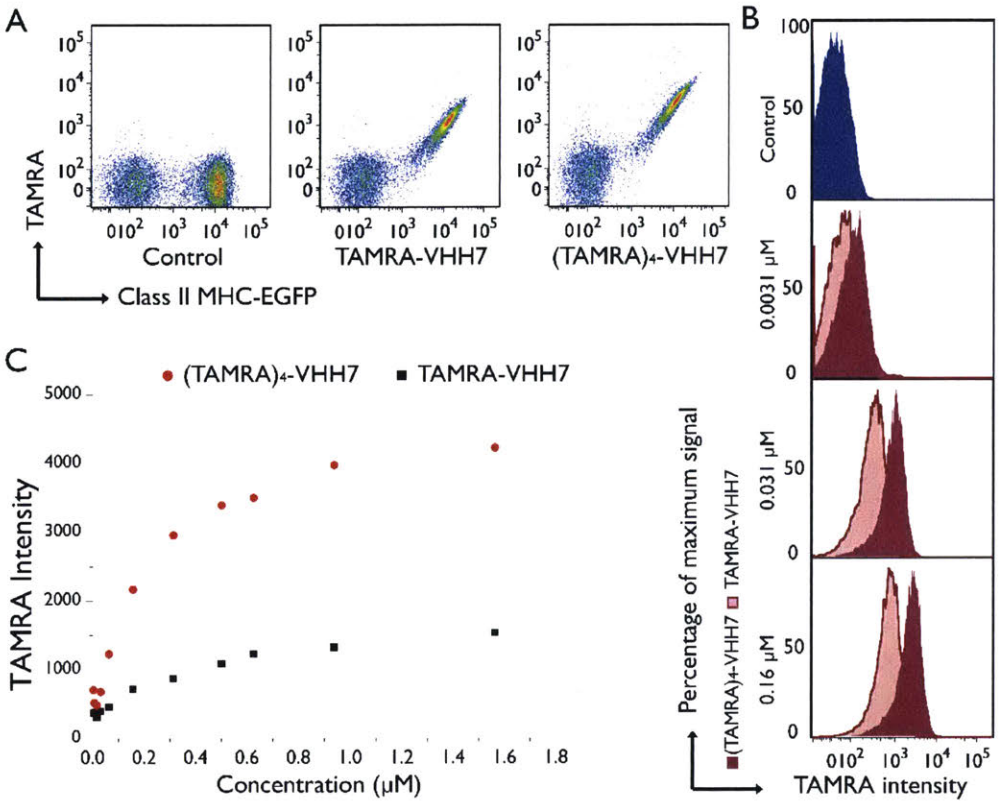

Figure 1.6. (A) Splenocytes isolated from Class II MHC-EGFP knock in mice received no treatment or were treated with a VHH7 probe containing a single TAMRA dye or the Holliday Junction probe with four TAMRA fluorophores, demonstrating that specificity of the VHH7 is not affected by the labelled Holliday Junction (B) increasing concentrations of VHH7 show a shift in intensity for single labelled TAMRA VHH-TAMRA (pink) and the $(TAMRA)_4$-Holliday Junction (maroon). (C) Quantitation of FACS data shows a ~4-fold increase in intensity for $(TAMRA)_4$-VHH7.

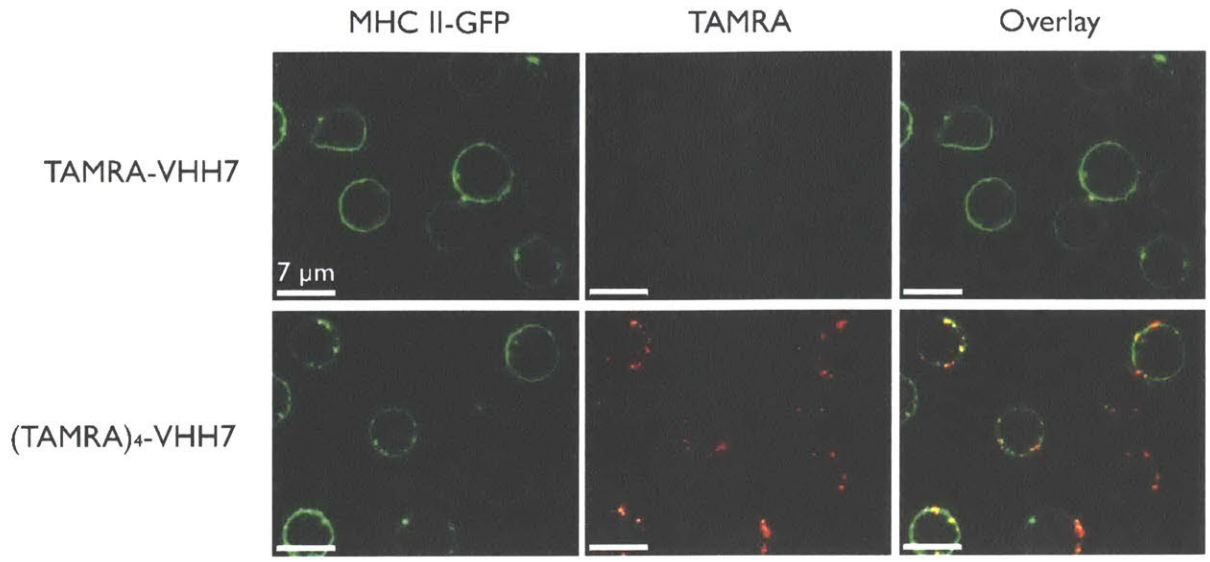

Figure 1.7. Splenic B cells expressing a Class II MHC-EGFP fusion were incubated with $(TAMRA)_4$-VHH7 or with VHH7-TAMRA single TAMRA dye. $(TAMRA)_4$-VHH7 shows enhanced fluorescence and co-localization with the EGFP fusion protein.

Full-sized antibodies, unlike VHH's, cannot be expressed in bacteria and are more difficult and expensive to produce. Therefore, increased fluorescence of full-sized IgGs is of importance, especially when using them as directly fluorophore-conjugated staining reagents. Full sized IgG's also provide an opportunity to install at least two LPXTG sortase recognition sites, one at each C terminus of the two identical heavy chains (HC). It might be possible to also modify the C-termini of the light chains with an LPXTG motif[24] and therefore install 4 Holliday junctions (and a theoretical maximum of 16 moles of fluorophore/mole of IgG).

The reaction of the full sized sortase-ready IgG specific for the surface marker DEC205 proceeded similarly as seen for VHH7. First two Gly3 peptides containing an azide and a Cy5 dye were sortagged onto each IgG HC. We then performed a "click" reaction to install a Holliday Junction containing a DBCO and three Alexa647 dyes. Cy5 and Alexa647 have similar excitation

and emission properties and for the purpose of this experiment are considered interchangeable. We generated two types of anti DEC205 IgG with different degrees of labeling; the first contains only the two sortagged Cy5 dyes, the second has two Holliday Junctions (eight dyes).

We used the A20 cell line as a B cell derivative with moderate levels of surface DEC205. As for VHH7, we saw a strong increase in fluorescence with the Holliday junction-labeled IgG's. The double Holliday junction probe (eight dyes) shows an approximate three-fold increase in fluorescence – only slightly less than the expected 4-fold increase, compared to the two-dye labeled antibody, confirmed by FACS analysis **(Figure 1.8A**). The two-dye labeled antibody was difficult to visualize by microscopy but double Holliday junction-labeled antibodies could readily be seen (**Figure1.8B**).

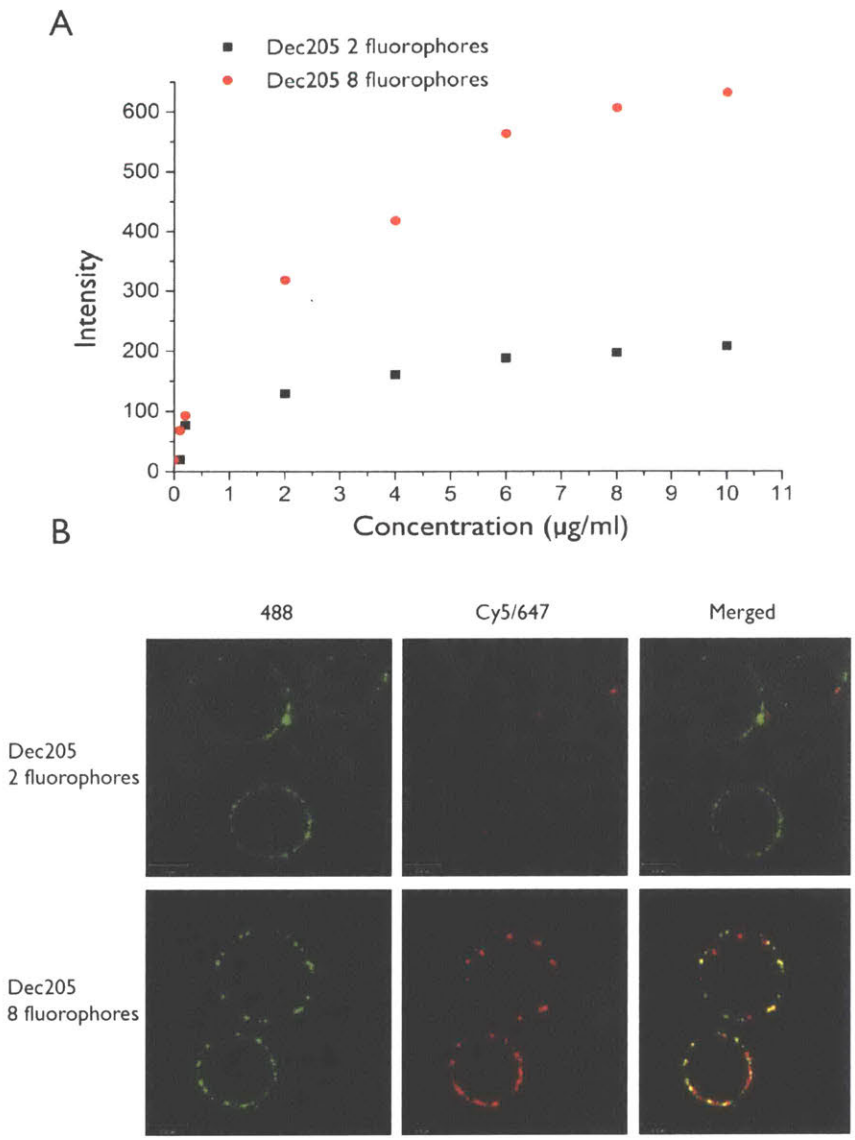

Figure 1.8. (A) Flow cytometry of A20 cells incubated with anti-DEC205 labeled with either 2 or 8 fluorophores. A ~3-fold increase in fluorescence was detected for anti-DEC205 modified with 8 fluorophores compared to anti-DEC205 labeled with 2 fluorophores. (B) A20 cells were captured on a poly-lysine coated slide and imaged by confocal microscopy. As expected, a far brighter signal is detected for anti-DEC205 labeled with 8 fluorophores.

1.3 Discussion and Conclusion

The Holliday junction-dye assembly is a simple and useful means of enhancing fluorescent signal strength, especially if applied with a quantitative and site-specific labeling strategy, as is the case for sortase-catalyzed reactions. Common antibody labeling approaches mostly exploit a reaction between primary amines and NHS-activated fluorophores, or a cysteine-selective modification using maleimide derivatives. In this situation, the site(s) at which the label is introduced may vary from molecule to molecule. For every preparation, the coupling efficiency between dye and protein must be determined empirically. Even then, the number and position of fluorophores on the labeled protein is not uniform. We position multiple fluorophores at the ends of Holliday junctions such that self-quenching is avoided, while simultaneously boosting signal intensity. Both a single domain antibody fragment (VHH) and full-size antibody were labeled with Holliday junctions. Their binding properties were not altered as shown by flow-cytometry and immunofluorescence. The Holliday junctions increase fluorophore intensity significantly, a trait especially useful when studying proteins that have low expression levels and that may be difficult to visualize by conventional labeling techniques. However, repeated in vivo introduction of any such modified product, will require a detailed assessment of immunogenicity. For the in vitro application reported here, this is obviously not an issue. It will be interesting to explore the possibility of adding sortase recognition sites to both the heavy and light chains of an IgG molecule: one could thus add four Holliday junctions and install 16 moles of fluorophore per mole of immunoglobulin. Since modification of Holliday junctions is not limited to the installation of fluorophores, but could include cytotoxic drugs or their precursors, the production of biologicals as protein-drug conjugates presents additional opportunities for application.

1.4 Experimental Section

1.4.1 Synthesis and Assembly of Holliday Junctions.

DNA oligonucleotides with 5' amino modification (C6) were purchased from Integrated DNA Technologies, Inc. (Coralville, IA) and purified by reverse-phase HPLC. 100μM oligonucleotide stock in sodium borate buffer (100mM sodium borate, pH 8.5) was combined with 10 molar equivalents of NHS activated fluorophore or sulfo-NHS activated DBCO (Click chemistry tools, Scottsdale, AZ) in a total volume of 1ml. NHS-activated TAMRA dye was purchased from Chempep, Inc (Wellington, FL) and Alexa 647 was purchased from Life technologies (Beverly, MA). The reaction was incubated at 40 °C overnight and purified on a NAP-10 column (GE healthcare Life Science, Piscataway, NJ). Equivalent molar ratios of each of the ssDNA strands were mixed and heated to 90°C, followed by slow cooling at 1°C per minute to 4°C. Products were separated by 3% agarose electrophoresis under non-denaturing conditions. DNA Bands were visualized by TOTO-3 iodide (Life Technologies), which was mixed at a 5:1 of ratio of base pairs to dye molecules. The DNA-dye mixtures were incubated at room temperature for 60 minutes and glycerol was added to 30% (v/v) prior to loading on the agarose gel. The intensity of TAMRA and TOTO-3 signals were measured by scanning on a Typhoon FLA 9500 gel scanner (GE Healthcare Life Sciences). Alternatively, DBCO labeled with oligonucleotide and the other unlabeled three oligonucleotides were mixed in equivalent molar ratios and assembled with previously described condition following by NHS activated fluorophores labeling.

1.4.2 Synthesis of the Peptide Probe for Sortase Reaction

Peptide GGGK(TAMRA)K(azide) with N terminal amine and C terminal CONH2 was synthesized following standard solid phase synthesis protocols[2]. All Fmoc amino acids were purchased from Chempep, Inc. The TAMRA dye was coupled to the lysine side chain by, first,

selective on-resin removal of the 4-Methyltrityl (MTT) protecting group in 1% TFA, 1%TIPS, DCM, followed by standard solid phase coupling to attach TAMRA to the lysine side chain. Fmoc-Lys(azide)-OH was used as building block to provide the bioorthogonal moiety. The peptide was purified by reverse phase HPLC and was confirmed by LCMS. Peptide GGGK(Cy5)K(azide) with N terminal amine and C terminal CONH2 was synthesized with a similar manner using Sieber amide resin (Novabiochem, Billerica, MA). NHS activated Cy5 is coupled with lysine side chain after selective on resin removal of [1-(4,4-dimethyl-2,6-dioxocyclohexylidene) ethyl] (DDe) protecting group with hydroxylamine hydrochloride/imidazole (1.3:1) in N-Methyl-2-pyrrolidone (NMP). Peptide was cleaved off the resin under mild acidic conditions (1% TFA, DCM). The peptide was purified by reverse phase HPLC and its identity was confirmed by LCMS.

1.4.3 C-Terminal Sortagging

Ca^{2+} independent heptamutant Sortase A derived from S. aureus (10 μM final concentration, 10× stock in 50 mM Tris, pH 7.4, 150 mM NaCl) and probe (1 mM final concentration, 50× stock) were added to the VHH7 (200 μM final concentration) in sortase buffer (50 mM Tris, pH 7.4, 150 mM NaCl). The resulting mixture was incubated at 20 °C for 2hrs. 0.5ml Ni-NTA was added to the reaction mixture and mixed for 20 min to remove sortase and unreacted protein. The mixture was filtered and the flow through was collected and purified by size exclusion chromatography (Superdex 75-GE Life Sciences). The resulting purified protein was concentrated in 10KD size cut-off centrifugal filter units. Concentrated protein was analyzed by SDS PAGE and LC/MS. Alternatively, immobilized Ca^{2+}-independent sortase was used when the target protein was of similar size as sortase to avoid sortase contamination in the following steps. Immobilization of sortase on CNBr-activated Sepharose (Sigma Aldrich, St. Louis, MO) was performed using procedures recommended by the manufacturer.

1.4.4 Assembly of the Holliday Junction-Protein Complex

Purified protein after the sortase reaction (100 nmol) was combined with 1.5 molar equivalents of assembled Holliday Junction in PBS buffer (5 mL total volume). The reaction mixture was incubated at 4 °C overnight. The mixture was purified by size exclusion chromatography (Superdex 200- GE Life Sciences) to separate any unreacted protein from product. The purified multi-labeled protein was concentrated in 30 kDa cut-off centrifugal filter units. Concentrated protein was analyzed by SDS PAGE.

1.4.5 Flow Cytometry

As shown in **Figure 1.9**, all data was acquired on a Fortessa instrument (BD Bioscience) and analyzed on a FLowjo software (Tree Star). Cells derived from homozygous class II MHC - EGFP knock in mice, which express class II MHC β-chain fused at its carboxy terminus with eGFP moiety and wild type C57/B6 mice were used for flow cytometry. Cells isolated from spleen were suspended in PBS (137mM NaCl, 2.7mM KCl, 10mM Na2HPO4, 1.8mM KH2PO4) with 2% fetal bovine serum (FBS) and passed through 40-μm cell strainers to obtain single-cell suspensions prior to antibody staining (30min at 4°C). Splenocytes from homozygous class II MHC-eGFP Knock in mice were stained at different concentrations of VHHs and derivatives. Splenocytes from wild type mice served as compensation controls. A20 cells were cultured in Dulbecco's modified Eagle's medium (DMEM) containing 10% IFS and various concentrations of Alexa647/Cy5 labeled anti-DEC205 antibodies and a commercial Alexa488 labeled anti-DEC205 antibody (ebioscience) as control.

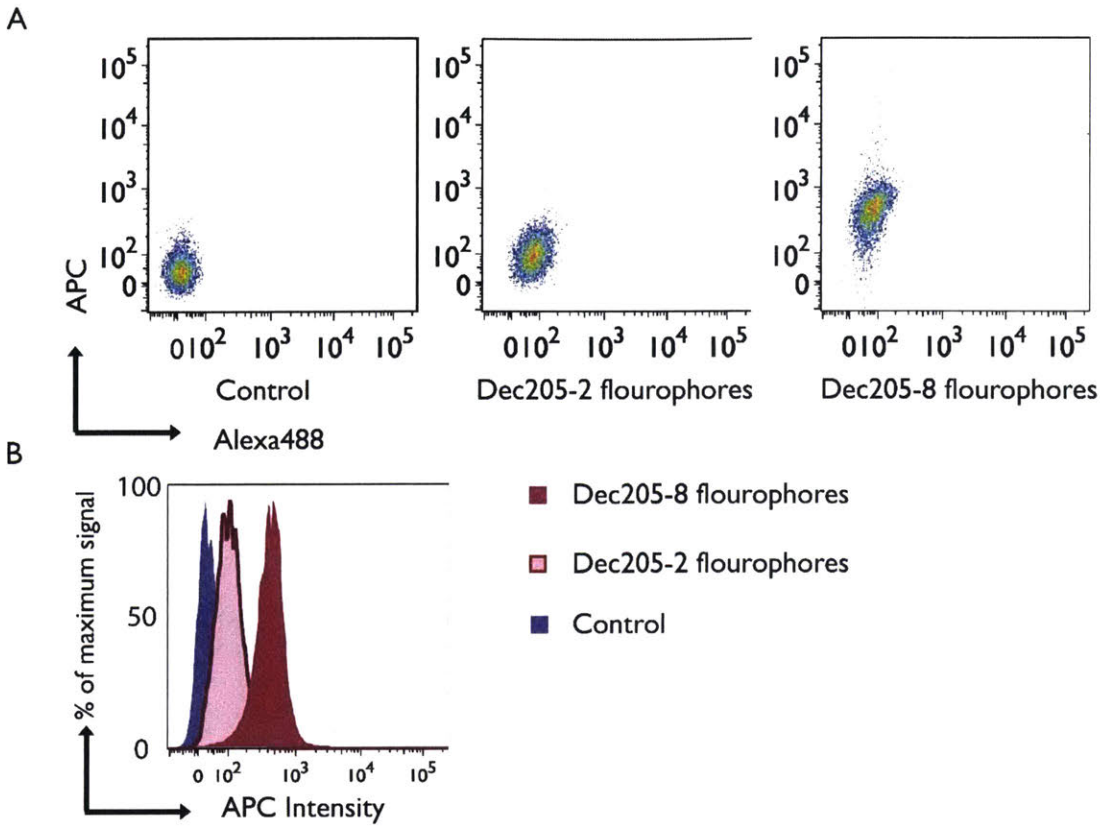

Figure 1.9 (A) Flow cytometry of A20 cells incubated with anti-DEC205 labeled with either 2 or 8 fluorophores and a control alexa488 labeled anti-DEC205 antibody that binds to a different epitope. (B) A shift in intensity for 2 fluorophores and 8 fluorophores labeled anti-DEC205 antibody at 8µg/ml.

1.4.6 Confocal Microscopy

Chambered cover glass slides were coated with poly-lysine (Sigma Aldrich). 200µl cells in PBS sorted by flow cytometry were added to the chambered slide and incubated at 4 °C for 30 min. Unattached cells were washed off with PBS with 2% FBS. Images were collected on a PerkinElmer ultraview spinning disk confocal microscope with Volocity acquisition software (PerkinElmer, Waltham, MA).

1.5 References

1. Hyeon, C.; Lee, J.; Yoon, J.; Hohng, S.; Thirumalai, D., Hidden complexity in the isomerization dynamics of Holliday junctions. *Nature chemistry* **2012,** *4* (11), 907-14.

2. Mazmanian, S. K.; Liu, G.; Ton-That, H.; Schneewind, O., Staphylococcus aureus sortase, an enzyme that anchors surface proteins to the cell wall. *Science* **1999,** *285* (5428), 760-3.

3. Witte, M. D.; Wu, T.; Guimaraes, C. P.; Theile, C. S.; Blom, A. E.; Ingram, J. R.; Li, Z.; Kundrat, L.; Goldberg, S. D.; Ploegh, H. L., Site-specific protein modification using immobilized sortase in batch and continuous-flow systems. *Nat Protoc* **2015,** *10* (3), 508-16.

4. Maruyama, T.; Dougan, S. K.; Truttmann, M. C.; Bilate, A. M.; Ingram, J. R.; Ploegh, H. L., Increasing the efficiency of precise genome editing with CRISPR-Cas9 by inhibition of nonhomologous end joining. *Nat Biotechnol* **2015,** *33* (5), 538-42.

5. Guimaraes, C. P.; Witte, M. D.; Theile, C. S.; Bozkurt, G.; Kundrat, L.; Blom, A. E.; Ploegh, H. L., Site-specific C-terminal and internal loop labeling of proteins using sortase-mediated reactions. *Nature Protocols* **2013,** *8* (9), 1787-99.

6. Harris, L. J.; Larson, S. B.; Hasel, K. W.; McPherson, A., Refined structure of an intact IgG2a monoclonal antibody. *Biochemistry* **1997,** *36* (7), 1581-97.

7. Kubala, M. H.; Kovtun, O.; Alexandrov, K.; Collins, B. M., Structural and thermodynamic analysis of the GFP:GFP-nanobody complex. *Protein Sci* **2010,** *19* (12), 2389-401.

8. *An Anti-Tubulin Darpin Caps the Microtubule Plus-End.* http://www.rcsb.org/structure/4DUI.

9. Eigenbrot, C.; Ultsch, M.; Dubnovitsky, A.; Abrahmsen, L.; Hard, T., Structural basis for high-affinity HER2 receptor binding by an engineered protein. *Proc Natl Acad Sci U S A* **2010,** *107* (34), 15039-44.

10. Porter, E. B.; Polaski, J. T.; Morck, M. M.; Batey, R. T., Recurrent RNA motifs as scaffolds for genetically encodable small-molecule biosensors. *Nature chemical biology* **2017,** *13* (3), 295-301.

11. Fry, R. Appreciating your past in order to transform the future. http://www.clevelandshrm.com/ (accessed 26.9.05).

12. Stacey, R. D., *Strategic Management and Organisational Dynamics*. Pitman: London, 1993.

13. Champagne, F. *The ability to manage change in health care organisations*; Commission of the Future of Health Care in Canada: November, 2002; p 36.

14. Lakowicz, J. R., *Principles of fluorescence spectroscopy*. 3rd ed.; Springer: New York, 2006; p xxvi, 954 p.

15. Vira, S.; Mekhedov, E.; Humphrey, G.; Blank, P. S., Fluorescent-labeled antibodies: Balancing functionality and degree of labeling. *Anal Biochem* **2010,** *402* (2), 146-150.

16. Toseland, C. P., Fluorescent labeling and modification of proteins. *Journal of chemical biology* **2013,** *6* (3), 85-95.

17. Hof, M.; Hutterer, R.; Fidler, V., *Fluorescence spectroscopy in biology : advanced methods and their applications to membranes, proteins, DNA, and cells*. Springer: Berlin ; New York, 2005; p xix, 305 p.

18. Sauer, M.; Hofkens, J.; Enderlein, J., *Handbook of Fluorescence Spectroscopy and Imaging: From Ensemble to Single Molecules*. John Wiley & Sons: 2010.

19. Wu, P.; Shui, W.; Carlson, B. L.; Hu, N.; Rabuka, D.; Lee, J.; Bertozzi, C. R., Site-specific chemical modification of recombinant proteins produced in mammalian cells by using the genetically encoded aldehyde tag. *Proceedings of the National Academy of Sciences* **2009,** *106* (9), 3000-3005.

20. Rush, J. S.; Bertozzi, C. R., New aldehyde tag sequences identified by screening formylglycine generating enzymes in vitro and in vivo. *J Am Chem Soc* **2008,** *130* (37), 12240-1.

21. Schmidt, S. R., *Fusion protein technologies for biopharmaceuticals: applications and challenges*. John Wiley & Sons: 2013.

22. Chen, I.; Howarth, M.; Lin, W.; Ting, A. Y., Site-specific labeling of cell surface proteins with biophysical probes using biotin ligase. *Nat Methods* **2005,** *2* (2), 99-104.

23. Crivat, G.; Taraska, J. W., Imaging proteins inside cells with fluorescent tags. *Trends Biotechnol* **2012,** *30* (1), 8-16.

24. Popp, M. W.; Antos, J. M.; Ploegh, H. L., Site-specific protein labeling via sortase-mediated transpeptidation. *Curr Protoc Protein Sci* **2009,** *Chapter 15*, Unit 15 3.

Chapter 2. VHHs Based Biosensors

The work presented in this chapter is a part of the following manuscript and is reproduced here with permission from the authors.

Guan-Yu Chen,[+] Zeyang Li,[+] Christopher S. Theile, Neelkanth M. Bardhan, Priyank V. Kumar, Joao N. Duarte, Takeshi Maruyama, Ali Rashidfarrokh, Angela M. Belcher, and Hidde L. Ploegh *Chemistry-A European Journal* 2015 Nov 23; 21(48): 17178–17183. doi:10.1002/chem.201503057

Guan-Yu Chen, [+] Zeyang Li, [+] Joao N Duarte, Alexandre Esteban, Ross W Cheloha, Christopher S Theile, Gerald R Fink, Hidde L Ploegh *Biosens Bioelectron.* 2017 Mar 15;89(Pt 2):789-794. doi: 10.1016/j.bios.2016.10.015.

2.1 Introduction of Immunosensors

2.1.1 Introduction

Antibody(Ab) and antibody fragment-based biosensors or immunosensors are compact tools capable of providing sensitive and rapid detection or capture of a range of pathogens or cells of interests for further analysis. The history of biosensors dates back to 1956 when Leland C. Clark described the first biosensor which was developed to detect glucose levels in serum samples using a membrane bound biologically sensitive element.[2] Over the past few decades, numerous types of biosensors have been developed for detection of a wide variety of substrates including small molecules, proteins, oligonucleotides, cells, viruses, and other. Immunosensors, a special type of biosensor, frequently applied for the detection of specific antigens or antibodies, are analytic devices that convert the signal generated by the binding of Abs or Ab derivatives to target into a measurable signal. In order to identify new and useful immunosensors, scientists must exploit recent advances in the development of nanomaterial solid supports with ideal surface properties, such as surfaces that employ antigen specific capture molecules for immunochemical reactions or antigen binding.

2.1.2 Selection of Antigen Binding Molecules

Abs or immunoglobulins (Igs) are highly soluble serum glycoproteins which can be divided into five main isotypes (IgA, IgD, IgE, IgG, and IgM) based on their heavy chain constant region sequences.[6] Polyclonal antibodies (pAb) can be easily raised in animals such as rat, rabbits, goats, and sheep. They are frequently used in immunosensors for pathogen detection. However, multiple epitopes may often be recognized by pAb since their source is a pool of Abs secreting B cells.[9] In cases where highly specific binding is required, monoclonal antibodies (mAb) are more desirable and can be generated through the use of hybridoma technology.[10] Splenocytes from an

immunized animal are commonly used as the source of Ab-producing B cells for myeoloma fusion. The resulting hybridoma cells are immortal cell lines secreting full size Abs.[11] The pool of hybridomas can be further screened against targeted antigens to identify suitable single cell candidates for monoclonal Ab production. Among the five main isotypes of Ig, IgG is the main type of Ab found in blood and extracellular fluid.[6] The general structure of an IgG is shown in **Figure 2.1.1,** and it consists of four polypeptide chains, i.e. two heavy chains and two light chains, which are joined together by disulfide bonds. The antigen-binding (Fab) region, composed of one constant and one variable domain from a paired heavy and light chain, provides the site responsible for antigen binding (**Figure 2.1.2**). Conjugation reactions may result in a decrease of antibody avidity.[12] Thus, immobilization strategies should be carefully designed so that Fabs are left unaltered throughout the process. High degree random conjugation may result in changes in antigen binding characteristics and, in more extreme scenarios, a complete loss of function.[13] In addition, different immobilization methods may lead to uniform or random orientation of Abs on solid support [14]. The ability to control the site of protein (Ab) modification is essential for avoiding the destruction or steric hindrance of antigen binding of immobilized Fabs. In principle, modification sites should be kept far away from the Fabs to achieve optimal results.

Though full-size Abs generated through immunization have been widely used for immunosensors since the beginning of biosensor development, recently developed recombinant molecules generated in vitro have many advantages over conventional Abs. The advantages of these alternative scaffolds include their compact sizes, excellent thermal and chemical stabilities, as well as low production costs.[15-16] For example, to obtain useful single domain antibodies (VHHs) from camelids (shown in **Figure 2.1.1B**), a cDNA library can be obtained from an immunized llama or alpaca to serve as a pool of DNA fragments for generation of the phage display library.[15] Phage that bind target during panning process can then be recovered, sequenced and transferred to a periplasmic expression vector to obtain the final VHH protein from *E. coli* expression. VHH binders with desired properties can be recombinantly expressed with tag

sequences, protein fusion partners, or artificial amino acids through covalent modification.[17] Similarly, DARPins **(Figure 2.1.1C)**, scFvs **(Figure 2.1.1D)**, and affibody scaffolds (**Figure 2.1.1E**) can also be screened in libraries as alternatives. In addition, peptide and oligonucleotide based binding molecules, such as aptamers **(Figure 2.1F)**, can be screened from a pool of random sequences to acquire molecules with desired binding specificity and affinity.[18]

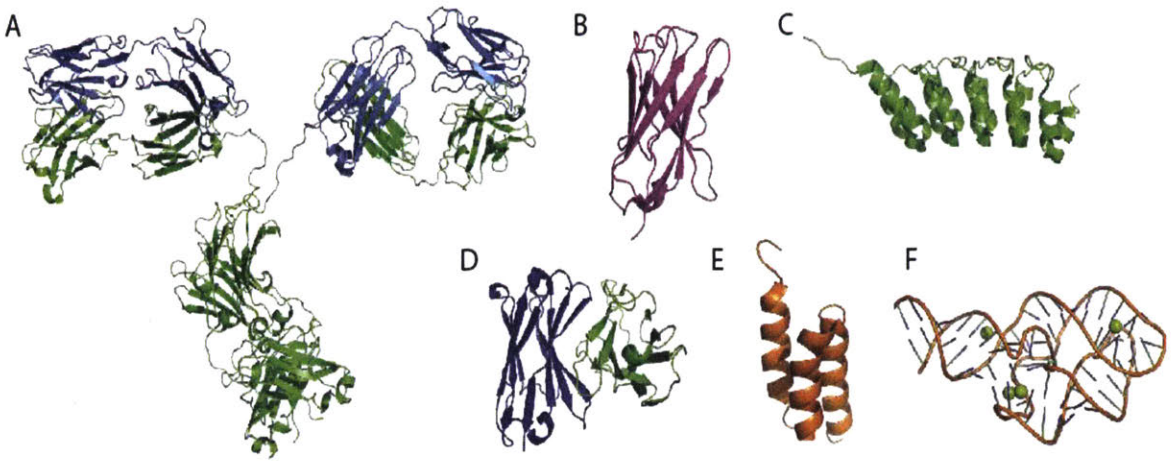

Figure 2.1.1 (A) Overall structure of Ab and alternative recombinant binder scaffolds used in biosensors. (A) IgG2a monoclonal antibody with two heavy chains colored in green and two light chains colored in blue (PDB:1IGT).[1] (B) The green fluorescent protein (GFP)-VHH (PDB: 3OGO).[3] (C) DARPin against tubulin beta chain (PDB: 4DUI).[4] (D) anti-fluorescein ScFv (PDB: 1X9Q).[5] (E) human epidermal growth factor receptor 2 (HER2) binding affibody (PDB: 2KZJ).[7] (F) 5-hydroxytryptophan aptamer (PDB: 5KPY).[8]

2.1.3. Immunosensor Types and Common Material Selection

The composition of support materials for an immunosensor can be selected based on analytic needs (**Table 2.1.1**). Optical transducers that exploit light absorption, luminescence, and fluorescence often require optically transparent materials as support. Surface plasmon resonance (SPR) sensors rely on the unique optical properties possessed by metallic nanostructures (gold, silver, etc.).[19] Electrochemical immunosensors produce electrical charges for the quantitative analysis of target molecules. Many novel nanomaterials, such as carbon nanotubes, graphene, indium tin oxide, nanowire, hydrogels, and metallic nanoparticles, are employed in order to construct a high-performance electrode for signal output.[20] Many attempts have been made to improve the electrochemical properties of supporting materials to increase electro-catalytic sensitivities, impart excellent electron transfer abilities and exhibit good biocompatibility.[20-21] Piezoelectric immunosensors exploit the piezoelectric effect which occurs in various crystalline substances. The piezoelectric immunosensor is known to be one of the most sensitive analytical instruments with the capability of detecting antigens in the picogram range.[22-23]

Immunosensor Type		Common Materials	References
Optical	Evanescent wave	Quartz, glass, graphene oxide (GO) sheets, hydrogels	19, 24-26
	Surface plasmon resonance (SPR)	Silver, gold, copper, aluminum	
Electrochemical	Conductive	Carbon, indium tin oxide, carbon nanotube, hydrogels, polythiophene	27-30
	Amperometric	Graphite, lipid, platinum, gold, nickel	
Piezoelectric	Bulk acoustic wave	Aluminium phosphate, aluminium nitride, zinc oxide, crystalized topaz, crystalized tourmaline, barium titanate, gallium orthophosphate, lead titanate	22-23, 31
	Surface acoustic wave		

Table 2.1.1 Immunosensor types and common materials used

2.1.4 Current conjugation methods

The performance of an immunosensor depends upon three key factors: 1) the binding affinity and specificity of antigen binding molecules, 2) the accessibility and proportion of binding sites intact after immobilization, and 3) the density of binding molecules coated on the surface of immunosensor. Different strategies for immobilization may result in different outcomes and efficiencies (**Figure 2.2**). Immobilized Abs can adopt several different orientations depending on the method applied. Adsorption-based methods often result in a "flat-on" orientation, with the Fc and Fab fragments lying flat on the surface.[32] This confirmation can result in hindrance of antigen

access to antibody binding sites, which can lead to a decrease in antigen binding capacity.[33] Specific orientation is preferrable but not as easily achieved as adsorption, since site specific modification of antigen binding molecules commonly require incorporation of a unique reactive group. Affinity based attachment using protein A and protein G provides another solution. These proteins display multiple binding sites specific to the Fc potion of Abs and lead to a predominantly "tail-on" attachment of Abs. Further improvement can be achieved by introducing a linker between protein A or protein G and the surface. The immobilization strategies should be also compatible with the targeted surface materials, such as gold, copper, iron, silicon, hydro-gel, carbon nanotubes, and graphene oxide. We presented the most popular conjugation methods for each different binding molecule category (**Table 2.1.2**).

Type of antigen binding molecules	Types of Immobilization	Functional Group	Orientation	References
Antibody	Adsorption	Various	Random	34-37
	Affinity	Antigen-antibody reaction	Partially oriented	37-39
		Protein A or G (non-covalent) binding	Partially oriented	36, 40
	Random crosslinking	Amine/carboxylic acid	Random	38-39, 41-42
		Thiol group	Random	39, 41, 43
		Sugar chain on C_H2	Partially Oriented	44-45
	DNA-directed	Nucleotide Binding Site ssDNA hybridization	Uniformly oriented	46-47
	C terminus	Enzyme mediated biotinylation	Uniformly oriented	44
VHH	C terminus	non-natural amino-acid	Uniformly oriented	48-49
	C terminus	Enzyme mediated Transpeptidation	Uniformly oriented	50-51
scFv	Tag mediated	Cysteine or Histidine containing linker	Partially Oriented	52-54
	E. coli surface displayed	Genetic fusion	Uniformly oriented	55
DARPins	Random crosslinking	Amine group	Random	56-57
Aptamer	Terminal modification	Thiol	Uniformly oriented	58-60

Table 2.1.2 A summary of popular conjugation methods

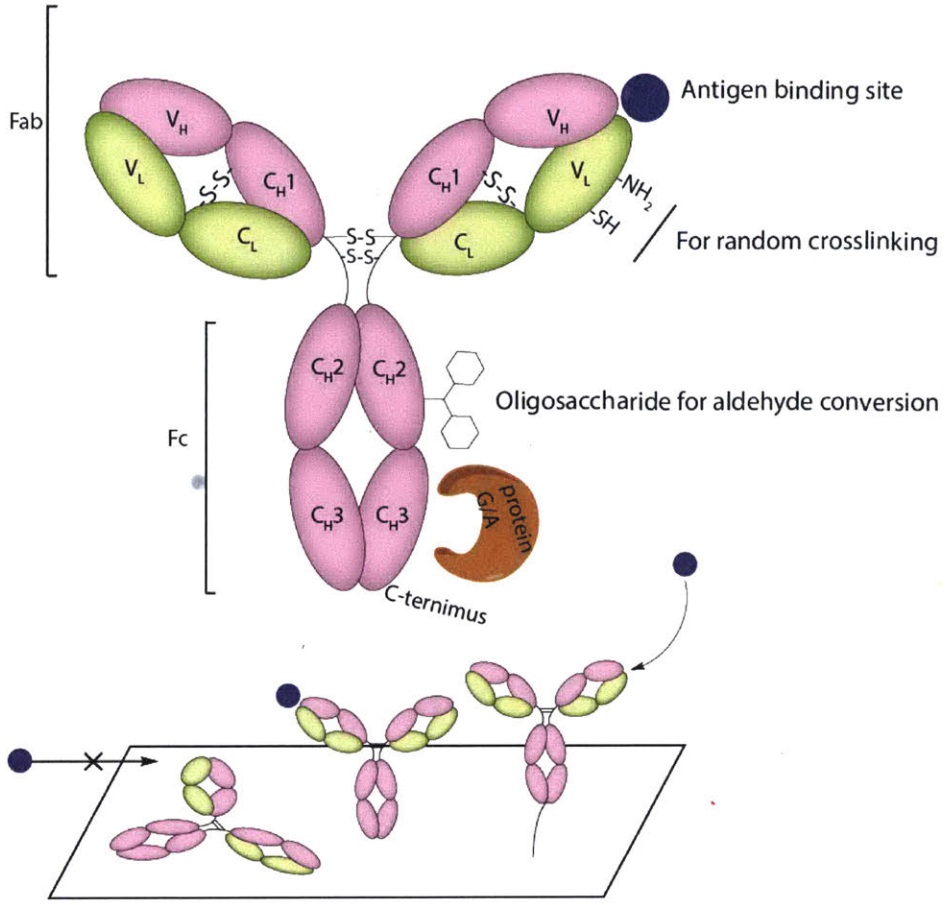

Figure 2.1.2 Functional groups on Abs used for conjugation and the result of random and oriented immobilization onto surfaces

Physical adsorption of Abs onto hydrophobic surfaces like polystyrene offers the simplest attachment. However, the process is uncontrollable in terms of orientation and stability, and often results in denaturation and detachment of protein from the surface.[32] Protein G and protein A are small bacteria-derived moieties bind in a specific orientation to Fc region.[40] This method offers non-covalent but mostly "tail-on" Ab attachment. Random crosslinking methods provide another mode of attachment as amine, carboxyl and thiol groups are abundant throughout the surface of

antibody. Amine and carboxyl coupling is commonly achieved by using carbodiimides as carboxyl activation reagents in tandem with succinimidyl ester (NHS) for improved efficiency.[41] This method, also known as EDC/NHS coupling, can be used to robustly create covalent linkage via amide bond formation (**Figure 2.1.3A** and **2.1.3B**). Reactive primary amine and carboxyl groups on Ab surface (lysine, aspartic acid and glutamic acid side chains) are abundant in Fab region due to its polar nature. Thus, it is impossible to control the orientation and predict the outcomes of Fab region immobilization as the immobilized product is a mixture of Abs modified at different molar equivalents and positions. Similarly, reactive thiol groups (cysteine side chains) can also be targeted for maleimide or iodoacetamide reaction (**Figure 2.1.3C**). Additionally, disulfide bonds can also be reduced as an alternative source of thiol groups. In addition to the classical maleimide reaction or gold surface attachment (**Figure 2.1.3D**), Baker and Chudasama groups reported the usage of pyridazinedone as a way to yield a more homogenous product with better retention of structure (**Figure 2.1.3E**).[43] Several other approaches are reported to achieve specific orientations. Kang *et. al.* reported a site specific biotinylation strategy using the sugar moiety on the Fc region (**Figure 2.1.3F**). [44] Oxidation of sugar chains yields reactive aldehyde groups, which can be used to covalently link Abs in an oriented manner without disturbing structural integrity. There are several other immobilizations methods reported recently. Bilgicer and co-workers exploited the conserved nucleotide binding site (NBS) on the Fab region to achieve site-specific labeling using UV-cross linking method.[46] Boozer and others reported a DNA-directed Ab immobilization method by using ssDNA pre-conjugated to Ab to form a self-assembled monolayer on the surface coated with complementary sequence.[47] Another Ab site-specific labeling strategy is to use formylglycine-generating enzyme (FGE) to install an aldehyde tag on a specific pentapeptide sequence, which may then react with aminooxy-containing surface linkers.[61]

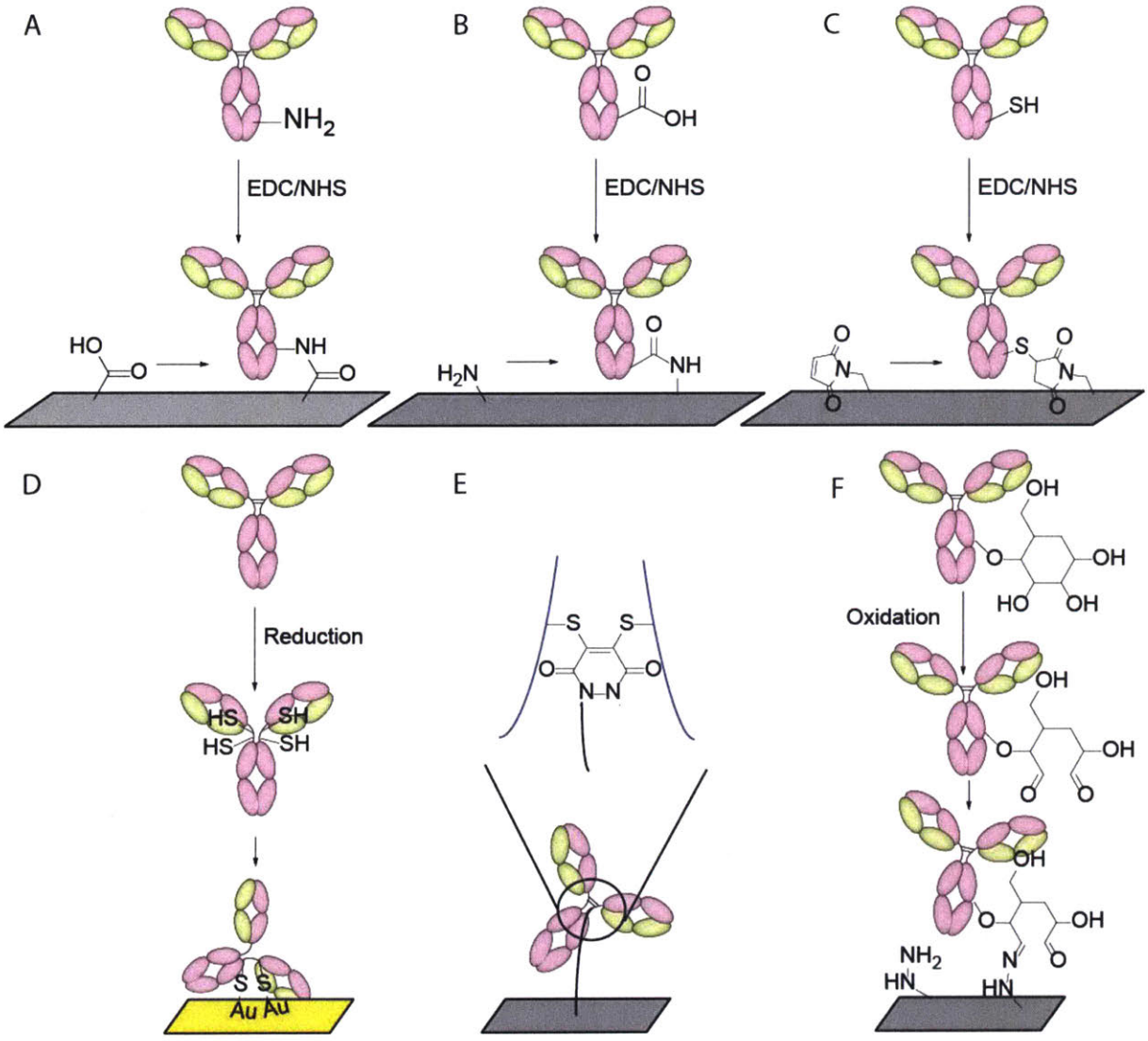

Figure 2.1.3 Ab immobilization scheme. (A) EDC/NHS coupling of Ab surface amine to carboxyl and (B) carboxyl groups to amine groups. (C) Sulfhydryl-reactive chemical group coupling to Ab surface thiol groups. (D) Reduction of antibody disulfides to reactive thiols for gold substrates binding. (E) Reduction of antibody disulfides for site specific pyridazinedone coupling. (F) Oxidation of sugar chains for reactive aldehyde groups.

VHHs, also known as nanobodies, are recombinant, antigen-specific, single-domain, variable fragments of camelid heavy chain-only antibodies. Compared to full size IgG's, VHHs can be expressed in high yield in bacterial systems. The small size (~14 kD) provides significant advantages in medical diagnostic and therapeutic applications.[62] However, due to their small size, VHH's have a significantly higher percentage of their surface involved in binding interactions compared to full size IgG's; therefore, site-specific installation of linker is particularly important for immunosensors that use VHHs. The Beekwilder group reported an oriented labeling method in which azide-functionalized VHH was attached to a cyclooctyne-tailored sensor surface (**Figure 2.1.4A**).[48] They emphasized the importance of oriented immobilization as it increased sensor efficiency up to 800-fold compared to random labeling. In addition, transpeptidase can also be used to create site specific modification on VHH since a short peptide recognition sequence can be easily incorporated into recombinant expression vectors. The Ploegh group incorporated the sortase recognition motif, LPXTG, at the C terminus of VHHs, which can then be used for installation of a short GGG peptide with a biorthogonal handle (**Figure 2.1.4B**).[50-51, 63-65]

ScFvs are a type of fusion protein which contains variable regions of the heavy (V_H) and light chains (V_L) of Abs connected via a short peptide linker. Shen et. al optimized a 15-mer peptide linker (RGRGRGRGRSRGGGS) to increase the adsorption efficiency on anionic charged biosensor surface.[52] Chen group developed a cancer marker monitoring platform produced through a dual-expression system in *E. coli* in which anti-cancer ScFvs and gold binding peptides are displayed on the surface of bacteria at the same time (**Figure 2.1.5**). In this case, ScFvs are fused at the C-terminus of the extracellular domain of a transmembrane protein (Lpp-OmpA) and to achieve a fixed orientation of ScFv on the *E. coli* surface.

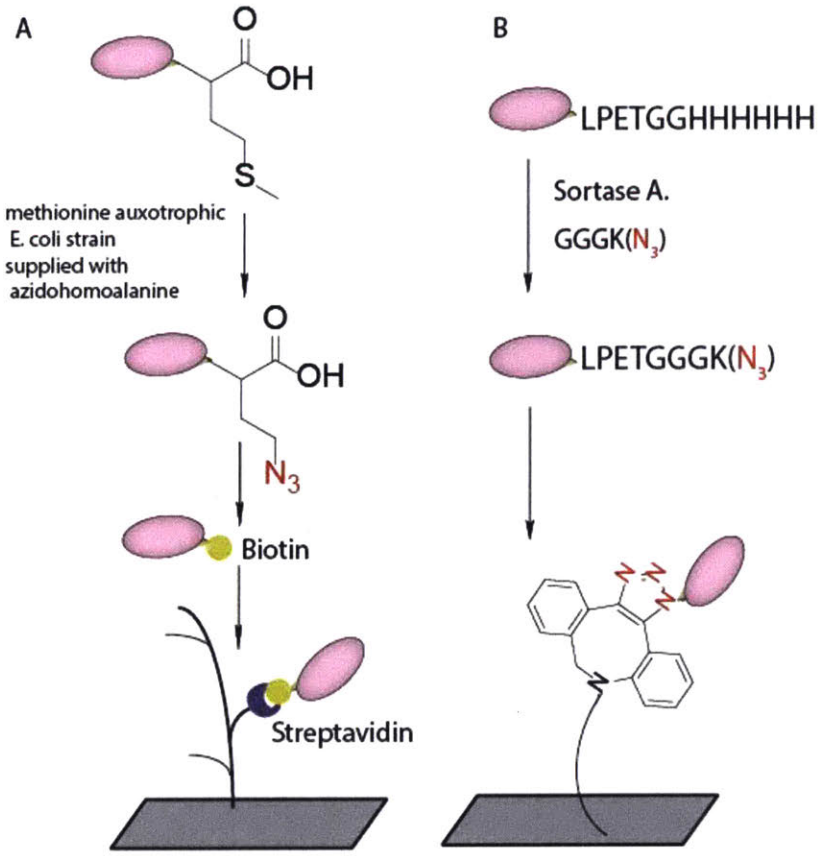

Figure 2.1.4 Oriented immobilization scheme for VHHs. (A) C-terminal N_3 group introduced by artificial amino acid incorporation followed by conversion to biotin for streptavidin binding. (B) C-terminal N_3 group attached via sortase mediated transpeptidation followed by site-specific attachment on DBCO modified surface.

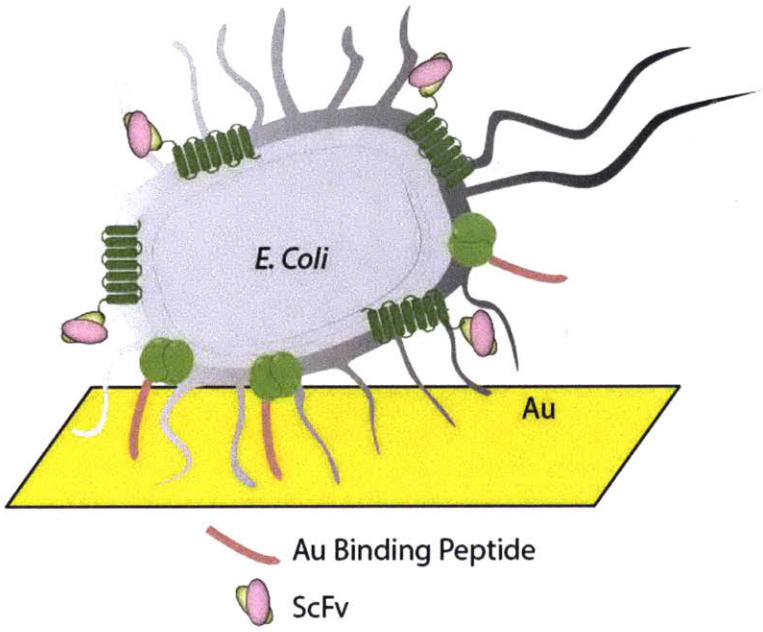

Figure 2.1.5. ScFv and gold-binding peptide dual-expression system in *E. coli*

Other novel alternatives, such as DARPins and Aptamers can also serve as the binding moiety in immunosensors. DARPins are a novel class of non-IgG scaffolds based on naturally occurring ankyrin repeats. DARPins are small in size (13-20 kDa) and highly soluble in aqueous solution. Deyev and others reported that DARPins can bind tightly to gold nanoparticles (GNPs) via adsorption.[56]

Aptamers are single-stranded DNA or RNA (ssDNA or ssRNA) oligonucleotides or peptides engineered through repeated in vitro selection or equivalent methods. However, aptamers have distinct limitations, especially for those composed of DNA or RNA. The rapid degradation of aptamers by nucleases in biological media is a serious problem. Such degradation causes instability which is unacceptable for biosensor application. Despite such limitations, many successful attempts have been made to create aptamer based biosensors in relatively nucleases free systems. One approach employed terminally functionalized thiol group for gold surface

binding.[59] Other functional groups such as primary amines or activated carboxylic acids are also commonly sued for covalent conjugation.[60]

2.1.5 Conclusions

The performance of immunosensors is closely associated with the antigen binding molecules and immobilization approach. While Abs have been increasingly used as detection elements in immunosensors, recent developments in antibody derivatives and other alternative binding molecules raises new opportunities and possibilities to create highly stable, efficient, and economically feasible diagnostic device. In this review, a wide range of immobilization strategies are presented for Ab and Ab alternatives and their applications on various nanomaterial surfaces are discussed. Pros and cons of each method are presented. The uniform orientation conferred by site-specific immobilization is essential for small Ab alternatives in order to retain their binding efficiency.

2.1.6 References

1. Ghosh, I.; Considine, N.; Maunus, E.; Sun, L.; Zhang, A.; Buswell, J.; Evans Jr, T. C.; Xu, M.-Q., Site-specific protein labeling by intein-mediated protein ligation. In *Heterologous Gene Expression in E. coli*, Springer: 2011; pp 87-107.

2. Heineman, W. R.; Jensen, W. B., Leland C. Clark Jr. (1918–2005). *Biosensors and Bioelectronics* **2006,** *21* (8), 1403-1404.

3. Guimaraes, C. P.; Witte, M. D.; Theile, C. S.; Bozkurt, G.; Kundrat, L.; Blom, A. E.; Ploegh, H. L., Site-specific C-terminal and internal loop labeling of proteins using sortase-mediated reactions. *Nature Protocols* **2013,** *8* (9), 1787-99.

4. Theile, C. S.; Witte, M. D.; Blom, A. E.; Kundrat, L.; Ploegh, H. L.; Guimaraes, C. P., Site-specific N-terminal labeling of proteins using sortase-mediated reactions. *Nature Protocols* **2013,** *8* (9), 1800-7.

5. Ton-That, H.; Liu, G.; Mazmanian, S. K.; Faull, K. F.; Schneewind, O., Purification and characterization of sortase, the transpeptidase that cleaves surface proteins of Staphylococcus aureus at the LPXTG motif. *Proceedings of the National Academy of Sciences of the United States of America* **1999,** *96* (22), 12424-9.

6. Vidarsson, G.; Dekkers, G.; Rispens, T., IgG subclasses and allotypes: from structure to effector functions. *Front Immunol* **2014,** *5*, 520.

7. Ton-That, H.; Schneewind, O., Anchor structure of staphylococcal surface proteins. IV. Inhibitors of the cell wall sorting reaction. *J Biol Chem* **1999,** *274* (34), 24316-20.

8. Clegg, R. M.; Murchie, A. I.; Zechel, A.; Carlberg, C.; Diekmann, S.; Lilley, D. M., Fluorescence resonance energy transfer analysis of the structure of the four-way DNA junction. *Biochemistry* **1992,** *31* (20), 4846-56.

9. Lipman, N. S.; Jackson, L. R.; Trudel, L. J.; Weis-Garcia, F., Monoclonal versus polyclonal antibodies: distinguishing characteristics, applications, and information resources. *ILAR J* **2005,** *46* (3), 258-68.

10. Singh, S.; Kumar, N.; Dwiwedi, P.; Charan, J.; Kaur, R.; Sidhu, P.; Chugh, V. K., Monoclonal Antibodies: A Review. *Curr Clin Pharmacol* **2017**.

11. Banker, D. D., Monoclonal antibodies. A review. *Indian J Med Sci* **2001,** *55* (12), 651-4.

12. Vira, S.; Mekhedov, E.; Humphrey, G.; Blank, P. S., Fluorescent-labeled antibodies: Balancing functionality and degree of labeling. *Anal Biochem* **2010,** *402* (2), 146-50.

13. Werthen, M.; Nygren, H., Effect of antibody affinity on the isotherm of antibody binding to surface-immobilized antigen. *J Immunol Methods* **1988,** *115* (1), 71-8.

14. Trilling, A. K.; Beekwilder, J.; Zuilhof, H., Antibody orientation on biosensor surfaces: a minireview. *Analyst* **2013,** *138* (6), 1619-27.

15. Bever, C. S.; Dong, J. X.; Vasylieva, N.; Barnych, B.; Cui, Y.; Xu, Z. L.; Hammock, B. D.; Gee, S. J., VHH antibodies: emerging reagents for the analysis of environmental chemicals. *Anal Bioanal Chem* **2016,** *408* (22), 5985-6002.

16. Muyldermans, S., Nanobodies: natural single-domain antibodies. *Annu Rev Biochem* **2013,** *82*, 775-97.

17. de Marco, A., Biotechnological applications of recombinant single-domain antibody fragments. *Microb Cell Fact* **2011,** *10*, 44.

18. Ray, P.; White, R. R., Aptamers for Targeted Drug Delivery. *Pharmaceuticals* **2010,** *3* (6), 1761-1778.

19. Rabbany, S. Y.; Donner, B. L.; Ligler, F. S., Optical immunosensors. *Crit Rev Biomed Eng* **1994,** *22* (5-6), 307-46.

20. Felix, F. S.; Angnes, L., Electrochemical immunosensors - A powerful tool for analytical applications. *Biosens Bioelectron* **2018,** *102*, 470-478.

21. Wen, W.; Yan, X.; Zhu, C.; Du, D.; Lin, Y., Recent Advances in Electrochemical Immunosensors. *Anal Chem* **2017,** *89* (1), 138-156.

22. Zu, H.; Wu, H.; Wang, Q. M., High-Temperature Piezoelectric Crystals for Acoustic Wave Sensor Applications. *IEEE Trans Ultrason Ferroelectr Freq Control* **2016,** *63* (3), 486-505.

23. Marrazza, G., Piezoelectric biosensors for organophosphate and carbamate pesticides: a review. *Biosensors (Basel)* **2014,** *4* (3), 301-17.

24. Akkoyun, A.; Bilitewski, U., Optimisation of glass surfaces for optical immunosensors. *Biosens Bioelectron* **2002,** *17* (8), 655-64.

25. Wiederoder, M. S.; Kendall, E. L.; Han, J. H.; Ulrich, R. G.; DeVoe, D. L., Flow-through microfluidic immunosensors with refractive index-matched silica monoliths as volumetric optical detection elements. *Sens Actuators B Chem* **2018,** *254*, 878-886.

26. Robinson, G. A., Optical immunosensors. *Biochem Soc Trans* **1991,** *19* (1), 18-20.

27. Liu, G.; Lin, Y., Nanomaterial labels in electrochemical immunosensors and immunoassays. *Talanta* **2007,** *74* (3), 308-17.

28. Munge, B. S.; Krause, C. E.; Malhotra, R.; Patel, V.; Gutkind, J. S.; Rusling, J. F., Electrochemical Immunosensors for Interleukin-6. Comparison of Carbon Nanotube Forest and Gold Nanoparticle platforms. *Electrochem commun* **2009,** *11* (5), 1009-1012.

29. Liu, H.; Malhotra, R.; Peczuh, M. W.; Rusling, J. F., Electrochemical immunosensors for antibodies to peanut allergen ara h2 using gold nanoparticle-peptide films. *Anal Chem* **2010,** *82* (13), 5865-71.

30. Piro, B.; Reisberg, S., Recent Advances in Electrochemical Immunosensors. *Sensors (Basel)* **2017,** *17* (4).

31. Hees, J.; Heidrich, N.; Pletschen, W.; Sah, R. E.; Wolfer, M.; Williams, O. A.; Lebedev, V.; Nebel, C. E.; Ambacher, O., Piezoelectric actuated micro-resonators based on the growth of diamond on aluminum nitride thin films. *Nanotechnology* **2013,** *24* (2), 025601.

32. Wiseman, M. E.; Frank, C. W., Antibody adsorption and orientation on hydrophobic surfaces. *Langmuir* **2012,** *28* (3), 1765-74.

33. Xu, H.; Zhao, X.; Grant, C.; Lu, J. R.; Williams, D. E.; Penfold, J., Orientation of a monoclonal antibody adsorbed at the solid/solution interface: a combined study using atomic force microscopy and neutron reflectivity. *Langmuir* **2006,** *22* (14), 6313-20.

34. Zourob, M., *Recognition receptors in biosensors*. Springer: New York ; London, 2010; p xvi, 863 p.

35. Ligler, F. S.; Taitt, C. A. R., *Optical biosensors : present and future*. 1st ed.; Elsevier: Amsterdam ; New York, 2002; p viii, 607 p.

36. Yang, V. C.-M.; Ngo, T. T., *Biosensors and their applications*. Kluwer Academic/Plenum Publishers: New York, 2000; p xviii, 360 p.

37. Rasooly, A.; Herold, K. E., *Biosensors and biodetection : methods and protocols*. Humana Press: New York, NY, 2009.

38. Hermanson, G. T., *Bioconjugate techniques*. Third edition. ed.; Elsevier/AP: London ; Waltham, MA, 2013; p xvii, 1146 pages.

39. Watson, R. R.; Preedy, V. R., *Genetically modified organisms in food : production, safety, regulation and public health*. Elsevier Science/Academic Press: Amsterdam ; Boston, 2016; p xxi, 494 p.

40. Choe, W.; Durgannavar, T. A.; Chung, S. J., Fc-Binding Ligands of Immunoglobulin G: An Overview of High Affinity Proteins and Peptides. *Materials (Basel)* **2016,** *9* (12).

41. Spicer, C. D.; Davis, B. G., Selective chemical protein modification. *Nat Commun* **2014,** *5*, 4740.

42. Howard, G. C.; Bethell, D. R., *Basic methods in antibody production and characterization*. CRC Press: Boca Raton, 2001; p 271 p.

43. Lee, M. T. W.; Maruani, A.; Richards, D. A.; Baker, J. R.; Caddick, S.; Chudasama, V., Enabling the controlled assembly of antibody conjugates with a loading of two modules without antibody engineering. *Chem Sci* **2017,** *8* (3), 2056-2060.

44. Kang, J. H.; Choi, H. J.; Hwang, S. Y.; Han, S. H.; Jeon, J. Y.; Lee, E. K., Improving immunobinding using oriented immobilization of an oxidized antibody. *Journal of Chromatography A* **2007,** *1161* (1), 9-14.

45. Makaraviciute, A.; Ramanaviciene, A., Site-directed antibody immobilization techniques for immunosensors. *Biosens Bioelectron* **2013,** *50*, 460-71.

46. Alves, N. J.; Champion, M. M.; Stefanick, J. F.; Handlogten, M. W.; Moustakas, D. T.; Shi, Y.; Shaw, B. F.; Navari, R. M.; Kiziltepe, T.; Bilgicer, B., Selective photocrosslinking of functional ligands to antibodies via the conserved nucleotide binding site. *Biomaterials* **2013,** *34* (22), 5700-10.

47. Boozer, C.; Ladd, J.; Chen, S.; Yu, Q.; Homola, J.; Jiang, S., DNA directed protein immobilization on mixed ssDNA/oligo(ethylene glycol) self-assembled monolayers for sensitive biosensors. *Anal Chem* **2004,** *76* (23), 6967-72.

48. Trilling, A. K.; Harmsen, M. M.; Ruigrok, V. J.; Zuilhof, H.; Beekwilder, J., The effect of uniform capture molecule orientation on biosensor sensitivity: dependence on analyte properties. *Biosensors & bioelectronics* **2013,** *40* (1), 219-26.

49. Rush, J. S.; Bertozzi, C. R., New aldehyde tag sequences identified by screening formylglycine generating enzymes in vitro and in vivo. *J Am Chem Soc* **2008,** *130* (37), 12240-1.

50. Chen, G. Y.; Li, Z.; Theile, C. S.; Bardhan, N. M.; Kumar, P. V.; Duarte, J. N.; Maruyama, T.; Rashidfarrokh, A.; Belcher, A. M.; Ploegh, H. L., Graphene Oxide Nanosheets Modified with Single-Domain Antibodies for Rapid and Efficient Capture of Cells. *Chemistry* **2015,** *21* (48), 17178-83.

51. Chen, G. Y.; Li, Z.; Duarte, J. N.; Esteban, A.; Cheloha, R. W.; Theile, C. S.; Fink, G. R.; Ploegh, H. L., Rapid capture and labeling of cells on single domain antibodies-functionalized flow cell. *Biosens Bioelectron* **2017,** *89* (Pt 2), 789-794.

52. Shen, Z.; Yan, H.; Zhang, Y.; Mernaugh, R. L.; Zeng, X., Engineering peptide linkers for scFv immunosensors. *Anal Chem* **2008,** *80* (6), 1910-7.

53. Shen, Z.; Mernaugh, R. L.; Yan, H.; Yu, L.; Zhang, Y.; Zeng, X., Engineered recombinant single-chain fragment variable antibody for immunosensors. *Anal Chem* **2005,** *77* (21), 6834-42.

54. Falco, C. N.; Dykstra, K. M.; Yates, B. P.; Berget, P. B., scFv-based fluorogen activating proteins and variable domain inhibitors as fluorescent biosensor platforms. *Biotechnol J* **2009,** *4* (9), 1328-36.

55. Fung-Ling Ng, K.-C. L., Chen-Yu Chang, Chih-Hsuan Hsu, Tsung-Yu Ho, Ming-Hsiu Hsieh, Ting-Han Kuo, Yu-Yun Wang, Ru-Huah Lin, Wei-Hung Hsu, Yu-Ting Lin, Ya-Chih Tai, Rui-Xing Wang, Nai-Chen Chi, Yu-An Chen, Yang-Chen Lin, Tzu-Yin Wei, Jing-Chin Lin, Hsiao-Ching Lee, Wen-Liang Chen, E.Cotector: The Fluorescent E. coli with Surface Displayed Anti-Cancer Marker scFv to Detect Specific Cancer Markers *PLOS Collections* **2016**.

56. Deyev, S.; Proshkina, G.; Ryabova, A.; Tavanti, F.; Menziani, M. C.; Eidelshtein, G.; Avishai, G.; Kotlyar, A., Synthesis, Characterization, and Selective Delivery of DARPin-Gold Nanoparticle Conjugates to Cancer Cells. *Bioconjug Chem* **2017,** *28* (10), 2569-2574.

57. Jost, C.; Pluckthun, A., Engineered proteins with desired specificity: DARPins, other alternative scaffolds and bispecific IgGs. *Curr Opin Struct Biol* **2014,** *27*, 102-12.

58. Na, W.; Liu, X.; Wang, L.; Su, X., Label-free aptamer biosensor for selective detection of thrombin. *Anal Chim Acta* **2015,** *899*, 85-90.

59. Eissa, S.; Zourob, M., Aptamer- Based Label-Free Electrochemical Biosensor Array for the Detection of Total and Glycated Hemoglobin in Human Whole Blood. *Sci Rep* **2017,** *7* (1), 1016.

60. Farokhzad, O. C.; Karp, J. M.; Langer, R., Nanoparticle-aptamer bioconjugates for cancer targeting. *Expert Opin Drug Deliv* **2006,** *3* (3), 311-24.

61. York, D.; Baker, J.; Holder, P. G.; Jones, L. C.; Drake, P. M.; Barfield, R. M.; Bleck, G. T.; Rabuka, D., Generating aldehyde-tagged antibodies with high titers and high formylglycine yields by supplementing culture media with copper(II). *BMC Biotechnol* **2016,** *16*, 23.

62. De Meyer, T.; Muyldermans, S.; Depicker, A., Nanobody-based products as research and diagnostic tools. *Trends in biotechnology* **2014,** *32* (5), 263-70.

63. Bardhan, N. M.; Kumar, P. V.; Li, Z.; Ploegh, H. L.; Grossman, J. C.; Belcher, A. M.; Chen, G. Y., Enhanced Cell Capture on Functionalized Graphene Oxide Nanosheets through Oxygen Clustering. *ACS nano* **2017,** *11* (2), 1548-1558.

64. Fang, T.; Duarte, J. N.; Ling, J.; Li, Z.; Guzman, J. S.; Ploegh, H. L., Structurally Defined alphaMHC-II Nanobody-Drug Conjugates: A Therapeutic and Imaging System for B-Cell Lymphoma. *Angew Chem Int Ed Engl* **2016,** *55* (7), 2416-20.

65. Li, Z.; Theile, C. S.; Chen, G. Y.; Bilate, A. M.; Duarte, J. N.; Avalos, A. M.; Fang, T.; Barberena, R.; Sato, S.; Ploegh, H. L., Fluorophore-Conjugated Holliday Junctions for Generating Super-Bright Antibodies and Antibody Fragments. *Angew Chem Int Ed Engl* **2015,** *54* (40), 11706-10.

2.2 Graphene Oxide Nanosheets Modified with Single Domain Antibodies for Rapid and Efficient Capture of Cells

2.2.1 Introduction

Peripheral blood can provide valuable information on an individual's immune status. Cell-based assays typically target leukocytes and their products. Characterization of leukocytes from whole blood requires their separation from the far more numerous red blood cells.[1] Current methods to classify leukocytes, such as recovery on antibody-coated beads or fluorescence-activated cell sorting require long sample preparation times and relatively large sample volumes.[2] A simple method that enables the characterization of cells from a small peripheral whole blood sample could overcome limitations of current analytical techniques. We describe the development of a simple graphene oxide surface coated with single domain antibody fragments. This format allows quick and efficient capture of distinct WBC subpopulations from small samples (~30 μL) of whole blood in a geometry that does not require any specialized equipment such as cell sorters or microfluidic devices.

2.2.2 Result

Graphene oxide (GO) is a derivative of graphene, which can be modified for various applications, including bioassays,[3] bioimaging[4] and biosensors to select for different cell types.[5] The biocompatibility of GO offers many features attractive for optical biosensing platforms, such as a large surface area, good water dispersibility, and ease of facial surface modification. Full-sized antibodies can be attached to GO to create biosensors for the capture of circulating tumor

cells from blood samples and for virus detection.[6] However, the full-sized antibody-GO platform has several drawbacks that prevent it from being used for high throughput screening. Full-sized antibodies are costly and not always easy to produce. Construction of the circulating tumor cell-antibody-GO biosensor requires special equipment to produce the necessary GO-gold surface.[5] Furthermore, antibodies are usually coupled to the GO surface via NHS ester or maleimide chemistries, which target free lysine or cysteine residues respectively, with possible loss of activity.[6-7] The use of NHS-lysine and maleimide-cysteine coupling complicates further functionalization of the antibody. For example, free lysine and cysteines not involved in covalent attachment to the GO surface could be functionalized with dyes, but attaining quantitative and homogeneous labeling is impossible. Attaching antibodies through biotin-streptavidin/NeutrAvidin interactions introduces additional complexity and usually relies on biotinylation strategies that again involve lysine or cysteine modifications.[5, 8]

We address these limitations by attaching single domain antigen-binding fragments derived from camelid heavy-chain-only antibodies, known as VHHs or nanobodies,[9] directly to the GO surface in a site-specific manner using sortase. VHHs are small (~15 KDa) and are easily expressed in bacteria; they are monomeric and have an excellent thermo-chemical stability profile, all of which make them suitable for diagnostic and therapeutic applications.[10] A sizable portion of the VHH surface is involved in binding interactions, and therefore site-specific modifications of a VHH at a position distal form the antigen binding site is essential to obtain a properly oriented coating, a prerequisite to build an efficient biosensor.[7,11] We used a sortase-mediated transpeptidation reaction in combination with 'click' chemistry to site-specifically attach a fluorescently labeled VHH to PEG linker-modified GO.[11-13] We thus installed an anti-murine Class II MHC VHH (VHH7)[14] and an anti-murine CD11b VHH (VHH DC13), both sortase-labeled with a TAMRA fluorophore, to GO nanosheets. The combination of these functionalized surfaces allowed us to selectively capture Class II MHC-positive (MHC^+) and CD11b-positive ($CD11b^+$)

cells from small volumes (~30 μl) of peripheral blood (**Figure 2.2.1**) with minimal handling in a device of simple geometry.

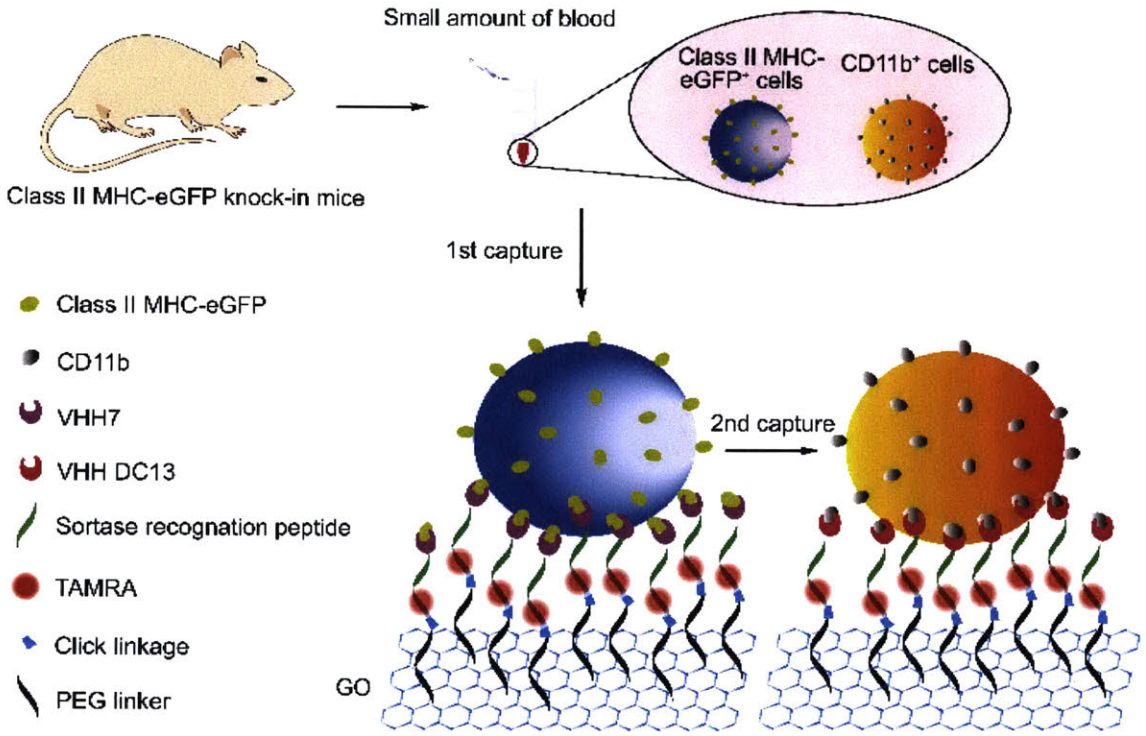

Figure 2.2.1. Schematic illustration of VHH7 and VHH DC13-based GO substrates for capture of Class II MHC-eGFP$^+$ and CD11b$^+$ cells from whole blood.

GO nanosheets (<2 nm thickness, 500 nm mean diameter) functionalized with carboxylic acids were dispersed in deionized water. For the preparation of nanosubstrates, GO was immobilized on a 3-aminopropyltriethoxysilane (APTES)- functionized glass slide by means of electrostatic forces between the oxide groups of GO and the amine-end of 3-APTES.[15] Scanning electron microscopy (SEM) images of GO nanosheets immobilized on a silicon substrate showed even and dense coverage of thin sheets on the surface, with spacing between adjacent sheets < 2 μm (**Figure 2.2.2**). The GO nanosheets were covalently functionalized with diamino-

functionalized polyethylene glycol (NH_2-$(PEG)_n$-NH_2) (**Figure 2.2.3**). The presence of epoxide, hydroxyl, carbonyl, carboxyl and amine groups was confirmed by X-ray photoelectron spectroscopy (XPS) (**Figure 2.2.4**). Dibenzocyclooctyne-N-hydroxysuccinimidyl ester (DBCO-NHS) was then reacted with the terminal amines of the PEG chains to install a 'click' chemistry handle onto the GO surface (**Figure 2.2.3**).

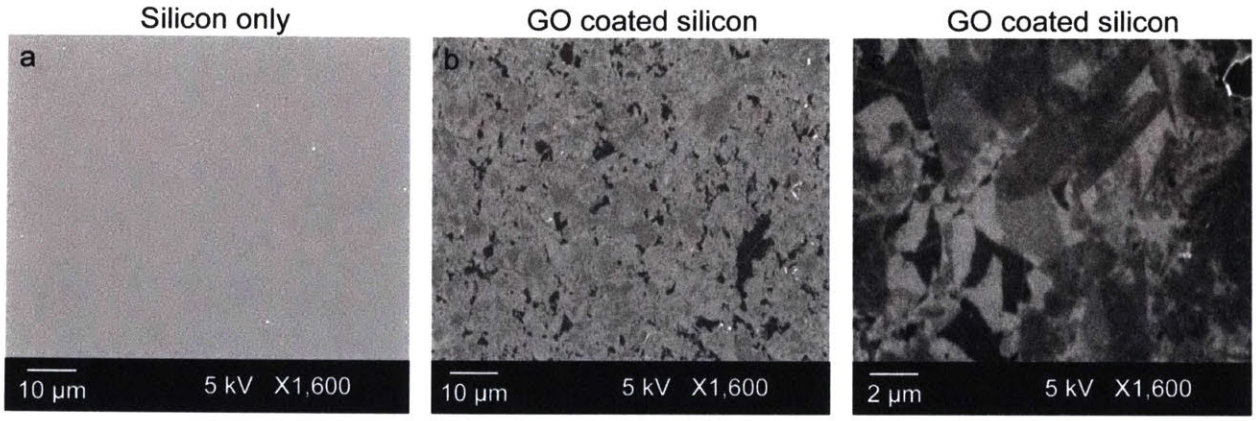

Figure 2.2.2 SEM images of GO immobilized on the substrate. (A) Silicon wafer (SiO_2 layer), (B, C) GO on the silicon substrate. Dense coverage of GO on the substrate is revealed in (B). The thin sheet morphology of GO is clearly observed in (C).

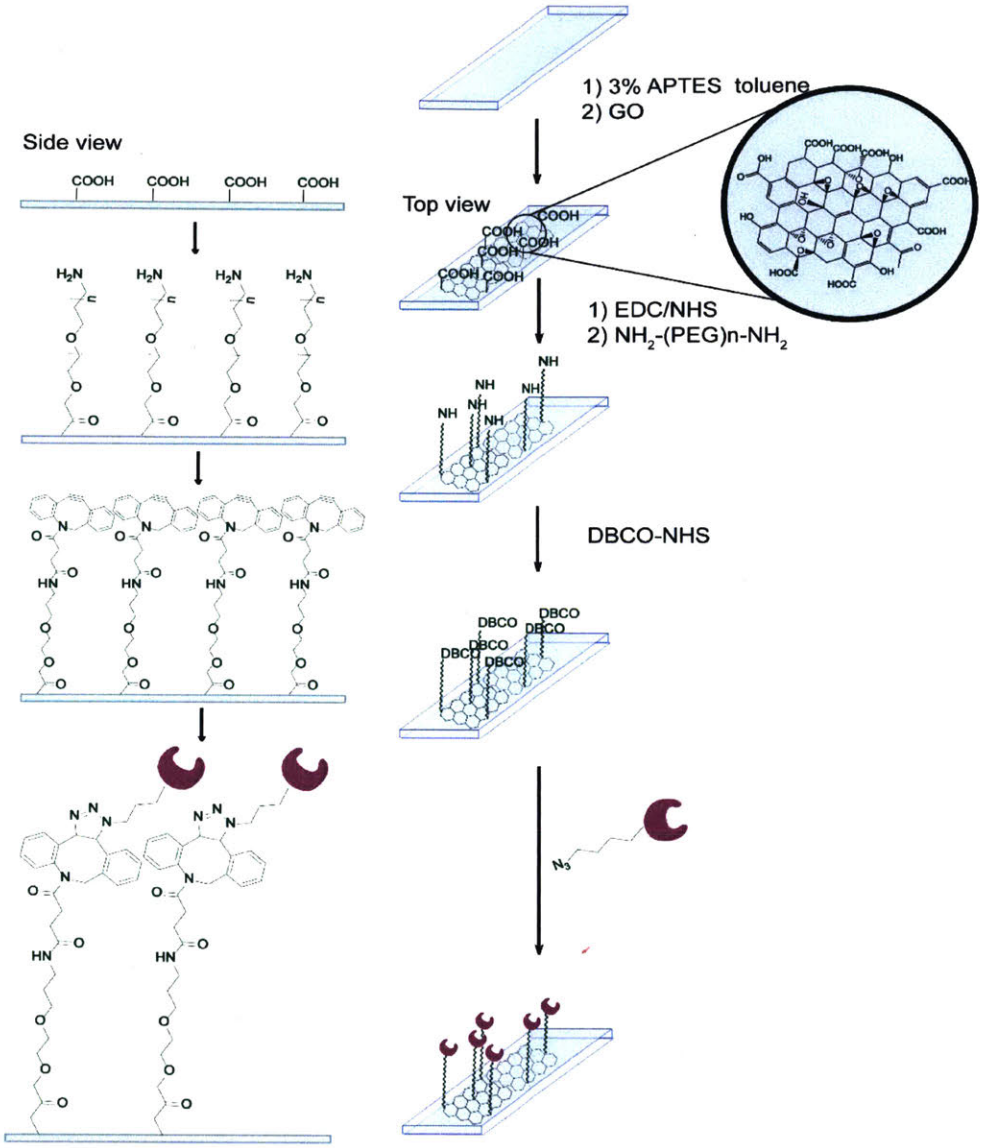

Figure 2.2.3 Glass slides are coated with 3% (3-aminopropyl)triethoxysilane (APTES) in toluene for 30 minutes and washed with toluene, ethanol, and then water. Following washes, slides are immersed in a GO (1 mg/ml) suspension for 1 hour. The carboxylic group on GO is then activated with N-hydroxysuccinimide (NHS) in a reaction catalyzed by 1-Ethyl-3-(3-dimethylaminopropyl)carbodiimide hydrochloride (EDC). A diamino-polyethylane glycol polyethylene glycol (PEG) linker is introduced with one end reacting with the N-hydroxysuccinimide (NHS) moiety. The other end of the PEG linker is further functionalized with an NHS-activated dibenzocycolctyne (DBCO). The protein, which has been labeled with an azide in a sortase-catalyzed reaction, is then "clicked" onto the DBCO in a strain-promoted cycloaddition.

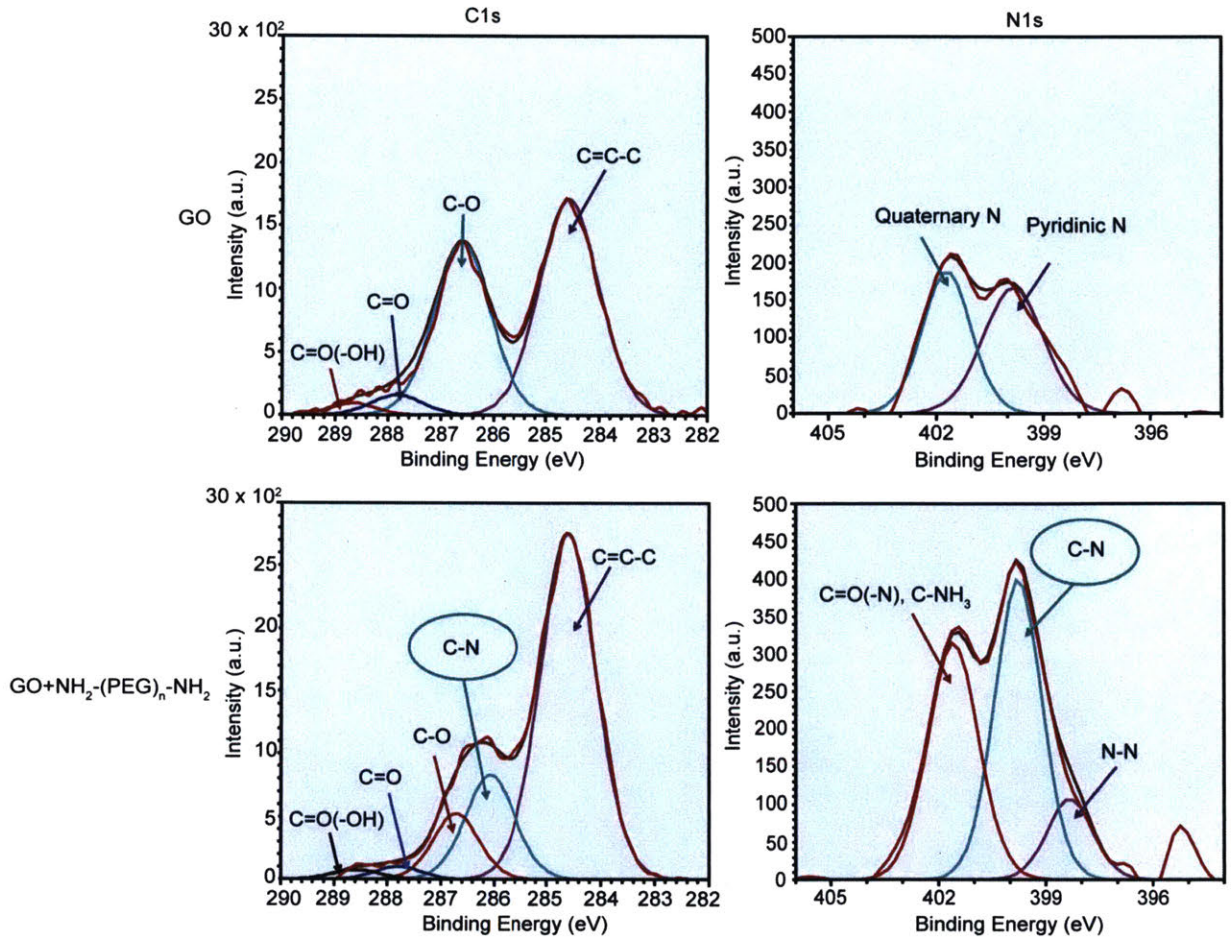

Figure 2.2.4 The C1s and N1s XPS spectra of amine-functionalized immobilized GO. The deconvolution spectrum in the C1s region of GO showed four different peaks centered at 284.6 eV, 286.7 eV, 287.8 eV and 288.7 eV, which corresponded to C=C-C, C-O, C=O and C=O(-OH), respectively. From the N1s XPS spectra, only a small amount of N was found in GO, corresponding to pyridinic and quaternary nitrogen. In the case of amine-functionalized GO, in addition to the aromatic C=C-C peak at 284.6 eV, C-N peak at 286.3 eV was detected in the C1s spectrum. The C-N peak at 399.5 eV was also found in the N1s spectrum. These results show that C-N peaks develop upon covalent bonding of the linker (NH_2) with GO according to an epoxide ring opening reaction, thus confirming that NH_2-(PEG)n-NH_2 was indeed immobilized onto the GO surface, consistent with previous experiments[2].

To assess the potential of GO-immobilized VHH for cell capture, we first engineered a sortase-ready version of VHH7 with an LPETG motif near the C-terminus.[14] Using standard sortagging protocols[14] we introduced a Gly_3 peptide equipped with a TAMRA fluorophore and an azide, to partner with the DBCO moiety during the 'click' reaction. We included the TAMRA fluorophore to create fluorescence microscopy overlays between the VHH-GO surface and a fluorescently stained cell (**Figure 2.2.5**). Thus modified VHH7 was covalently coupled in a uniform orientation onto a GO nanosheet upon reaction of the DBCO and azide groups in a cycloaddition (**Figure 2.2.6A**). Atomic force microscopy (AFM) images showed that the VHH7-immobilized GO nanosheets exhibited a clear difference in height profile with a vertical size ranging from 20 to 80 nm (**Figure 2.2.6B**), attributable to immobilization of VHH7 on the nanosheets.

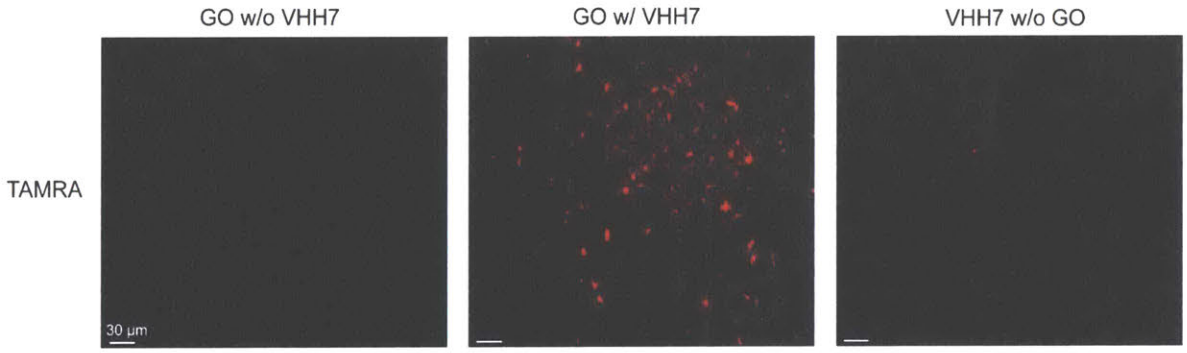

Figure 2.2.5 Confocal microscopy images of the glass slide with (middle) or without VHH7 immobilization (left), or the GO uncoated glass slide with VHH7 immobilization (right). VHH7 modified with both a TAMRA moiety and an azide was grafted onto the GO coated or uncoated substrate. The TAMRA signal (middle) indicates that VHH7 was successfully immobilized on the GO substrate.

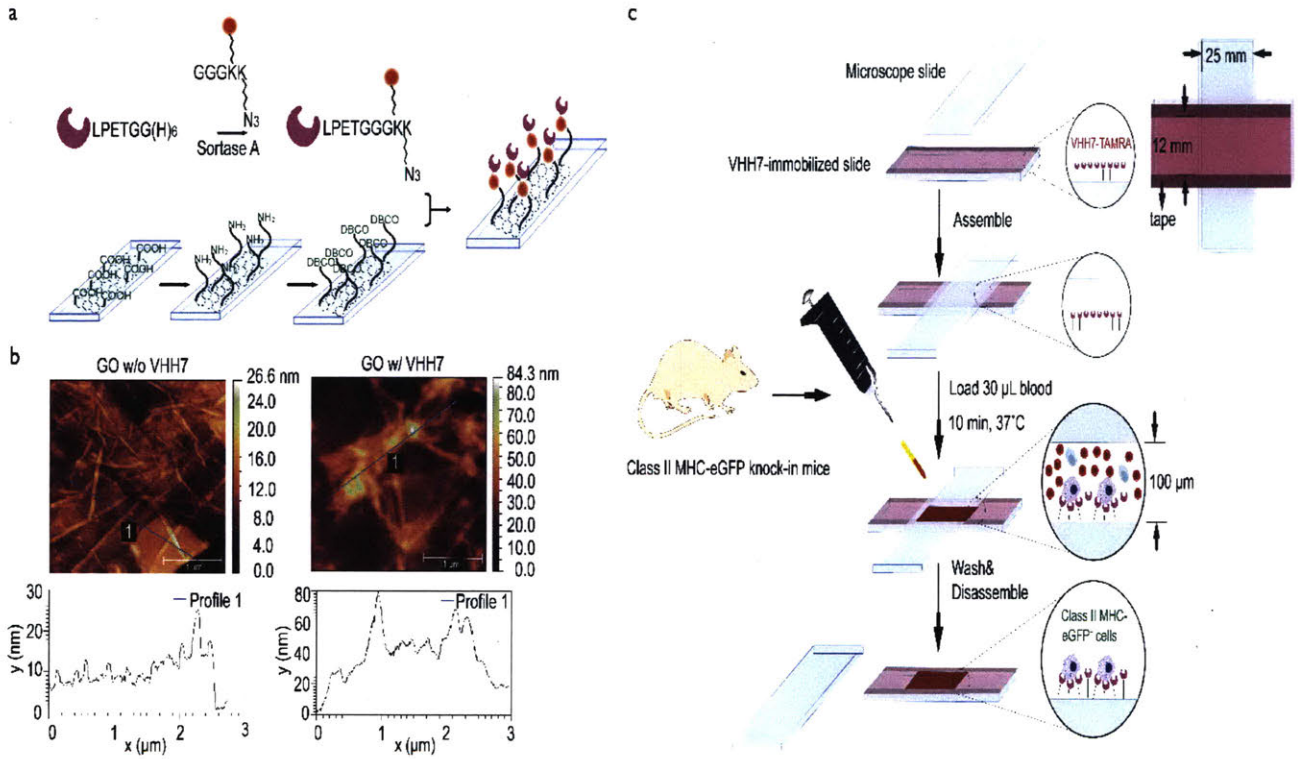

Figure 2.2.6 Uniform attachment and characterization of a murine Class II MHC-specific targeting nanobody, VHH7, on GO nanosheets. (A) Overview of sortase-mediated site-specific ligation of VHH7 onto GO nanosheets. VHH7 was C-terminally modified via a sortase-mediated ligation to install a TAMRA fluorophore and an azide. The GO nanosheet was functionalized with a DBCO handle for a "click" reaction with the azide-modified VHH7. (B) AFM images of GO nanosheets and GO nanosheets with VHH7 immobilized on silicon substrates. The height difference between GO nanosheets with or without VHH7 immobilization was ~20-80 nm. The topography of the slide observed under the AFM is characteristic of protein bound to GO.[6] (C) Whole blood analysis from Class II MHC-eGFP knock-in mice. A small volume of blood (30 μL) was loaded into the assembled chamber and incubated at 37˚C for 10 min. The chamber was then disassembled and the cell-bearing substrate slide was gently washed 3x with PBS. After washing, cells were analyzed by fluorescence microscopy and quantitative image analysis.

The VHH7-GO functionalized slide was assembled with a second glass slide to form a cell capture chamber. Two strips of double-sided tape served as spacers to yield a chamber of approximately 12 mm × 25 mm x ~0.1 mm for a total volume of ~30 µl. The VHH is thus directly attached to one of the surfaces of the capture chamber. Assembly of this device requires no more than two-sided tape and a second, unmodified glass slide (**Figure 2.2.6C**). Delivery of ~30 µl of whole blood or a cell suspension is then achieved by contacting the opening of the chamber with the tip of a mechanical pipetting device. Within seconds, discharge of the intended volume then fills the chamber by capillary action. Wash steps are conducted in similar fashion by delivery of buffer to one open side of the chamber, and wicking off buffer at the opposite end of the chamber, using filter paper to ensure flow across the chamber surfaces.

To verify the specificity of GO-immobilized VHH7 for murine Class II MHC$^+$ cells, mouse B lymphoma (A20) and human B lymphoma (Raji, murine Class II MHC-negative) cell lines were labeled with a fluorescent cell tracker dye, diluted in PBS and loaded into the VHH-GO device for 10 min at 37°C. Different cell densities were applied to optimize loading conditions (**Figure 2.2.7A, B**). When ~2.2x10^4 A20 cells were seeded, ~83% of the cells were captured. As the number of loaded cells increased to 6-7x10^4, approximately half of the cells were retained. There was little difference in the total number of cells retained when the number of cells loaded was increased to ~20x10^4, as just ~4.3x10^4 were captured. For A20 cells, the functionalized nanosubstrate showed a capture yield of A20 cells of ~80 % for ~2.2×10^4 loaded cells, compared to ~17 % for an unmodified GO surface (**Figure 2.2.7C**). Human Raji cells showed no significant difference in binding to the VHH7-functionalized (~21%) and the unmodified GO surface (~15%), demonstrating the specificity of VHH7 for its target (**Figure 2.2.7D**). GO nanosheets modified with VHH7 thus efficiently captured murine Class II MHC$^+$ cells (**Figure 2.2.7E** and **Figure 2.2.8**).

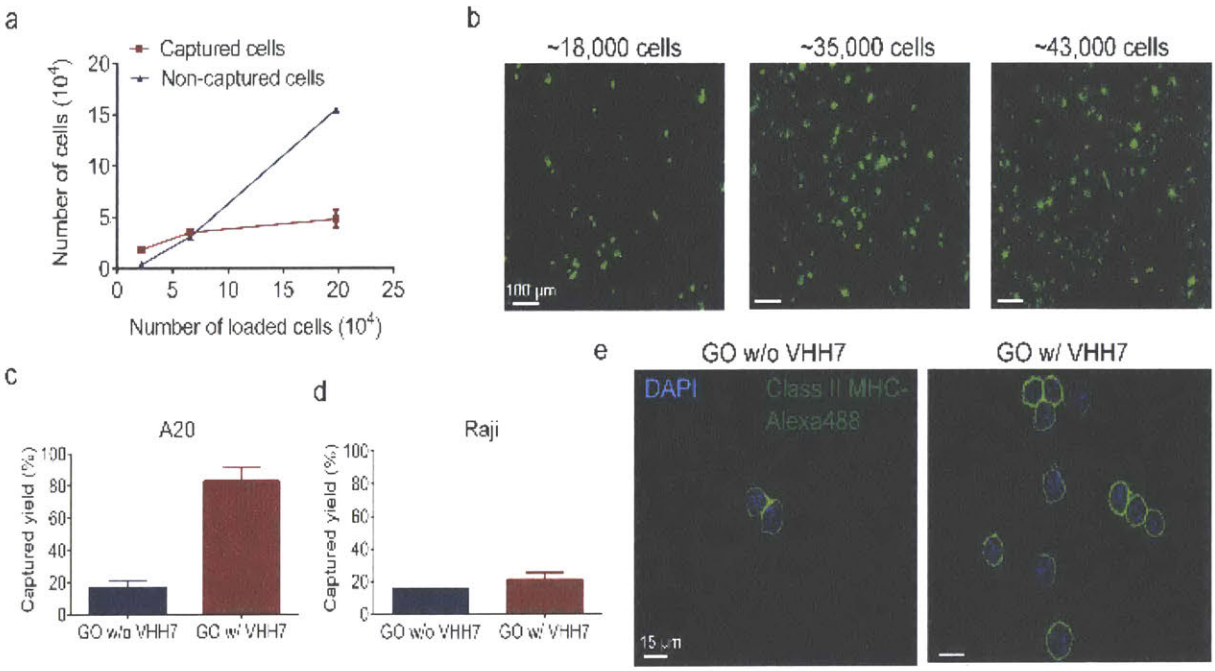

Figure 2.2.7 Quantification and characterization of captured cells. (A) Quantification of bound cells at different cell loading numbers. (B) Microscopic observation of bound Class II MHC$^+$ cells. (C) Quantification of captured A20 cells (murine Class II MHC$^+$) on substrates with and without VHH7 immobilization. (D) Capture of Raji cells (murine Class II MHC-negative). (E) Immunofluorescence images of captured A20 cells stained with Alexa488-labeled anti-Class II MHC and DAPI.

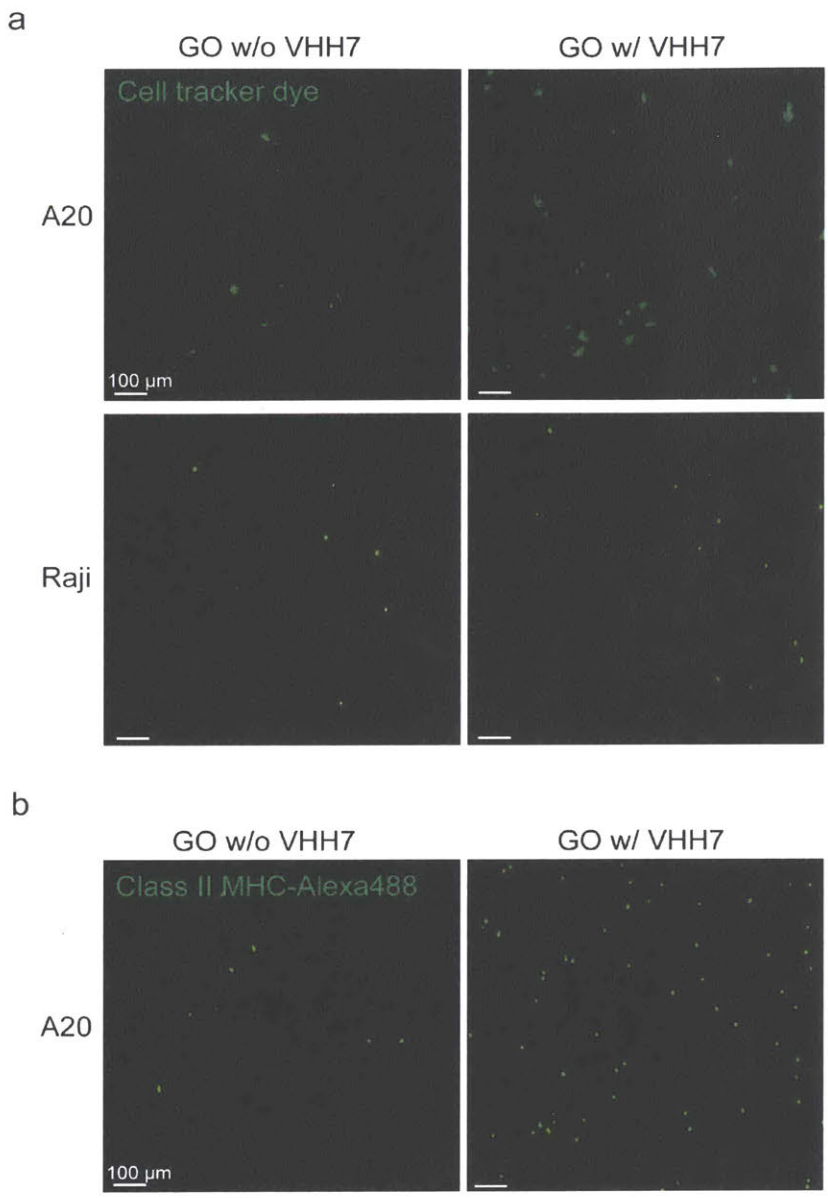

Figure 2.2.8 Fluorescence microscopy of captured cells. (A) A20 and Raji cells were labeled with a fluorescent cell tracker dye, followed by cell capture and image analysis as described in Figure 3. (B) A20 cells without cell tracker labeling were captured on the VHH7-GO substrate and stained with Alexa488-labeled anti-Class II MHC (10 x magnification).

We next tested performance of the VHH7-modified nanosubstrate on whole blood. Fresh blood was obtained from Class II MHC-eGFP knock-in mice for ready visualization of Class II MHC$^+$ cells by their GFP fluorescence (**Figure 2.2.9**). Analysis of Class II MHC-eGFP$^+$ cells showed an average capture efficiency of ~74 % (n=5) on the VHH7-functionalized nanosubstrate (~11,000 cells). Conversely, without VHH7, only ~14 % of eGFP$^+$ cells (~2,000 cells) were retained (**Figure 2.2.10A, B** and **Table 2.2.1**), in agreement with what was observed with the A20 cell line. A similarly low capture yield (~11%) was seen when using an irrelevant VHH for immobilization (**Figure 2.2.11**). We saw co-localization of the Class II MHC-eGFP signal with the VHH7-TAMRA signal (**Figure 2.2.10C, D**). When we counterstained VHH7-immobilized cells with Alexa647-labeled VHH7 and DAPI, we observed excellent colocalization of Alexa647-labeled VHH7 with Class II MHC-eGFP, showing that GO-VHH7 immobilized cells remained available for further staining *in situ* (**Figure 2.2.10E**), with only minimal consumption of labeled antibody owing to the small volume of the chamber (~30 µL). Most eGFP$^+$ captured cells ranged from 10-15 µm in diameter, the size of B cells (**Figure 2.2.10C**). The identity of this population was further confirmed with Alexa647-labeled anti-IgG antibody for surface staining of B cell receptors (BCRs) (**Figure 2.2.12**). B cells captured from OB-1-Class II MHC eGFP mice, which possess a BCR specific for ovalbumin[16] and its fragments retained the ability to bind and internalize an Alexa647-labeled ovalbumin fragment, the FGD-17mer peptide,[16-17] which ultimately co-localized with Class II-MHC-eGFP$^+$ compartments (**Figure 2.2.13**).

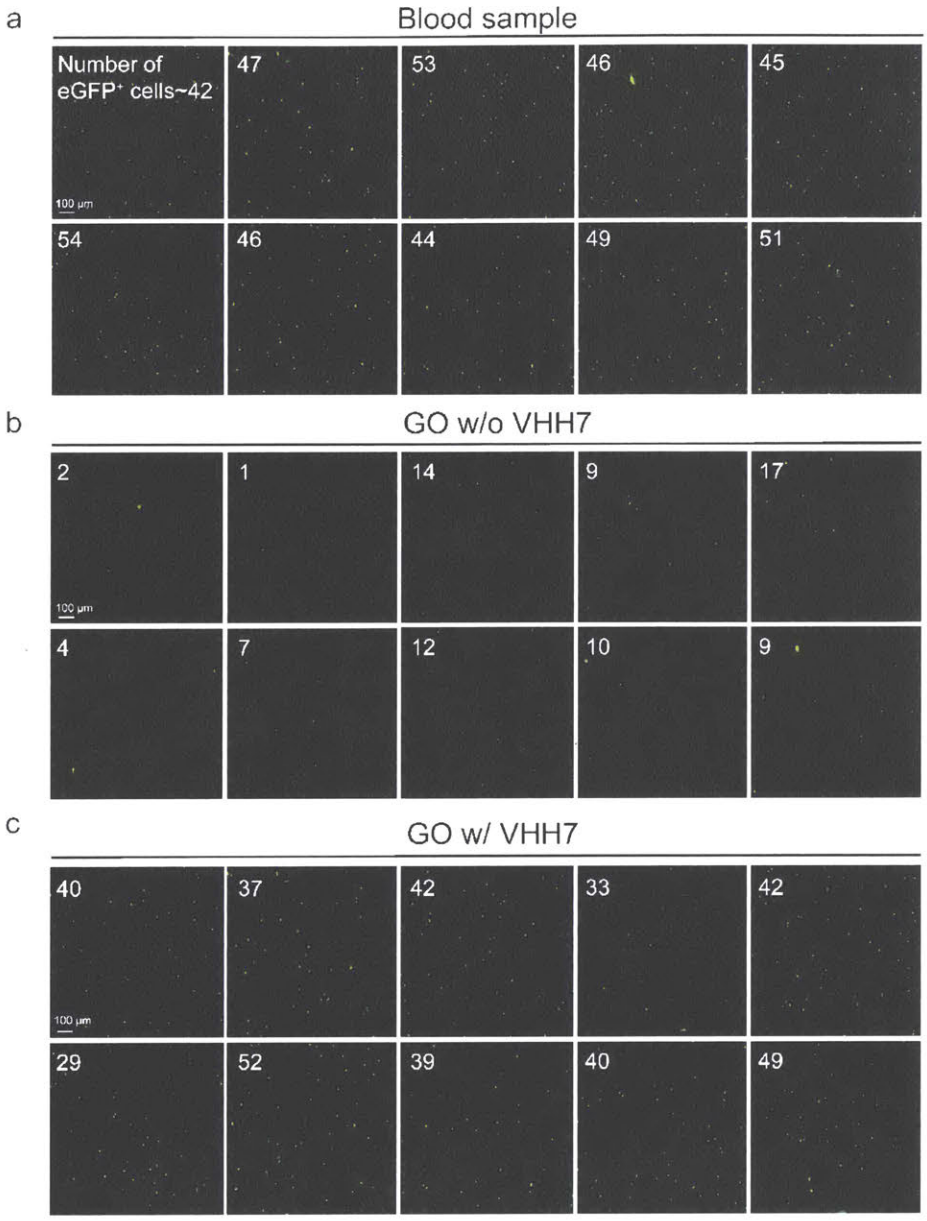

Figure 2.2.9 Fluorescence microscopy of captured MHC II-eGFP+ cells from whole blood. (A) Total Class II MHC-eGFP$^+$ cells in 30 µL of blood. Cells captured on the GO substrate (B) without VHH7 immobilization or (C) with VHH7 immobilization. Ten representative fields of vision for each individual substrate were examined to enumerate the total number of Class II MHC-eGFP$^+$ cells (**Table 2.2.1**).

	Sample number	Total number of Class II MHC-eGFP$^+$ cells in sample	Number of captured Class II MHC-eGFP$^+$ cells	Captured yield
GO w/o VHH7	blood1	14,310	2,550	17.8%
	blood2	15,090	2,130	14.1%
	blood3	13,080	1,620	12.4%
	blood4	15,420	2,100	13.6%
	blood5	15,570	1,770	11.4%
	Average captured yield			13.9±2.5%
GO w/ VHH7	blood1	14,310	12,120	84.7 %
	blood2	15,090	10,740	71.2 %
	blood3	13,080	9,900	75.7 %
	blood4	15,420	9,690	62.8 %
	blood5	15,570	11,400	73.2 %
	Average captured yield			73.5±7.9%

Table 2.2.1 Quantitation of captured Class II MHC-eGFP+ cells from different blood samples.

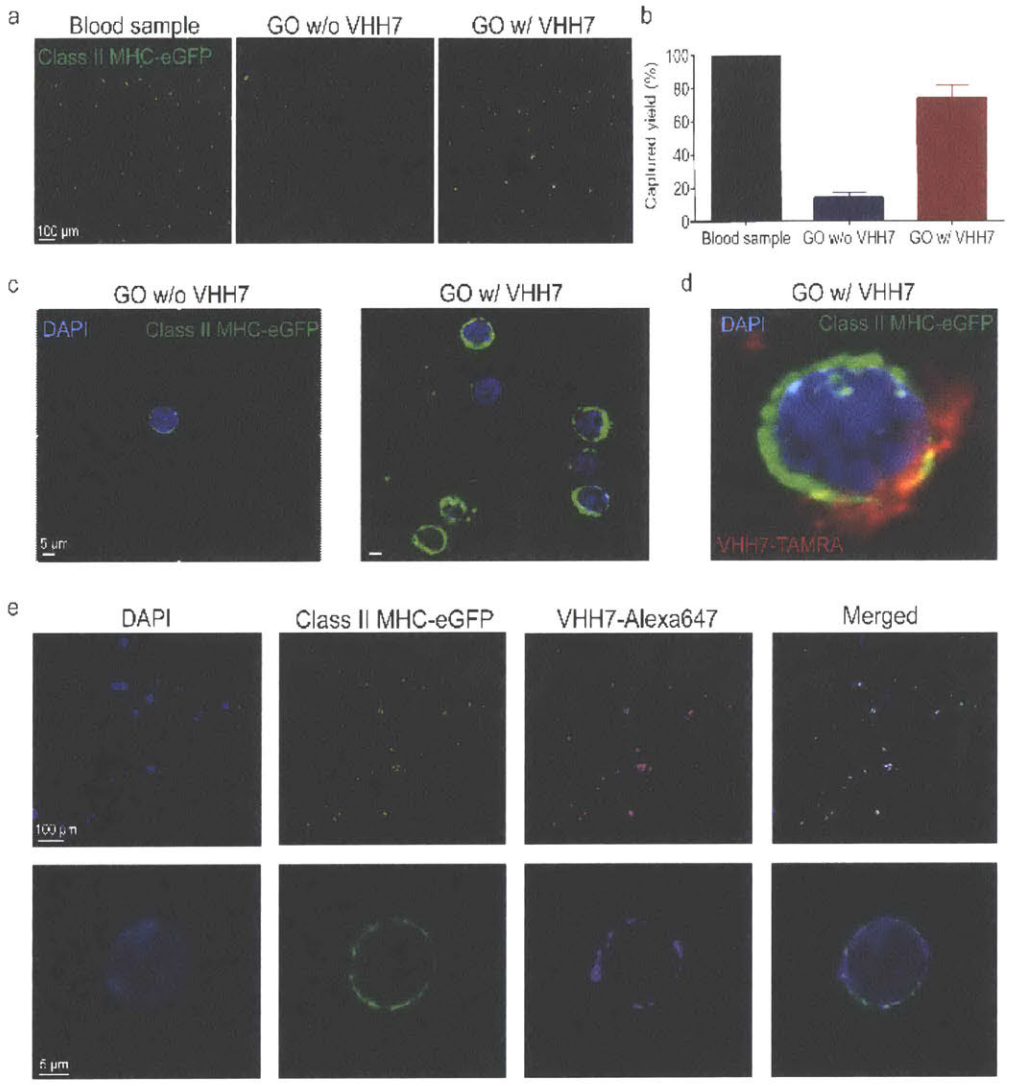

Figure 2.2.10 Quantification and characterization of Class II MHC-eGFP+ cells from 30 µl of whole blood. (A) Fluorescence microscopy of cells captured on VHH7-modified and unmodified GO substrates. (B) Quantification of captured cells. (C) Confocal microscopy of captured cells. (D) Higher magnification of a captured cell, showing colocalization of the Class II MHC-eGFP signal with VHH7-TAMRA. (E) Confocal microscopy images of VHH7-captured cells after staining with Alexa647-labeled VHH7.

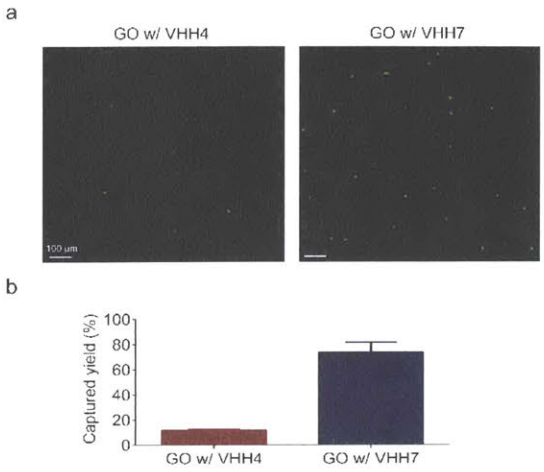

Figure 2.2.11. VHH7-modified nanosubstrates allow capture of Class II MHC-eGFP+ cells from whole blood. (A) Fluorescence microscopy of MHC II-GFP+ cells captured on anti-human Class II MHC VHH4- or VHH7-immobilized GO substrates. (B) Quantification of captured Class II MHC-eGFP+ cells.

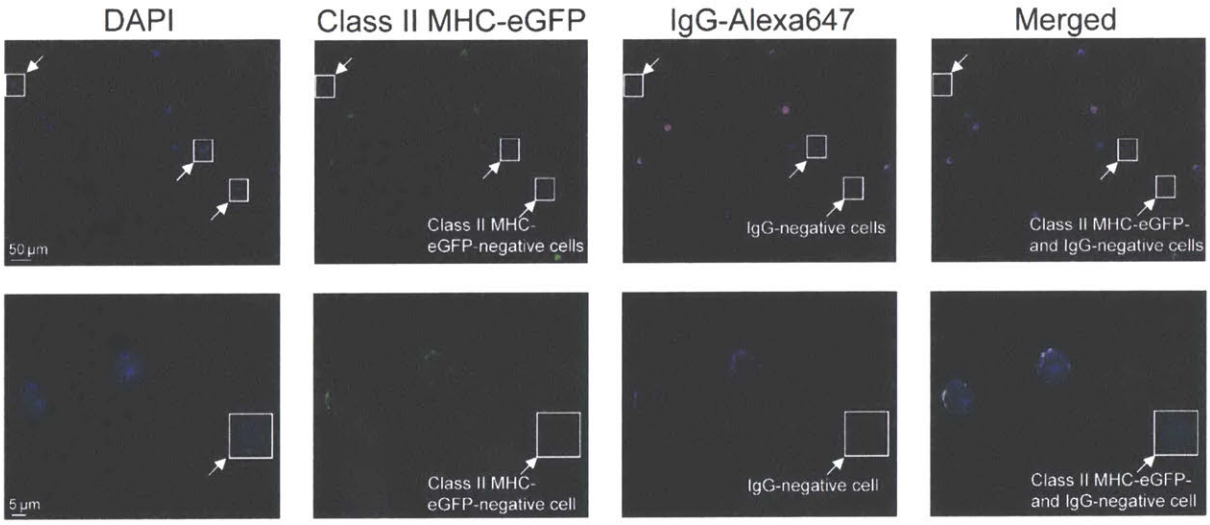

Figure 2.2.12. Characterization of captured Class II MHC-eGFP+ cells. Captured cells were stained with DAPI and Alexa647-labeled anti-IgG. Captured Class II MHC-eGFP+ cells can be stained with anti-IgG antibody and thus identifies them as B cells. Arrows indicate the Class II MHC-eGFP- and IgG-negative cells.

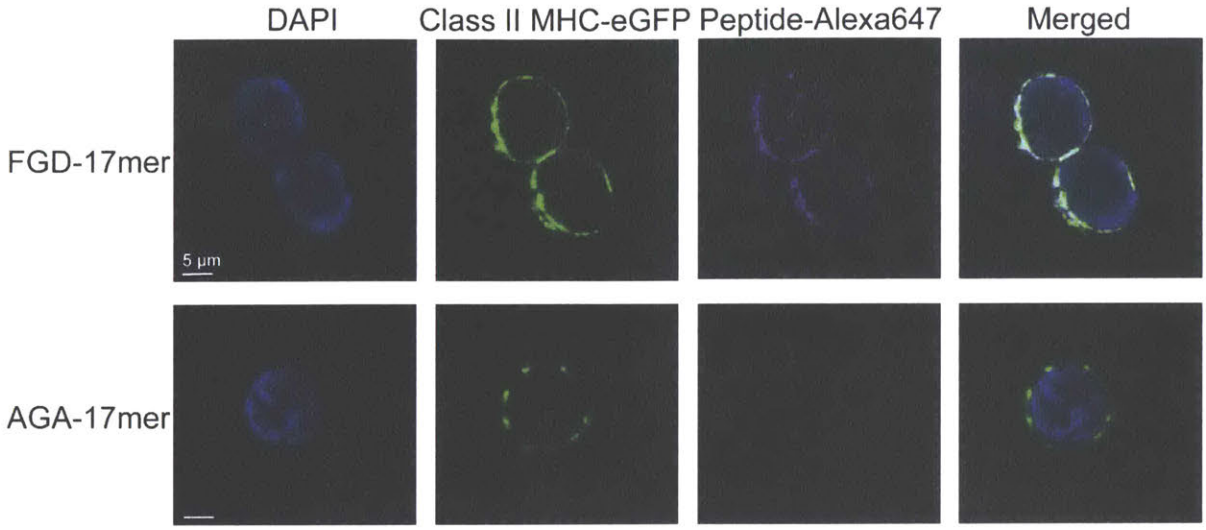

Figure 2.2.13. Captured cells retain endocytic capability. Cells from OB1/Class II MHC-eGFP+ knock-in mice were captured, followed by incubation with Alexa647-labeled FGD-17mer (OB1 BCR-positive) and AGA-17mer (OB1 BCR-negative) peptide for 10 min at 37°C. OB1 B cells bind the FGD 17-mer but not the AGA 17-mer. Confocal microscopy confirmed that the captured B cells retained the ability to internalize the FGD-17mer. The peptide-Alexa647 signal colocalized with the GFP singal on Class II MHC-eGFP+ cells.

To calculate the fraction of Class II MHC-negative cells bound to the VHH7-GO nanosubstrate, we disassembled the chamber after cell capture and stained captured cells using Alexa647-labeled anti CD45 (a surface marker for leukocytes) or Alexa647- labeled anti CD3 (a surface marker for T cells). After image acquisition, we used the merged information to identify Class II MHC-eGFP$^+$ cells, as shown in **Figure 2.2.13A** and **B**. Confocal microscopy showed that all cells captured were CD45$^+$. Class II MHC-eGFP$^+$ cells comprised the majority (~76%), of captured cells, CD3$^+$ cells constitute up to ~21%, and the remaining leukocyte population is ~3% of the total (**Figure 2.2.13C**). This observation is consistent with earlier observations that the captured cells from whole blood often contain non-specifically bound leukocytes.[18]

To further demonstrate the utility of our method, we immobilized VHH DC13, specific for murine CD11b$^+$, onto a GO substrate, to capture other leukocytes. We analyzed the capture efficiency of GO-immobilized VHH DC13 alone and in conjunction with VHH7-GO. Capture efficiency and yield were similar to those observed for VHH7-Class II MHC$^+$ B-cells. Confocal microscopy showed that the majority of captured cells are CD11b$^+$ with fewer Class II MHC-eGFP$^+$ cells and CD11b/Class II MHC-eGFP double positive cells (**Figure 2.2.14**)

To improve recovery of CD11b$^+$ populations, we created a capture chamber that allows the sample to pass sequentially over two surfaces, functionalized with VHH7 and VHH DC13 respectively (**Figure 2.2.15A**, **Figure 2.2.16**). Blood obtained from Class II MHC-eGFP knock-in mice was exposed first to the VHH7-modified substrate for 10 min, followed by flushing with PBS to transfer the sample onto the adjacent VHH DC13-modified substrate, where incubation continued for another 10 min. Captured cells were counterstained with Alexa647-labeled anti-CD11b and DAPI and visualized by confocal microscopy. CD11b$^+$ cells (which are Class II MHC-eGFP negative cells) comprised the majority of captured cells on the VHH DC13-modified substrate (**Figure 2.2.15B**). Compared with cells directly captured on a VHH DC13-modified surface (**Figure 2.2.14**), the combination of VHH7 and VHH DC13 significantly improves purity of captured of CD11b$^+$ cells (95% instead of 66% of the VHH DC13 alone **Figure 2.2.15C**). Overall CD11b$^+$ cell capture yield (~3,500 cells) in the tandem array showed no loss compared to a surface functionalized with only VHH DC13 (**Figure 2.2.15D**)

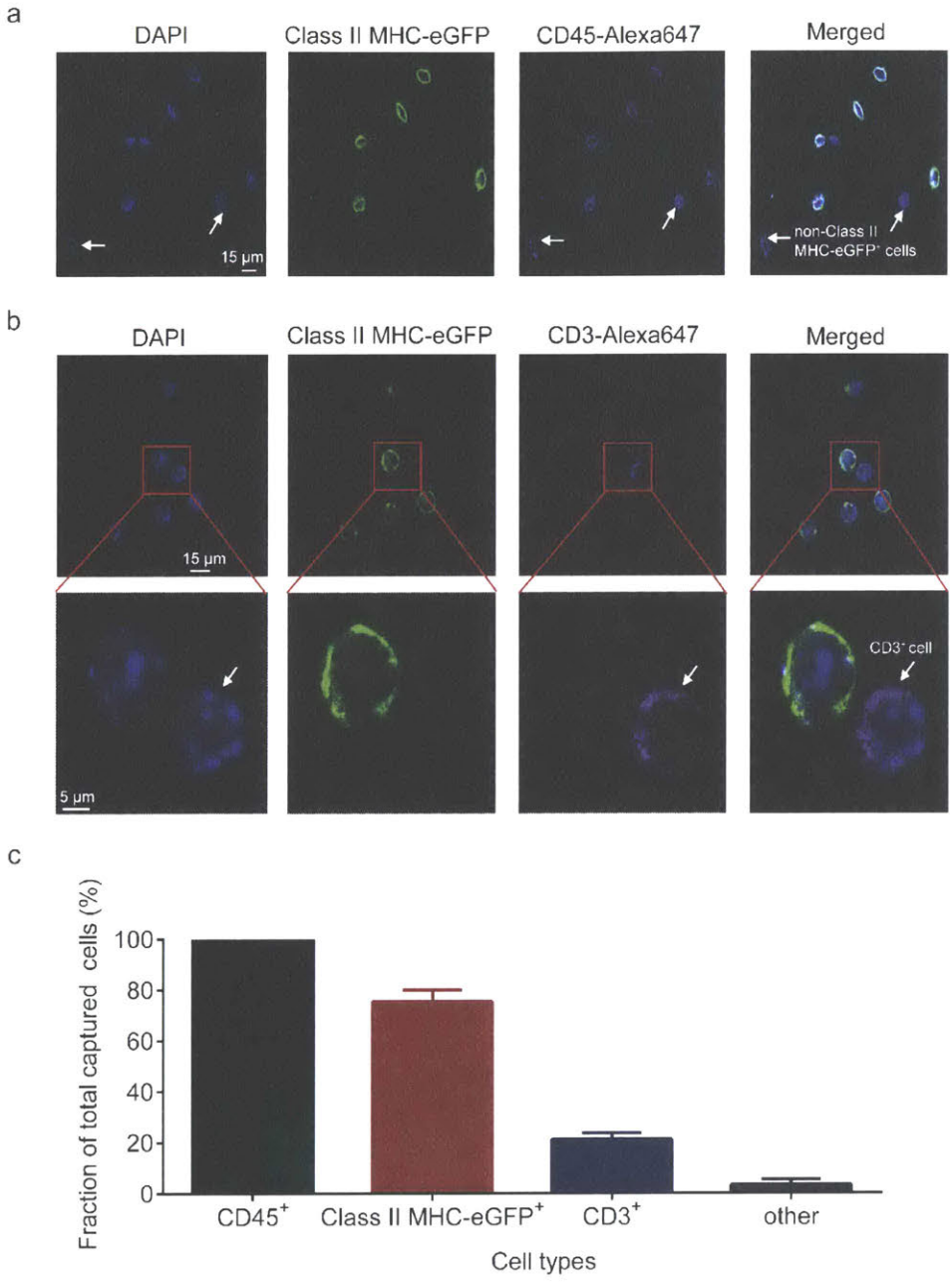

Figure 2.2.14. Identification of non-specifically bound leukocytes on VHH7-immobilized substrates. (A-B) Confocal microscopy images of Class II MHC-eGFP+ cells, and after staining with Alexa647-labeled CD45, Alexa647-labeled-CD3 and DAPI, as indicated. CD45 is present on all WBCs and CD3 is present on T cells. (C) Quantification of bound Class II MHC-eGFP+, CD3+ and remaining cells (other) on the substrates. The percentages of Class II MHC-eGFP+ or CD3+ cells were scored on 100-120 cells.

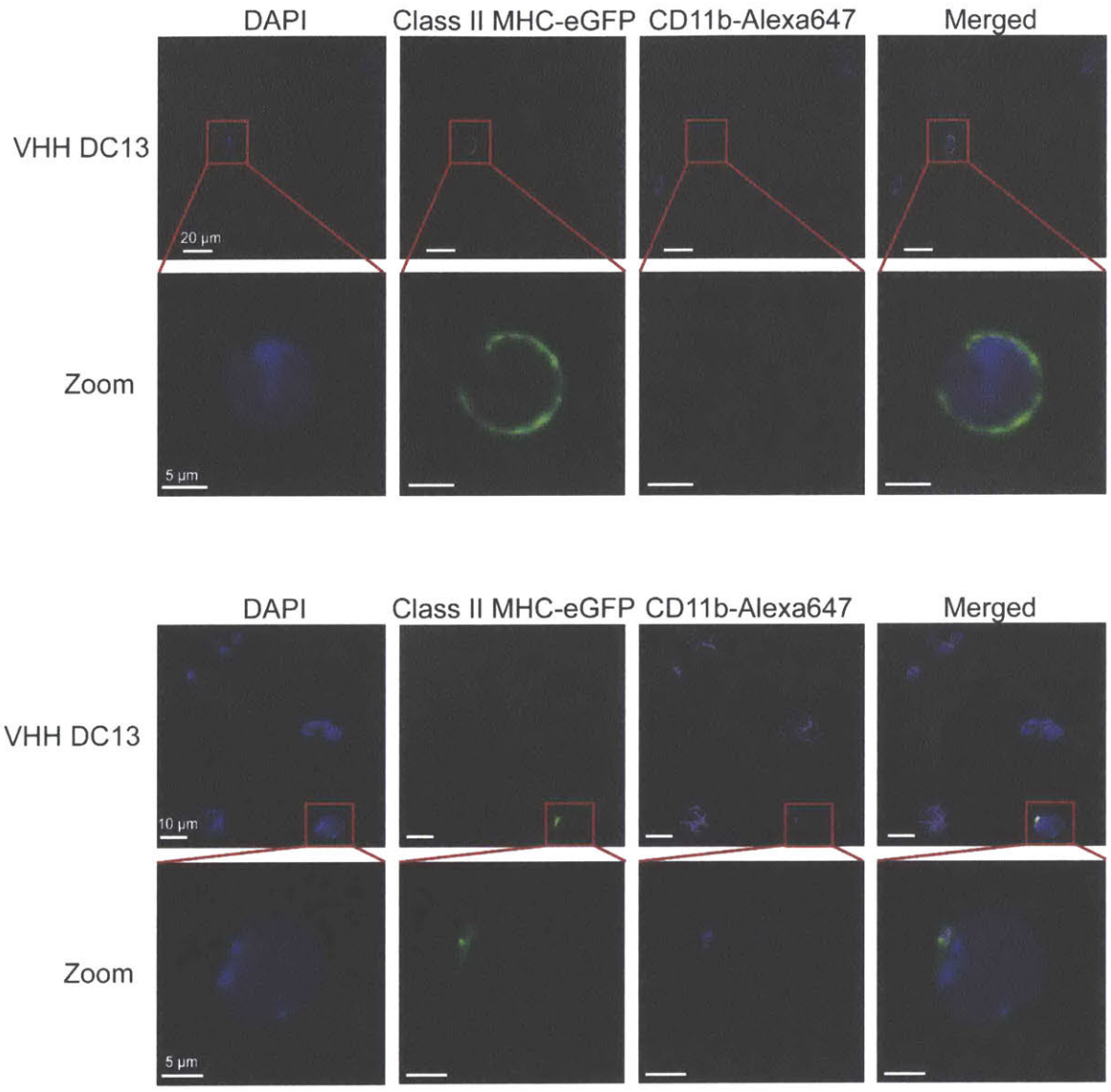

Figure 2.2.14. Identification of non-specifically bound leukocytes on VHH DC13-immobilized substrates alone. (D-E) Confocal microscopy images of Class II MHC-eGFP and CD11b positive cells, and after staining with Alexa647-labeled CD11b and DAPI, as indicated.

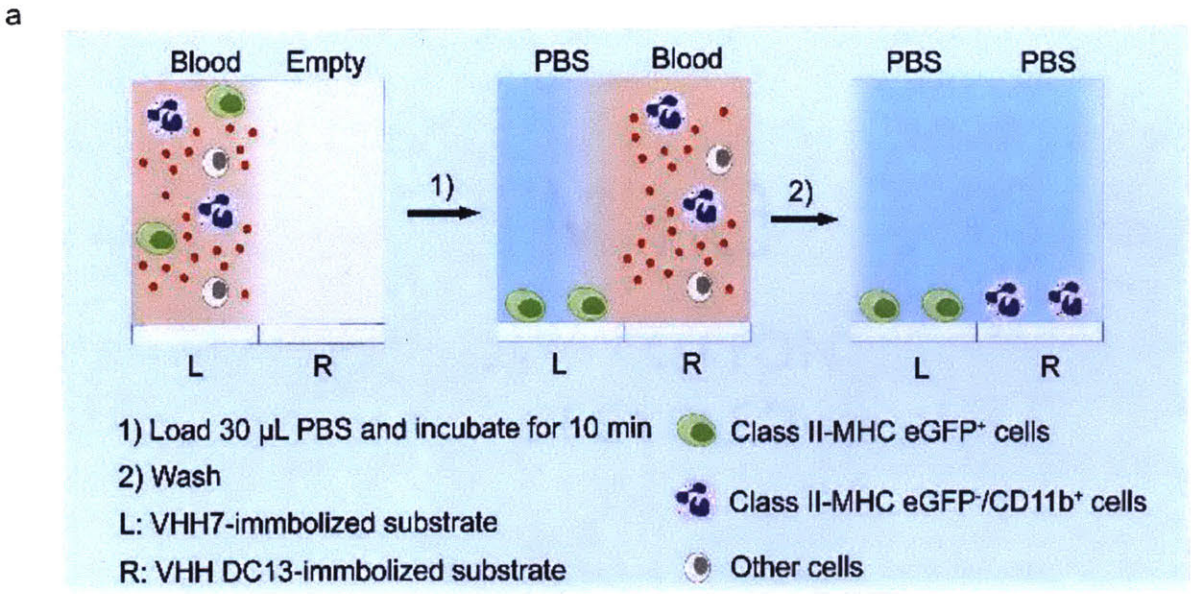
a
Blood
Empty
PBS
Blood
PBS
PBS
1)
2)
L
R
L
R
L
R
1) Load 30 µL PBS and incubate for 10 min
2) Wash
L: VHH7-immbolized substrate
R: VHH DC13-immbolized substrate
Class II-MHC eGFP+ cells
Class II-MHC eGFP-/CD11b+ cells
Other cells

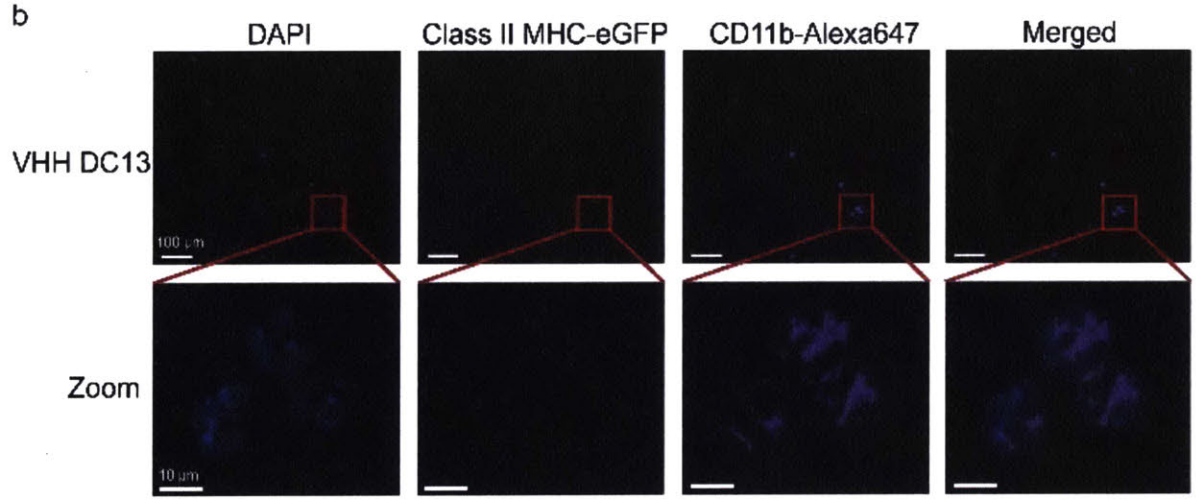
b
DAPI
Class II MHC-eGFP
CD11b-Alexa647
Merged
VHH DC13
Zoom
100 µm
10 µm

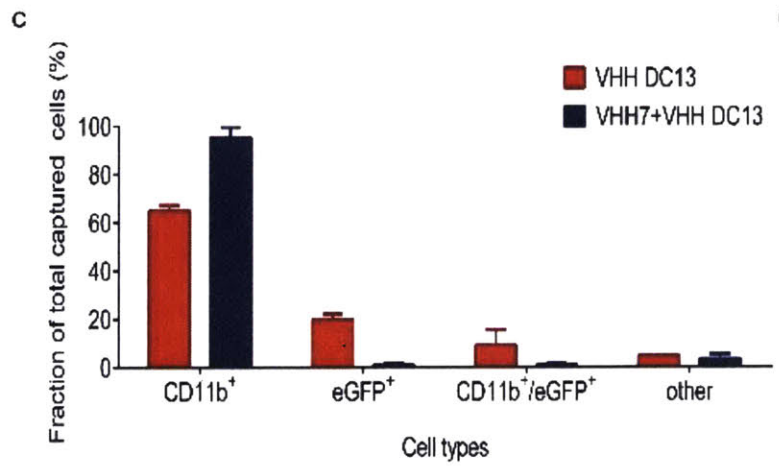
c
Fraction of total captured cells (%)
VHH DC13
VHH7+VHH DC13
100
80
60
40
20
0
CD11b+
eGFP+
CD11b+/eGFP+
other
Cell types

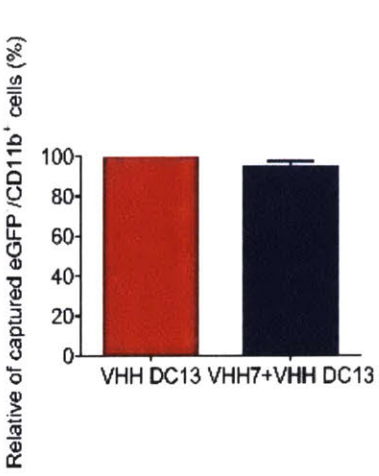
d
Relative of captured eGFP /CD11b+ cells (%)
100
80
60
40
20
0
VHH DC13
VHH7+VHH DC13

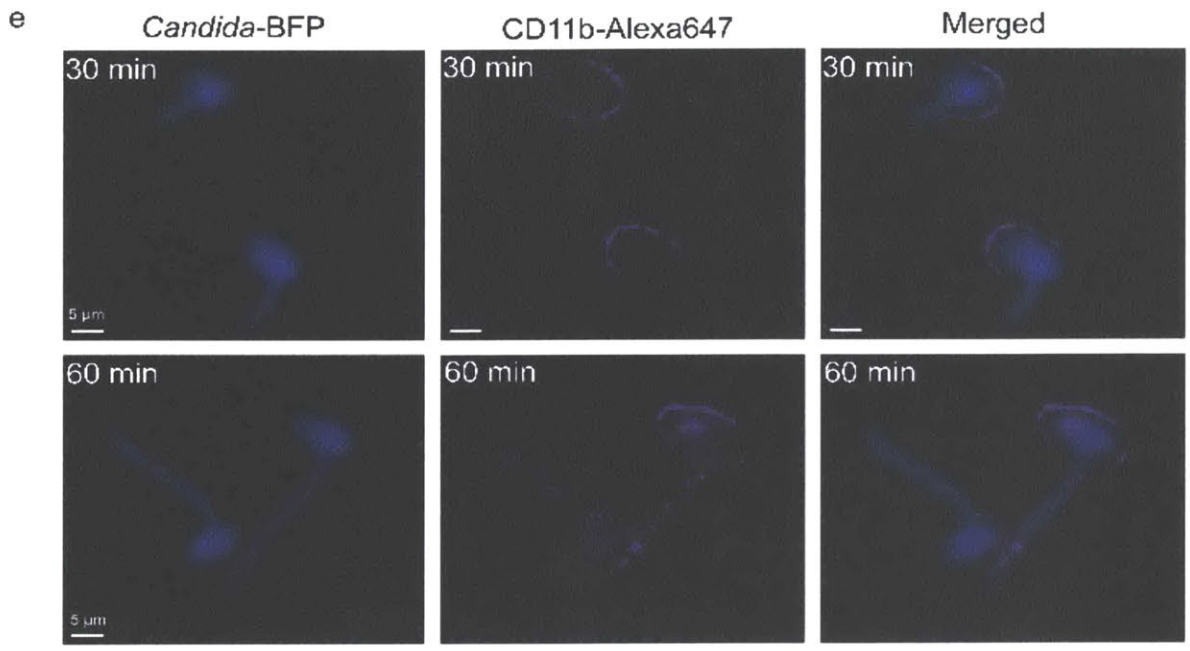

Figure 2.2.15 Quantification and characterization of captured CD11b+ cells by combined VHH7-VHH DC13-modified substrates. (A) Cells were first passed over a VHH7 coated surface and captured subsequently on VHH DC13-modified substrates. (B) Characterization of captured cells. (C) Fraction of captured cells. (D) Comparison of the yield of CD11b+/eGFP- cells captured on a single (VHH DC13 alone) or dually modified VHH7-VHH DC13 substrate. (E) Confocal microscopy of captured cells engaged in phagocytosis of Candida albicans. Captured cells were stained with Alexa647-labeled anti-CD11b antibody while Candida albicans expressed blue fluorescent protein to facilitate their detection.

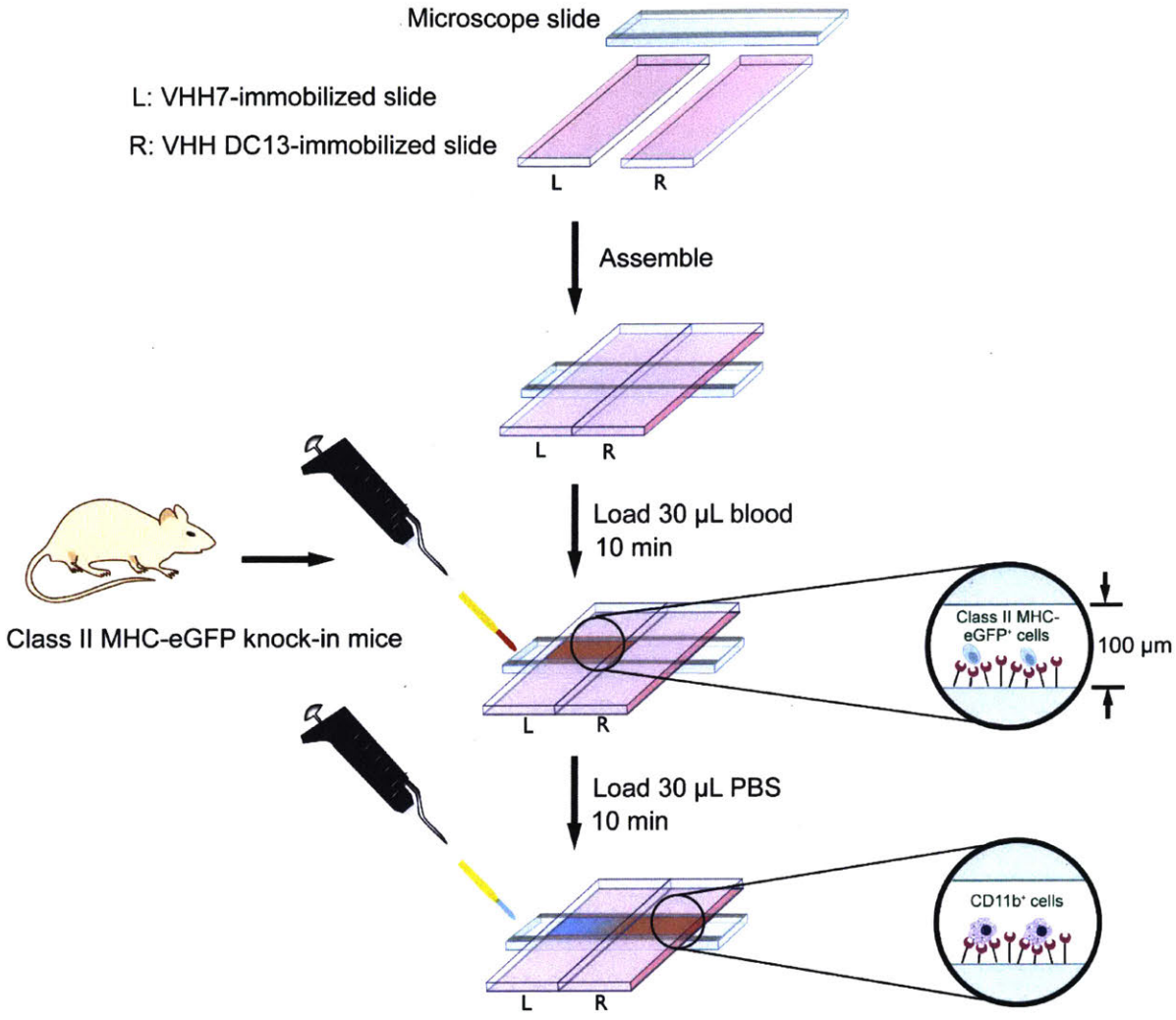

Figure 2.2.16 Whole blood analysis from Class II MHC-eGFP knock-in mice in the combination of two VHHs (VHH7 and VHH DC13)-modified substrates. As indicated in Fig. 2c, a small volume of blood (30 µL) was loaded into the assembled chamber and incubated for 10 min. After that, 30 µL of PBS was loaded into the same side of assembled chamber which allowing cells to pass over two surface functionalized with VHH7 and VHH DC13. After incubation for another 10 min, the chamber was then disassembled and the cell-bearing VHH DC13-immobilized substrate slide was gently washed 3x with PBS. After washing, cells were analyzed by fluorescence microscopy.

CD11b$^+$ cells captured on VHH DC13-modified substrates contain a bi- or multilobed nucleus characteristic of neutrophils (**Figure 2.2.15B**).h Alexa647-labeled anti Gr-1 (a surface marker for neutrophils) (**Figure 2.2.17**). Neutrophils are part of the first line of defence against fungal pathogens such as *Candida albicans*, using their dectin-1 receptor to initiate phagocytosis of *Candida albicans.* The dually functionalized VHH7-VHH DC13 GO surface successfully captured CD11b$^+$ cells in the process of phagocytosing *Candida albicans* in the blood (**Figure 2.2.15E**, **Figure 2.2.18**). Confocal microscopy shows that during phagocytosis of *Candida albicans,* cell morphology changes (compare 30 and 60 min time points). A common limitation of working with primary neutrophils is their short lifespan. *In vivo*, cells can be rapidly captured (~20 min) in good yield (~95%) by dually functionalized VHH-modified substrates, thus providing rapid access to pure immobilized neutrophils with detection of phagocytic function.

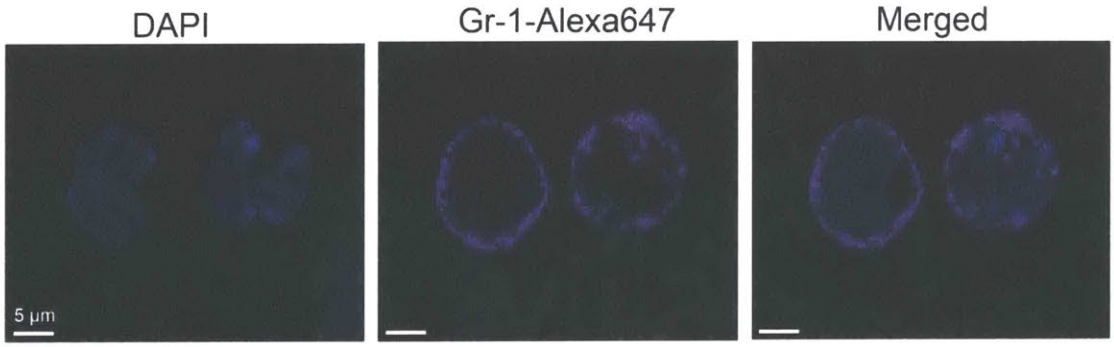

Figure 2.2.17 Characterization of captured CD11b+ cells after passing over two surfaces functionalized with VHH7 and VHH DC13. Confocal microscopy images of CD11b+ cells captured on VHH DC13-modified substrates and stained with DAPI and Alexa647-labeled anti-Gr-1 antibody. Captured cells contain divided lobes and can be stained with anti-CD11b (Fig. 4b) and anti-Gr-1 antibody, thus identifies them as neutrophils.

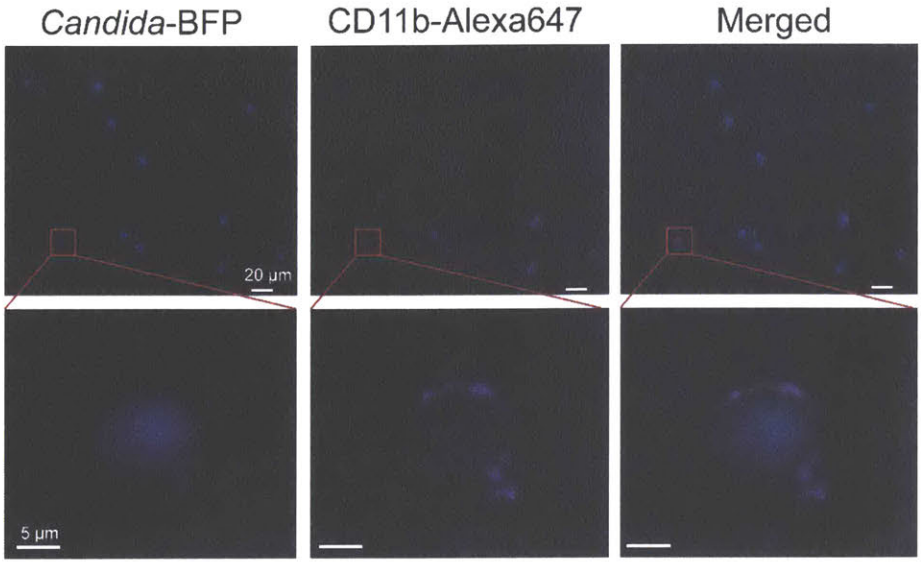

Figure 2.2.18 Combination of VHH7 and VHH DC13-modified nanosubstrates allows identification the phagocytosis of Candida albicans in CD11b+ cells. Fresh blood from Class II MHC-eGFP+ knock-in mice was incubated with Candida albicans-BFP (Candida-BFP) for 30 min followed by captured the cells as described in Figure 2.2.16 and Figure 2.2.10D. Confocal microscopy confirmed that most CD11b+ cells with Candida albicans phagocytosis can be captured on VHH DC13-midified substrates.

2.2.3 Experimental

2.2.3.1 Preparation of GO-coated nanosubstrates

Coating of glass slides and silicon wafers (TED PELLA) with GO was performed as described below. First a standard 25 mm×75 mm glass microscope slide was cleaned by immersion in acetone and subsequent sonication for 30 min. The slide was washed with ethanol, then water and dried under a stream of nitrogen gas. The cleaned slide was immersed in 3% (v/v) 3-aminopropyltriethoxysilane (3-APTES) in toluene for 30 min, washed with toluene, ethanol and

then water before being dried under a stream of nitrogen gas. GO (GnO1LD2H2O, ACS Material) was immobilized on a slide surface by immersing the functionalized glass slide into the GO solution (1 mg/ml) for 1 hr, then washed with PBS before VHH4, VHH7 and VHH DC13 immobilization.

2.2.3.2 C-terminal sortagging of VHH

Peptide GGGK(TAMRA)K(azide) with N terminal amine and C terminal $CONH_2$ was synthesized following standard solid phase synthesis protocol. TAMRA was coupled to the lysine side chain by selective removal of the 4-Methyltrityl (MTT) group under mild acidic conditions (trifluoroacetic acid/triisopropylsilane/dichloromethane (TFA/TIPS/DCM) (1:1:98)) on resin, followed by standard solid phase coupling to the lysine side chain. Fmoc-Lys(azide)-OH (Chempep Inc.) was used as building block to enable subsequent reaction with the bioorthogonal DBCO moiety. The peptide was purified by reverse phase HPLC and its identity was confirmed by LCMS. (1:1:98)) on resin, followed by standard solid phase coupling to the lysine side chain. Fmoc-Lys(azide)-OH (Chempep Inc.) was used as building block to enable subsequent reaction with the bioorthogonal DBCO moiety. The peptide was purified by reverse phase HPLC and its identity was confirmed by LCMS.

Peptide GGGC(Alexa647) with N terminal amine and C terminal $CONH_2$ was synthesized using standard solid phase synthesis protocols. The maleimide-activated Alexa647 was coupled post-cleavage to the cysteine side chain. The dye-coupled peptide was further purified by reverse phase HPLC. The maleimide-activated Alexa647 was coupled post-cleavage to the cysteine side chain. The dye-coupled peptide was further purified by reverse phase HPLC.

$Ca2^+$-independent heptamutant Sortase A (plasmid available from Addgene, Plasmid# 51141) (10 μM final concentration, 10X stock in 50 mM Tris, pH 7.4, 150 mM NaCl) and probe (0.5 mM final concentration, 50X stock) were added to VHH4, VHH7 or VHH DC13 (15 μM final

concentration) in sortase buffer (50 mM Tris, pH 7.4, 150 mM NaCl). The resulting mixture was incubated at 4°C for 2 hr. Ni-NTA resin (0.5 ml packed volume) was added to the reaction mixture and agitated for 20 min to remove sortase and unreacted VHH4, VHH7 or VHH DC13 by adsorption. Unbound materials were purified on a PD-10 desalting column (GE Healthcare Life Sciences) and further purified by size exclusion chromatography (Superdex 75, GE Healthcare Life Sciences). The resulting purified protein was concentrated in 10 KD size centrifugal filter units. Concentrated protein was analyzed by SDS PAGE and LC/MS.

2.2.3.3 Immobilization of VHH to GO nanosheets

GO-coated glass slides were activated with 2 mM (1-ethyl-3-[3-dimethylaminopropyl] carbodiimide) and 5 mM N-hydroxysulfosuccinimide in 0.1 M MES (2-[morpholino]ethanesulfonic acid, 0.5 M NaCl, pH=6.0) for 15 minutes at 25°C. Slides were washed and coupled with 0.5 mM poly(ethylene glycol) bis(amine) (MW 3,000) in PBS at 25°C for 6 hr followed by installation of dibenzocyclooctyne-sulfo-N-hydroxysuccinimidyl ester in PBS for 6 hr. The resulting slide was washed and incubated with 50 mM purified VHH4, VHH7 or VHH DC13 in PBS for 12 hr to allow reaction of the protein's single azide substituent with the DBCO moiety installed on the GO.

2.2.3.4 Synthesis of VHH7-immobilized GO nanosubstrate

Surface morphology of GO-coated substrates was examined using a Jeol 5600LV scanning electron microscope (SEM). High-resolution X-ray photoelectron spectroscopy (HR-XPS) measurements were performed using a PHI Quantera SXM. Topology profiles of GO with and without VHH7 were examined on an atomic force microscope (AFM, XE-70, Park System) using the aluminum coating silicon probe (resonant frequency=300 kHz, force constant=40 N/m) working in tapping mode (scanning rate=1 Hz). The TAMRA signal on VHH7 was also examined by confocal microscopy (PerkinElmer Ultraview spinning disk) equipped with an ORCA-ER CCD

camera (Hamamatsu Photonics). Images were captured and analyzed using Volocity software (PerkinElmer).

2.2.3.5 Preparation of a functionalized chamber for cell capture

Functionalized GO substrates (25 mm× 75 mm) were blocked with 1% BSA in PBS for 1 hr at 37°C, followed by 3 washes with PBS. A GO substrate slide was then assembled with a second blocked but otherwise unmodified glass slide to form a cell capture chamber. The actual chamber is created by placing two pieces of double sided tape (6.5 mm× 75 mm) along the long sides of the glass slide at a distance of ~12 mm across (see Fig 2.). The taped glass slide is then placed perpendicularly onto a functionalized GO substrate slide to form a capture chamber measuring 12 mm× 25 mm x 0.1 mm. This device has a total volume of ~30 µL. Loading is accomplished by direct injection, using a mechanical pipettor, of the ~30 µL volume by apposing the pipette tip to the rim of the chamber. Expulsion of the desired volume then rapidly fills the chamber. Washing is accomplished by delivering the desired volume of washing solution to one side of the open chamber, and wicking off liquid from the opposing open end of the chamber to ensure even flow over the modified surface of the device.

2.2.3.6 Cell culture and capture experiments

Murine A20 and human Raji B cell lymphomas were maintained in RPMI1640 medium containing 10% inactivated fetal calf Serum (IFS), 55 µM β-mercaptoethanol, 1 mM sodium pyruvate and 1% penicillin/streptomycin. For cell capture experiments, cells were collected and labeled with CellTracker™ Green CMFDA dye (C7025, Invitrogen). Different A20 cell densities (~2.2×10^4, ~6-7×10^4 and ~20×10^4 cells/30 µl) were adjusted by mixing labeled cells with PBS. The cell suspensions (30 µl) were loaded into the capture chamber and incubated at 37°C for 10 min. Raji (~2.2×10^4 cells/30 µl; negative for murine Class Ii MHC) and capture chambers not

modified with VHH7 served as negative controls. After washing, captured cells were examinedby fluorescence microscopy. To capture cells from whole blood, samples were obtained from Class II MHC-eGFP knock-in mice and collected in heparinized tubes. Blood samples (30 µL) were then loaded into the capture chamber. For quantitative analyses, the average number of captured cells was calculated by counting ten representative fields of visionfrom three independent capture experiments for each group (ie ~$2.2x10^4$ cells/30 µl of A20 cells).

2.2.3.7 Immunofluorescence microscopy and analysis

A20 cells were loaded into the functionalized capture chamber (~2.2×10^4 cells) and incubated at 37°C for 10 min. After 3 washes with PBS, cells were fixed as described[2], washed with PBS and incubated with the anti-murine Class II MHC (I-A/1-E) Alexa488-labeled antibody (107616 Biolegend), in a 1:1000 dilution, for 1 hr at 25°C. For Class II MHC-eGFP$^+$ cells captured from whole blood, cells were fixed and incubated with Alexa-647-labeled VHH7 (1 µM) for 20 min or stained with Alexa647-conjugated anti-mouse IgG (A-21235, Life Technologies), Alexa647-conjugated anti-mouse CD45 (103123, Biolegend) or CD3 (100209, Biolegend) for 1 hr at 25°C in the dark. After washing, the cells were counterstained with 4,6-diamidino-2-phenylindole (DAPI, Vector Labs) and visualized by confocal microscopy. Images were captured and analyzed using Volocity software. Approximately 100-120 cells in the images for CD45, Class II MHC and CD3 were counted for quantification of CD45$^+$, Class II MHC-eGFP$^+$ and CD3$^+$ cells. For CD11b$^+$ cells captured from whole blood, cells were fixed and stained with Alexa647-conjugated anti-mouse CD11b (101218, Biolegend) or Alexa647-conjugated anti-mouse Gr-1 (108418, Biolegend) for 1 hr at 25°C in the dark. After washing, the cells were counterstained with DAPI and visualized by confocal microscopy. Approximately 100-120 cells in the images for CD11b and Class II MHC were counted for quantification of CD11b$^+$/eGFP$^-$ (CD11b positive but Class II MHC-eGFP

negative), CD11b^{+}/eGFP^{+} (CD11b and Class II MHC-eGFP double positive) and CD11b+/eGFP^{-} (CD11b negative but Class II MHC-eGFP positive) cells.

2.2.3.8 Incubation of captured cells with OB1 peptide

Alexa647-labeled FGD-17mer and AGA-17mer peptide were prepared and characterized as described[3]. Cells from OB1/Class II MHC-eGFP^{+} knock-in mice[4] were captured, followed by incubation with Alexa647-labeled FGD-17mer and AGA-17mer peptide for 10 min at 37°C. After washing, the cells were counterstained with DAPI and visualized by confocal microscopy.

2.2.3.9 Phagocytosis of *Candida albicans* in whole blood

Fresh blood from Class II MHC-eGFP^{+} knock-in mice was incubated with *Candida albicans* which expressed blue fluorescent protein (*Candica*-BFP) for 30 and 60 min at 37°C as we described[5], followed by loading into two VHHs (VHH7 and VHH DC13)-immobilized substrates as described in Fig. S12. Captured cells were fixed and stained with Alexa647-conjugated anti-mouse CD11b. After PBS washing, the cells were visualized by confocal microscopy.

2.2.3.10 Statistical analysis

Data were analyzed by one-way ANOVA and represented as the mean ±standard deviation based on at least 3 independent capture experiments.

2.2.4 Discussion and Conclusion

Sortase conjugation of VHH7 in a uniform orientation onto GO nanosubstrates allows efficient capture of Class II MHC$^+$ cells from small amounts of blood. We generated a simple flow system for cells to pass successively over two surfaces, functionalized with VHH7 and VHH DC13 respectively, a configuration that increases the capture percentage of CD11b$^+$ cells. Sortase conjugation also allows site-specific and quantitative installation of additional fluorophores for co-localization microscopy with a fluorescent or fluorescently stained cells. This VHH-based sensing system is compatible with small blood or reagent sample volumes, rapid processing, stability, ease of manufacture and low cost. Stability of GO-VHH adducts might even eliminate the need for a cold chain and thus enable use of devices of this type outside the setting of the laboratory. Our method can easily be extended to other VHHs or biologicals for isolation, identification and analysis of other cell types in a minimally invasive approach.

2.2.5 References

1. Sethu, P.; Moldawer, L. L.; Mindrinos, M. N.; Scumpia, P. O.; Tannahill, C. L.; Wilhelmy, J.; Efron, P. A.; Brownstein, B. H.; Tompkins, R. G.; Toner, M., Microfluidic isolation of leukocytes from whole blood for phenotype and gene expression analysis. *Analytical chemistry* **2006,** *78* (15), 5453-61.

2. Witte, M. D.; Wu, T.; Guimaraes, C. P.; Theile, C. S.; Blom, A. E.; Ingram, J. R.; Li, Z.; Kundrat, L.; Goldberg, S. D.; Ploegh, H. L., Site-specific protein modification using immobilized sortase in batch and continuous-flow systems. *Nat Protoc* **2015,** *10* (3), 508-16.

3. Mei, Q.; Zhang, Z., Photoluminescent graphene oxide ink to print sensors onto microporous membranes for versatile visualization bioassays. *Angew Chem Int Ed Engl* **2012,** *51* (23), 5602-6.

4. Sreejith, S.; Ma, X.; Zhao, Y., Graphene oxide wrapping on squaraine-loaded mesoporous silica nanoparticles for bioimaging. *Journal of the American Chemical Society* **2012,** *134* (42), 17346-9.

5. Yoon, H. J.; Kim, T. H.; Zhang, Z.; Azizi, E.; Pham, T. M.; Paoletti, C.; Lin, J.; Ramnath, N.; Wicha, M. S.; Hayes, D. F.; Simeone, D. M.; Nagrath, S., Sensitive capture of circulating tumour cells by functionalized graphene oxide nanosheets. *Nature nanotechnology* **2013,** *8* (10), 735-41.

6. Jung, J. H.; Cheon, D. S.; Liu, F.; Lee, K. B.; Seo, T. S., A graphene oxide based immuno-biosensor for pathogen detection. *Angew Chem Int Ed Engl* **2010,** *49* (33), 5708-11.

7. Trilling, A. K.; Harmsen, M. M.; Ruigrok, V. J.; Zuilhof, H.; Beekwilder, J., The effect of uniform capture molecule orientation on biosensor sensitivity: dependence on analyte properties. *Biosensors & bioelectronics* **2013,** *40* (1), 219-26.

8. Jeon, S.; Moon, J. M.; Lee, E. S.; Kim, Y. H.; Cho, Y., An electroactive biotin-doped polypyrrole substrate that immobilizes and releases EpCAM-positive cancer cells. *Angew Chem Int Ed Engl* **2014,** *53* (18), 4597-602.

9. Muyldermans, S., Nanobodies: natural single-domain antibodies. *Annu Rev Biochem* **2013,** *82*, 775-97.

10. De Meyer, T.; Muyldermans, S.; Depicker, A., Nanobody-based products as research and diagnostic tools. *Trends in biotechnology* **2014,** *32* (5), 263-70.

11. Trilling, A. K.; Hesselink, T.; van Houwelingen, A.; Cordewener, J. H.; Jongsma, M. A.; Schoffelen, S.; van Hest, J. C.; Zuilhof, H.; Beekwilder, J., Orientation of llama antibodies strongly increases sensitivity of biosensors. *Biosensors & bioelectronics* **2014,** *60*, 130-6.

12. Mao, H.; Hart, S. A.; Schink, A.; Pollok, B. A., Sortase-mediated protein ligation: a new method for protein engineering. *Journal of the American Chemical Society* **2004,** *126* (9), 2670-1.

13. Ton-That, H.; Mazmanian, S. K.; Faull, K. F.; Schneewind, O., Anchoring of surface proteins to the cell wall of Staphylococcus aureus. Sortase catalyzed in vitro transpeptidation reaction using LPXTG peptide and NH(2)-Gly(3) substrates. *The Journal of biological chemistry* **2000,** *275* (13), 9876-81.

14. Witte, M. D.; Cragnolini, J. J.; Dougan, S. K.; Yoder, N. C.; Popp, M. W.; Ploegh, H. L., Preparation of unnatural N-to-N and C-to-C protein fusions. *Proceedings of the National Academy of Sciences of the United States of America* **2012,** *109* (30), 11993-8.

15. Chen, G. Y.; Pang, D. W.; Hwang, S. M.; Tuan, H. Y.; Hu, Y. C., A graphene-based platform for induced pluripotent stem cells culture and differentiation. *Biomaterials* **2012,** *33* (2), 418-27.

16. Dougan, S. K.; Ogata, S.; Hu, C. C.; Grotenbreg, G. M.; Guillen, E.; Jaenisch, R.; Ploegh, H. L., IgG1+ ovalbumin-specific B-cell transnuclear mice show class switch recombination in rare allelically included B cells. *Proceedings of the National Academy of Sciences of the United States of America* **2012,** *109* (34), 13739-44.

17. Li, Z.; Theile, C. S.; Chen, G. Y.; Bilate, A. M.; Duarte, J. N.; Avalos, A. M.; Fang, T.; Barberena, R.; Sato, S.; Ploegh, H. L., Fluorophore-Conjugated Holliday Junctions for Generating Super-Bright Antibodies and Antibody Fragments. *Angew Chem Int Ed Engl* **2015,** *54* (40), 11706-10.

18. Hou, S.; Zhao, H.; Zhao, L.; Shen, Q.; Wei, K. S.; Suh, D. Y.; Nakao, A.; Garcia, M. A.; Song, M.; Lee, T.; Xiong, B.; Luo, S. C.; Tseng, H. R.; Yu, H. H., Capture and stimulated release of circulating tumor cells on polymer-grafted silicon nanostructures. *Adv Mater* **2013,** *25* (11), 1547-51.

19. Branzk, N.; Lubojemska, A.; Hardison, S. E.; Wang, Q.; Gutierrez, M. G.; Brown, G. D.; Papayannopoulos, V., Neutrophils sense microbe size and selectively release neutrophil extracellular traps in response to large pathogens. *Nature immunology* **2014,** *15* (11), 1017-25.

20. Strijbis, K.; Tafesse, F. G.; Fairn, G. D.; Witte, M. D.; Dougan, S. K.; Watson, N.; Spooner, E.; Esteban, A.; Vyas, V. K.; Fink, G. R.; Grinstein, S.; Ploegh, H. L., Bruton's Tyrosine Kinase (BTK) and Vav1 contribute to Dectin1-dependent phagocytosis of Candida albicans in macrophages. *PLoS pathogens* **2013,** *9* (6), e1003446.

21. Esteban, A.; Popp, M. W.; Vyas, V. K.; Strijbis, K.; Ploegh, H. L.; Fink, G. R., Fungal recognition is mediated by the association of dectin-1 and galectin-3 in macrophages. *Proceedings of the National Academy of Sciences of the United States of America* **2011,** *108* (34), 14270-5.

22. Agrawal, N.; Toner, M.; Irimia, D., Neutrophil migration assay from a drop of blood. *Lab on a chip* **2008,** *8* (12), 2054-61.

2.3 Rapid Capture and Labeling of Cells on Single Domain Antibody-Functionalized Flow Cell

Current techniques to characterize leukocyte subgroups in blood require long sample preparation times and sizable sample volumes. A simplified method for leukocyte characterization using smaller blood volumes would thus be useful in diagnostic settings. Here we describe a flow system comprised of two functionalized graphene oxide (GO) surfaces that allow the capture of distinct leukocyte populations from small volumes blood using camelid single-domain antibody fragments (VHHs) as capture agents. We used site-specifically labeled leukocytes to detect and identify cells exposed to fungal challenge. Combining the chemical and optical properties of GO with the versatility of the VHH scaffold in the context of a flow system provides a quick and efficient method for the capture and characterization of functional leukocytes.

2.3.1 Introduction

Peripheral blood represents an attractive source of material for clinical studies, given the minimally invasive procedure required for sample collection and the capacity of such samples to report on perturbations of the immune and inflammatory status. Immunological assays usually involve enumeration and characterization of white blood cells or leukocytes (WBC's). The tracking of cell surface proteins mostly relies on fluorophore-conjugated antibodies or the intrinsic fluorescence provided by fluorescent protein fusions[1-3]. We have generated red blood cells (RBCs) that contain modified surface proteins equipped with a sortase tag. The presence of this tag allows covalent installation of a wide range of probes[4-5]. Despite the development of several methods to label cells from blood[6-8], none affords selective labeling of specific leukocytes due to the short lifespan of these cells[9]. Existing methods to characterize leukocytes *ex vivo* require comparatively long sample preparation times that involve isolation, labeling, and washing steps, all of which may

affect the responsiveness of leukocytes[10]. In addition, many leukocyte subtypes share surface markers. For instance, both B cells and monocytes express class II MHC products and-similarly-both monocytes and neutrophils express CD11b[11-12]. A fast and reliable method that allows the isolation of specifically labeled leukocytes from blood would thus be useful.

Graphene oxide (GO) provides an attractive option to improve the sensitivity of biosensors [13-15]. Typical GO-based biosensors are created by covalently immobilizing antibodies via exposed lysine residues of antibodies to the activated carboxyl group on GO[16]. However, this method results in random orientation of the antibody. Orienting single domain antigen-binding fragments, also known as VHHs or nanobodies, on sensor surfaces by click chemistry leads to greatly improved sensitivity for biosensors [17-18]. The small size of VHHs (~15 KDa) and their excellent thermal and chemical stability profile make them suitable for numerous diagnostic and therapeutic applications [19-21]. Since a large percentage of the VHH surface is involved in binding interactions, it is essential to create a uniform orientation using site-specific modifications[17-18] to improve the biosensor's performance. To achieve consistency in orientation, we previously used a combination of sortase-mediated trans-peptidation reactions and 'click' chemistry to site-specifically link VHHs with linkers coated onto GO[10, 22]. The use of these techniques allowed for quick and efficient capture of a distinct leukocyte subpopulation from small volumes of blood.

Here we use transgenic mice that express dectin-1-LPETG-$(HA)_3$, a sortase-modifiable protein[16, 23-24], on CD11b positive ($CD11b^+$) cells. These engineered $CD11b^+$ cells can be labeled with a sortase-catalyzed reaction under native conditions (**Figure 2.3.1**). In this system, blood samples pass over two surfaces functionalized with an anti-murine Class II MHC VHH (VHH7) and an anti-murine CD11b VHH (VHH DC13), respectively. To demonstrate the potential value of this for further diagnostic applications, we also examined whether surfaces functionalized with a VHH can capture labeled blood cells engaged in the phagocytosis of *Candica albicans*.

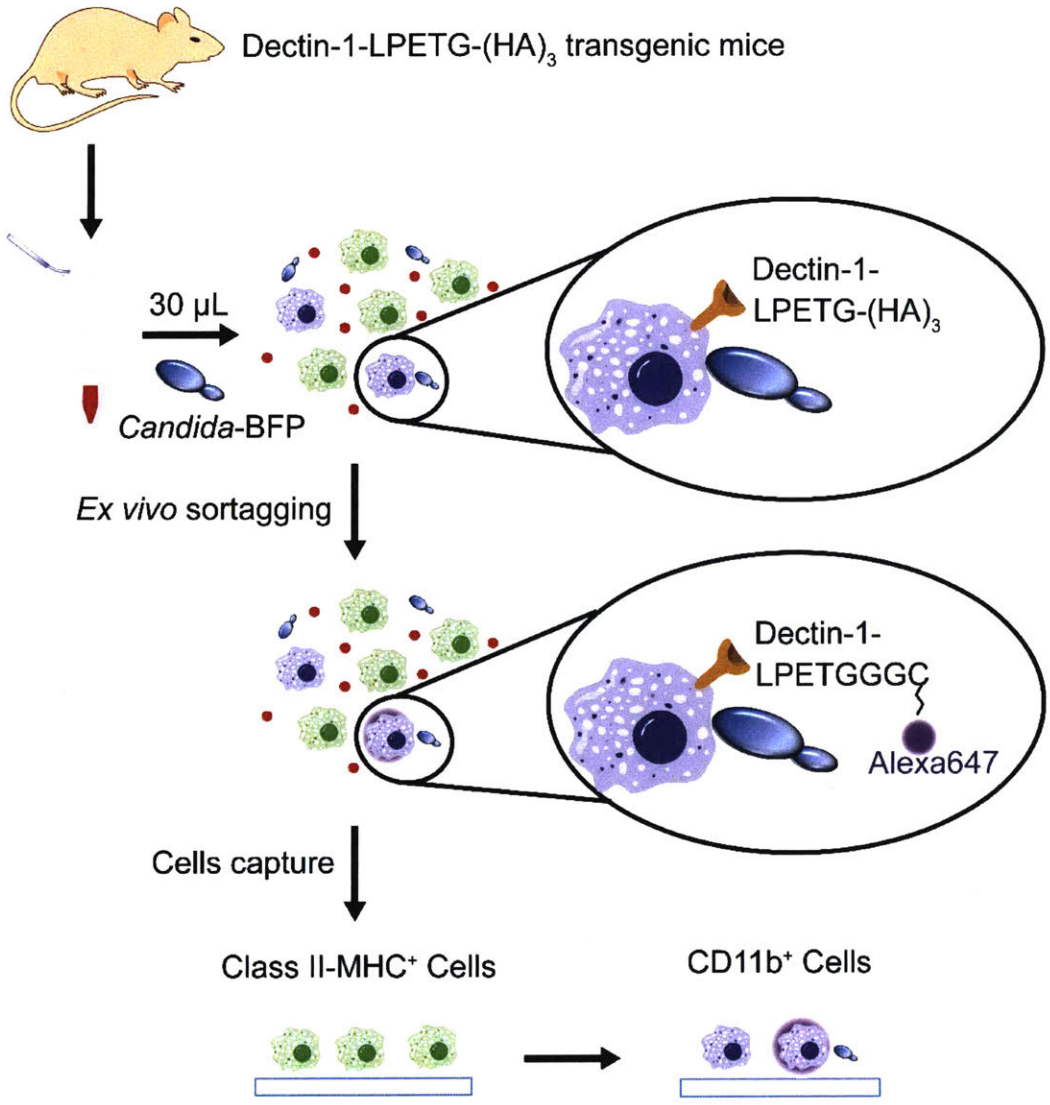

Figure 2.3.1 Schematic illustration of VHH-functionalized flow cell for capture of sortase-labeled cells from small blood sample volumes. The thin sheet morphology of GO is clearly

2.3.2 Experimental Section

2.3.2.1 Preparation of labeled VHH for immobilization

We synthesized the probe used for VHH labeling, GGGK-[TAMRA]-K-N_3, with an N terminal amine and a C terminal $CONH_2$ following standard solid phase synthesis protocols[22]. Calcium-independent heptamutant Sortase A (10 μM final concentration) and probe (1 mM final concentration) were added to the VHH (200 μM final concentration) in PBS at 20 °C for 2 hr. Ni-NTA (0.5 ml, Qiagen) was then added to the reaction mixture and mixed for 20 min to remove sortase and any unreacted VHH. The desired product, the VHH-peptide adduct, was purified by size exclusion chromatography (Superdex 75- GE Life Sciences).

2.3.2.2 Immobilization of VHH to GO nanosheets

GO-coated glass slides were activated with 2 mM 1-ethyl-3-(3-dimethylaminopropyl)carbodiimide (EDC) and 5 mM N-hydroxysulfosuccinimide (NHS) in 0.1 M MES (2-[morpholino]ethanesulfonic acid, 0.5 M NaCl, pH=6.0) for 15 minutes at 25°C. Slides were coupled with 0.5 mM poly(ethylene glycol) bis(amine) (MW 3,000) at 25°C, followed by installation of dibenzocyclooctyne-sulfo-N-hydroxysuccinimidyl ester (DBCO-NHS ester) in PBS for 6 hr. Slides were incubated with 50 μM VHH7 or VHH DC13 labeled with peptide GGGK-TAMRA-K-N_3 in PBS for 12 hr. The VHH7 and VHH DC13-GO functionalized nanosubstrates were assembled with another glass slide to form a chamber with two different coating surfaces [10, 22].

2.3.2.3 Generation of dectin-1-LPETG-$(HA)_3$ transgenic mice

Mice expressing dectin-1-LPETG-$(HA)_3$ were generated as described by Beard et al.[25] A fragment containing the tagged version of murine dectin-1 cDNA was cloned into the ColA1/neomycin/hygromycin targeting vector, which contains the ColA1-targeting arms. The linearized targeting vector was introduced into B6;129 ES cells by electroporation and cells were selected with G418. Selected clones were checked for the desired insertion by PCR using the

primers: 5'-GCACAGCATTGCGGACATGC-3', 5'-CCCTCCATGTGTGACCAAGG- 3' and 5'-GCAGAAGCGCGGCCGTCTGG-3'. The ES cells were injected into a blastocyst which was then implanted into pseudopregnant females to obtain chimeras. The chimeric animals were crossed with C57BL/6 wild-type animals. Those showing germ-line transmission of the modified dectin construct were selected. The mice were then crossed to B6.129P2-Lyz2tm1(cre)Ifo/J animals (Jackson laboratory) to express the transgene exclusively in lysozyme positive cells. To eliminate expression of endogenous dectin-1, the animals were further crossed with dectin-1-deficient mice kindly provided by Dr. Stuart Levitz and Dr. Gordon D. Brown [16, 26]. These mutant mice were then bred to obtain homozygous for sortaggable dectin-1.

2.3.2.4 Immunofluorescence microscopy

To capture cells from whole blood, samples (30 µl) were obtained from wild type (WT) or transgenic mice and collected in heparinized tubes. These samples were then loaded into the VHH-functionalized flow system for cell capture. After 3 washes with PBS, cells captured on the VHH DC13-immobilized substrate were fixed with 4% paraformaldehyde solution in PBS, followed by a PBS wash and staining with Alexa647-conjugated anti-mouse CD11b (101218, Biolegend), Alexa647-conjugated anti-mouse Gr-1 (108418, Biolegend) or Alexa647-conjugated anti-mouse HA-tag (3444, Cell Signaling Technology) antibody (1:1000 dilution) by incubation for 1 hr at 25°C. Cells captured on the VHH7-immobilized substrate were fixed and incubated with anti-mouse IgG Alexa568-conjugated antibody (A-11031, Life Technologies) for 1 hr at 25°C in the dark. After a wash with PBS, captured cells were counterstained with 4,6-diamidino-2-phenylindole (DAPI, Vector Labs) and visualized by confocal microscopy. Images were captured and analyzed using Volocity software (PerkinElmer).

2.3.2.5 Fluorescence-activated cell sorting (FACS) analysis of peripheral blood leukocytes

Peripheral blood was collected from both wild-type and dectin-1-LPETG-$(HA)_3$ transgenic animals. After lysis of red blood cells, freshly isolated leukocytes were stained with an anti-HA-tag antibody (D5-1722, Columbia Biosciences) conjugated with PE. Cells were analyzed by FACS and different white blood cell types were discriminated by their SSC and FSC profile. Modified dectin-1-LPETG-$(HA)_3$ was detected at the cell surface using anti-HA antibody.

2.3.2.6 Sortase labeling

To label cells expressing dectin-1-LPETG-$(HA)_3$, 30 µL of 50 µM sortase A (sortase) and 500 µM GGGC-Alexa647 peptide were preincubated in PBS on ice for 15 min, followed by mixing with 60 µL of blood from either wild type or transgenic animals. Mixtures were incubated on ice for 60 min with occasional gentle mixing. The mixture was loaded into the VHH-functionalized flow chamber for cell capture. After a wash with PBS, cells were fixed and stained with DyLight550-conjugated anti HA-tag antibody (ab117513, Abcam) or DAPI and visualized by confocal microscopy.

2.3.2.7 Capture of labeled cells from whole blood engaging in phagocytosis of *Candida albicans*

Fresh blood from transgenic mice was incubated for 30 min at 37°C with *Candida albicans* that express blue fluorescent protein (*Candica*-BFP)[24], followed by incubation with GGGC-Alexa647 peptide and sortase to label dectin-1-LPETG-$(HA)_3$ positive cells. The sample was then loaded into the VHH-functionalized flow chamber for cell capture. Cells were fixed and visualized by confocal microscopy.

2.3.3 Results and Discussion

2.3.3.1 Principle

Surfaces functionalized with VHH7 and VHH DC13 can selectively capture Class II MHC-positive (MHC^+) and $CD11b^+$ cells from small volumes of peripheral blood[10, 22]. We now show that this device can also capture primary cells from dectin-1-LPETG-$(HA)_3$ transgenic mice. GO was immobilized on a 3-APTES-functionized glass slide through electrostatic forces between the oxide groups of GO and the amine-end of 3-APTES[27]. To enable conjugation with a dibenzocyclooctyl (DBCO) click partner localized to the GO nanosheet, we engineered a sortase-ready version of VHH7 and VHH DC13 with an LPETG motif near the C-terminus. A Gly_3 peptide containing a TAMRA fluorophore and an azide to enable coupling with DBCO during the 'click' reaction was introduced using standard sortagging protocols[28]. The TAMRA fluorophore was included to verify protein immobilization (**Figure 2.3.2A**). The modified VHH7 and VHH DC13 VHH were thus covalently linked to GO nanosheet in a uniform manner (**Figure 2.3.2B**). The VHH7 and VHH DC13-GO functionalized nanosubstrates were assembled with an additional glass slide to form a cell capture chamber (**Figure 2.3.3**). Two pieces of double sided tape were placed on the side of the empty glass slide before pressing onto VHH7 and VHH DC13-immobilized substrates to generate two adjacent chambers of overall 12 mm × 50 mm size. The cell capture chamber has a height of 0.1 mm and each therefore contains ~30 µL of fluid. Other cell-capture devices, such as antibody-coated bead-based pull down assays and flow cytometry-based cell sorting, require longer sample preparation times and usually larger sample volumes[29-30]. This VHH-based device allows quick and efficient capture of distinct leukocyte subpopulations from small blood sample volumes.

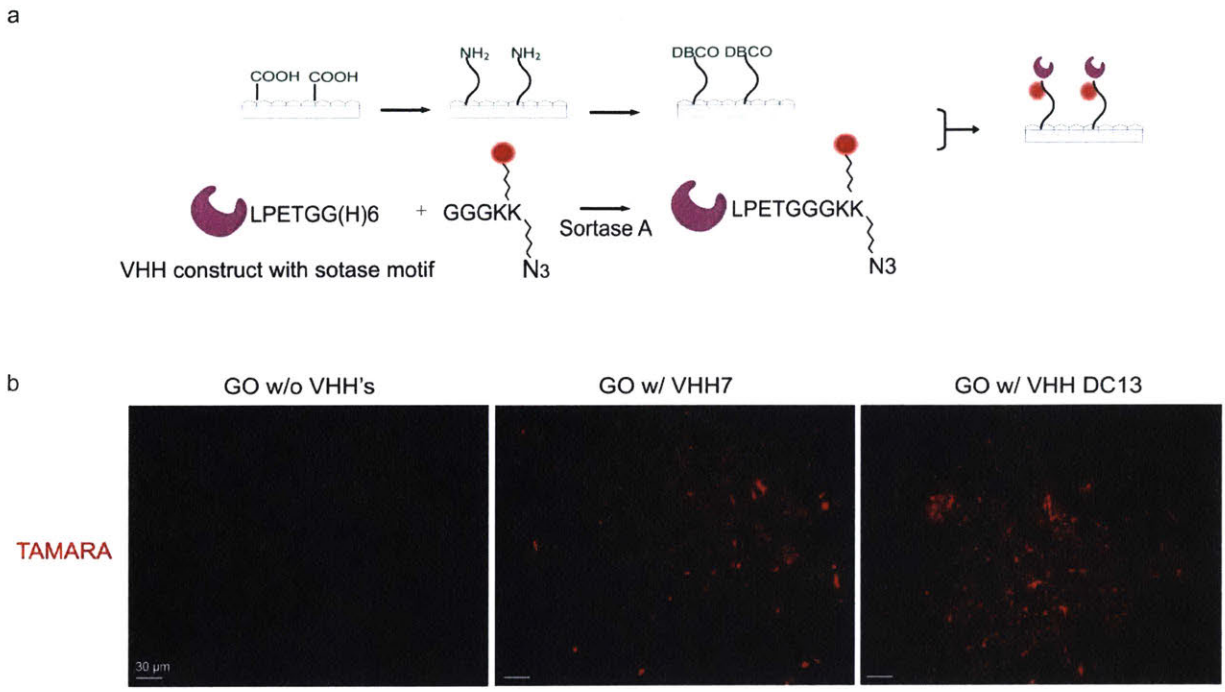

Figure 2.3.2 Sortase-mediated labeling of the VHH system. (A) Overview of sortase-mediated site-specific ligation of VHH's onto GO nanosheets. (B) Confocal microscopy images of the glass slide without (left panel) or with VHH7 (middle panel) and VHH DC13 (right panel) immobilization. VHH7 and VHH DC13 were C-terminally modified via a sortase-mediated ligation to install a TAMRA fluorophore and an azide. The GO nanosheet was functionalized with a dibenzocyclooctyne (DBCO) handle for a "click" reaction with the azide-modified VHH7 and VHH DC13. The TAMRA signal indicates successful immobilization of VHH7 and VHH DC13 on the GO substrate.

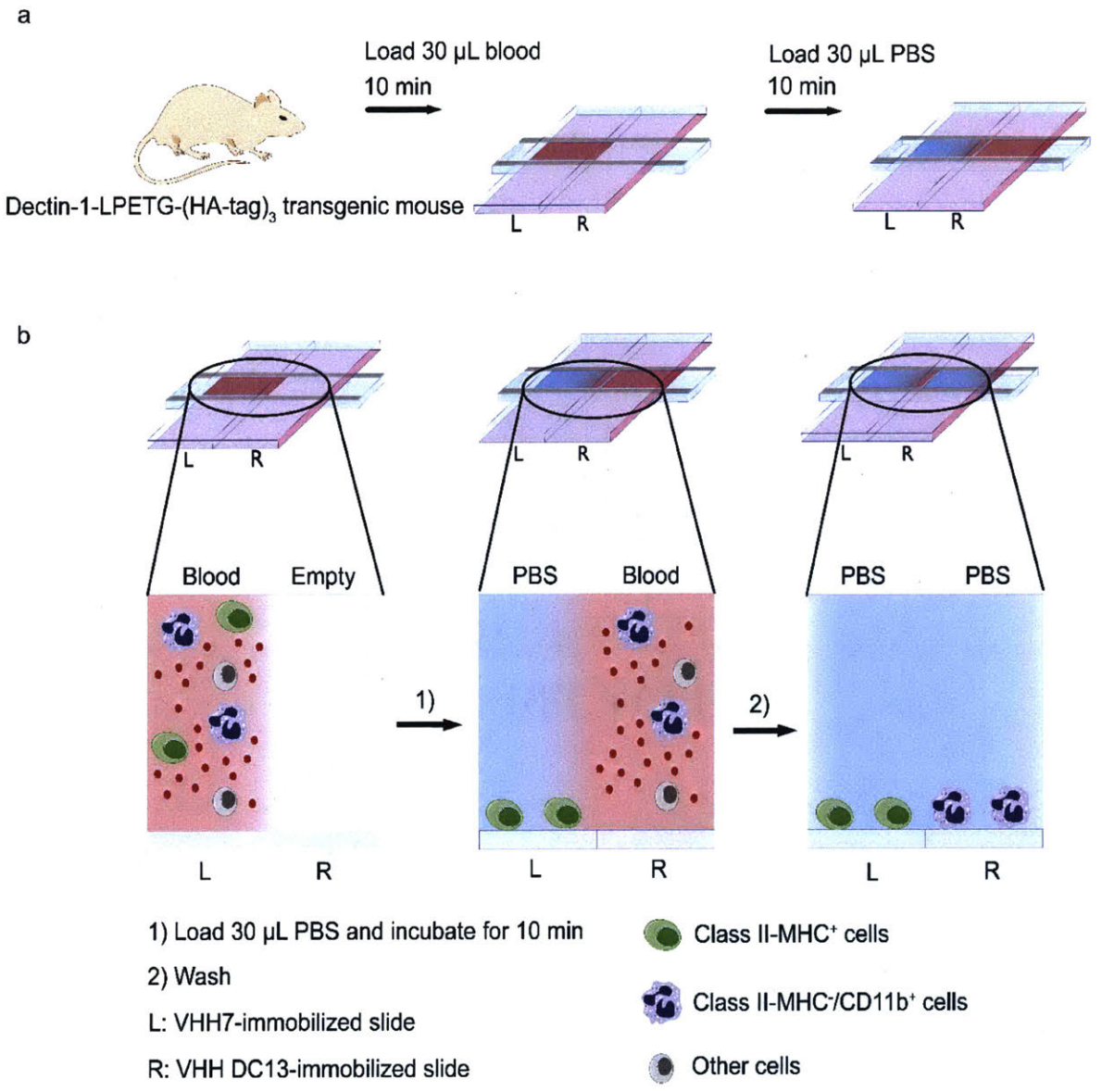

Figure 2.3.3 Whole blood analysis from transgenic mice in the VHH's-functionalized flow system. (A) A small volume of blood (30 µl) was loaded into the assembled chamber and incubated on VHH7-modified substrate for 10 min. After that, 30 µl of PBS was loaded into the same side of the assembled chamber, allowing cells to pass through the second surface functionalized with VHH DC13. (B) After incubation for another 10 min, the chamber was then disassembled and the cell-bearing VHH's-immobilized substrate slide was gently washed 3x with PBS. After washing, cells were analyzed by confocal microscopy.

2.3.3.2 Capture of cells from transgenic mice

Dectin-1 is a major β-glucan receptor on neutrophils and monocytes ($CD11b^+$ cells) and plays an important role in the phagocytosis of *Candida albicans*[24, 31-32]. The use of a site-specific labeling method has allowed us to monitor the behavior of fluorophore-labeled functional dectin-1 on the cell surface[24, 32]. However, since most dectin-1 positive neutrophils have a short lifespan [9], it is difficult to image labeled leukocytes from whole blood if long isolation and processing times are involved. We first tested the performance of two VHH-modified substrates for rapid capture of $CD11b^+$ cells from transgenic mice that express engineered sortase-ready dectin-1. Fresh peripheral blood samples were obtained from transgenic mice that express dectin-1-LPETG-$(HA)_3$ on the surface of neutrophils and other lysozyme-positive leukocytes[4, 24, 32-33] (**Figure 2.3.4**). The expression of the endogenous untagged version of dectin-1 was eliminated by crossing these animals with dectin-1 deficient mice. Flow cytometry analysis of leukocytes from whole blood collected from the transgenic animals showed that ~11-20% of total granulocytes and monocytes are HA-tagged (**Figure 2.3.4B**, **Figure 2.3.5**), with tagged cells representing ~1-2% of the total cell population (**Figure 2.3.5**). These experiments confirm the expression of dectin-1-LPETG-$(HA)_3$ specifically in lysozyme-positive cells such as granulocytes and monocytes (i.e. $CD11b^+$ cells). We next evaluated the potential of the VHH-functionalized flow cell to capture dectin-1-LPETG-$(HA)_3$ cells from the transgenic mice. Class II MHC^+ cells (mostly B cells) can be depleted by first passing the sample through the VHH7-coated surface (**Figure 2.3.6**), thus improving the capture specificity of $CD11b^+$ cells on the second VHH DC13-modified substrate[10, 22]. Confocal microscopy showed that a large proportion (~96%) of $CD11b^+$ cells from transgenic mice were retained on VHH DC13-modified nanosubstrates (**Figure 2.3.4C**, **Figure 2.3.7**).

Most of the captured CD11b$^+$ cells contain multilobular nuclei, a defining characteristic of neutrophils[9, 31]. The identification of this population was further confirmed by cell-surface staining with Alexa647-conjugated anti Gr-1 (a surface marker for neutrophils) (**Figure 2.3.8**). In addition, a fraction of the captured CD11b$^+$ cells was stained with Alexa647-conjugated anti HA-tag antibody (**Figure 2.3.4D**), thereby confirming that the VHH-functionalized flow cell can capture and identify dectin-1-LPETG-$(HA)_3$ cells.

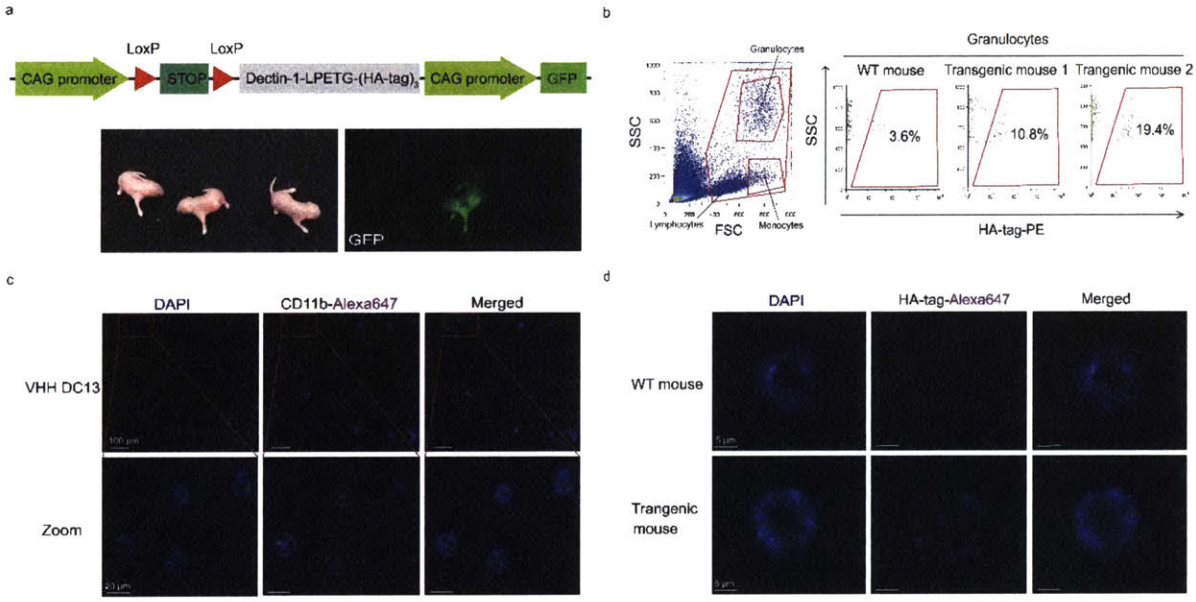

Figure 2.3.4 Whole blood analysis from dectin-1-LPETG-(HA-tag)3 transgenic mice. (A) Generation of dectin-1-LPETG-(HA-tag)3 transgenic mice. (B) FACS analysis of murine peripheral blood granucytes expressing dectin-1-LPETG-(HA-tag)3. (C-D) Confocal microscopy images of captured cells from transgentic mice after further staining with DAPI, Alexa647-labeled anti-CD11b and Alexa647-labeled anti-HA-tag antibody. A small volume of blood (30 µL) from transgenic mice was loaded into the VHH's-functionalized flow system and incubated on each VHH-immobilized substrate at room temperature for 10 min. The chamber was then disassembled and the cell-bearing VHH DC13-immobilized substrate slide was gently washed 3x with PBS. After washing, cells were analyzed by confocal microscopy.

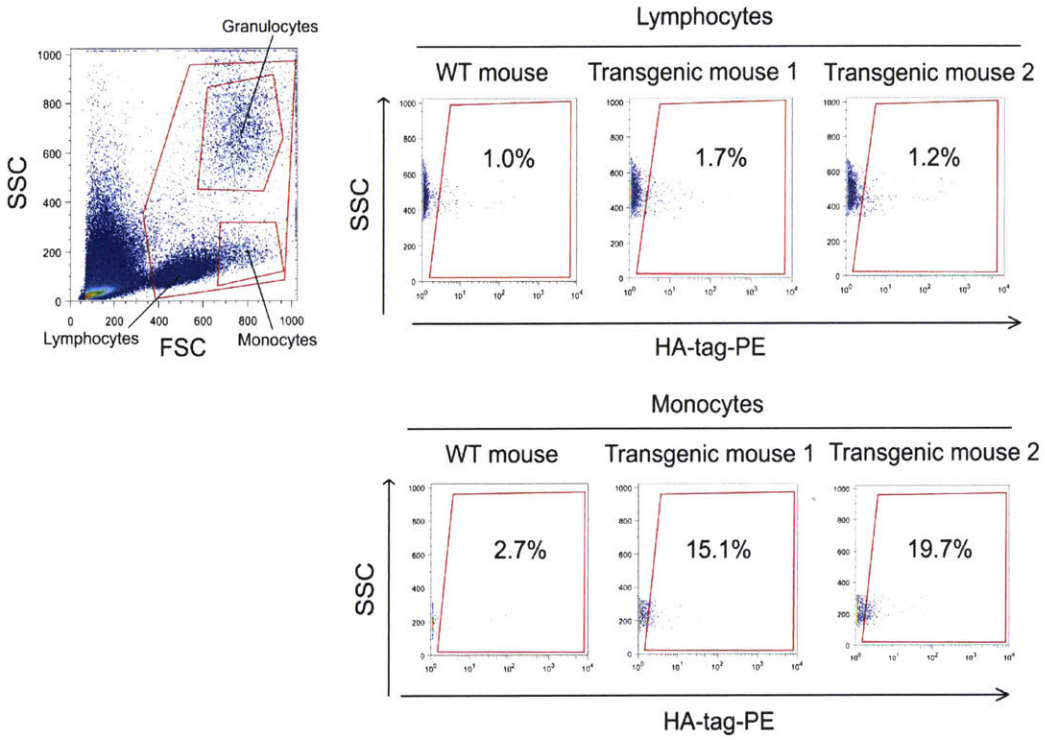

Figure 2.3.5 FACS analysis of murine peripheral blood leukocytes expressing dectin-1-LPETG-(HA-tag)3. Leukocytes were collected and stained with anti-HA-tag antibodies conjugated with PE to detect expression levels of dectin-1-LPETG-(HA-tag)3. Gates were set to select lymphocytes or monocytes depending on their Side-Scatter (SSC) and Forward-Scatter (FSC) intensity. Numbers are percentages of cells expressing surface-exposed tagged dectin-1. WT: wild-type animals (C57Bl/6).

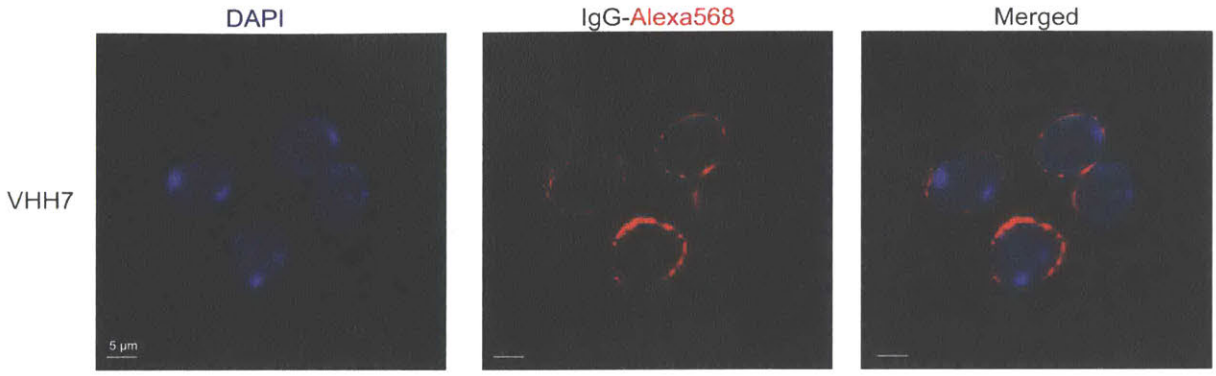

Figure 2.3.6 VHH7-modified nanosubstrates allow capture of IgG+ cells from transgenic mice. We have demonstrated that VHH7-modified substrate captured Class II MHC-eGFP+ cells from Class II MHC-eGFP knock-in mice, and most of the captured Class II MHC-eGFP+ cells can be stained with anti-IgG antibody and thus identifies them as B cells1. Cells from transgenic mice can be captured on VHH7-modified substrates and stained with anti-IgG antibody, confirming that most B cells can be depleted by first passing through an additional VHH7 coated surface.

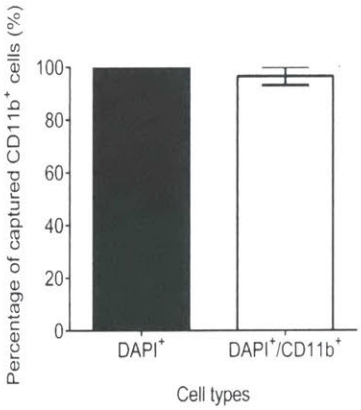

Figure 2.3.7 Identification of captured $CD11b^+$ cells after passing through the VHH's-functionalized flow system. Captured cells on VHH DC13-modified substrates were stained with DAPI and Alexa647-labeled anti-CD11b antibody and subjected to confocal microscopy analysis. Most captured cells can be co-stained with DAPI and anti-CD11b antibody (~96%). The percentages of DAPI positive ($DAPI^+$) or DAPI and CD11b double positive ($DAPI^+/C11b^+$) cells were scored on 100-120 cells.

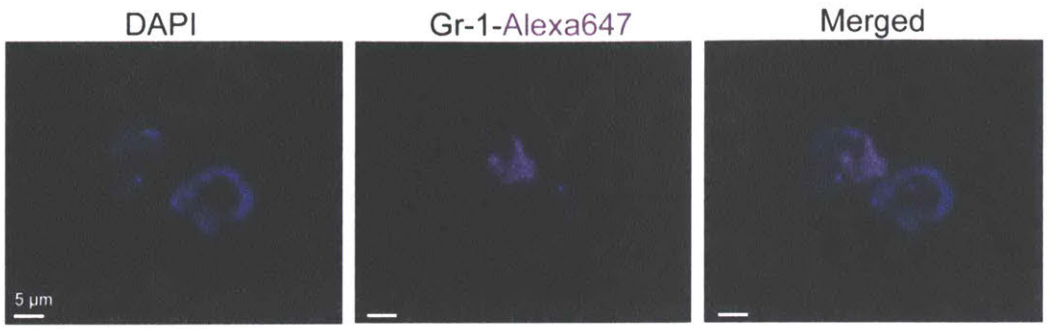

Figure 2.3.8 Characterization of neuthrophils ($CD11b^+$ cells) captured in the VHH's-functionalized flow system. Captured cells from transgenic mice blood were stained with DAPI and Alexa647-labeled anti-Gr-1 antibody. Captured cells contain divided lobes and can be stained with anti-CD11b (Fig. 2c) and anti-Gr-1 antibody.

2.3.3.3 Capture of sortase-labeled cells from transgenic mice

To determine whether the C terminus of dectin-1-LPETG-$(HA)_3$ can be labeled on intact blood cells, GGGC-Alexa647 peptide (500 μM) with or without sortase (50 μM) was gently mixed with blood and incubated on ice for 60 min (**Figure 2.3.9A**). Sortase A acts as a transpeptidase which recognizes the LPETG motif and cleaves between the Thr and Gly residues, forming a thioester intermediate. An N-terminal polyglycine-based peptide then serves as nucleophile to resolve the thioester to form the final ligated product, which contains a natural amide bond linkage in the peptide backbone [34-36]. Here we use GGGC-Alexa647 peptide as the nucleophile to selectively label the C terminal LPETG of dectin-1 prior to capturing the desired cell population with our VHH-functionalized flow cell. (**Figure 2.3.9B**). Blood from wild type mice was used as a control, and all captured cells were stained with DAPI. Confocal microscopy images revealed the surface of sortase-labeled cells exhibited a clear fluorophore signal when compared with cells not exposed to sortase or with the wild type control. Labeled cells captured on the substrates were stained with DyLight 550-conjugated anti-HA antibody, which showed a decrease in signal intensity resulting from loss of the HA tag upon sortase labeling (**Figure 2.3.10**). The flow cell is thus able to efficiently capture labeled cells of low abundance in peripheral blood and enables the analysis of individual captured cells via immunofluorescence staining.

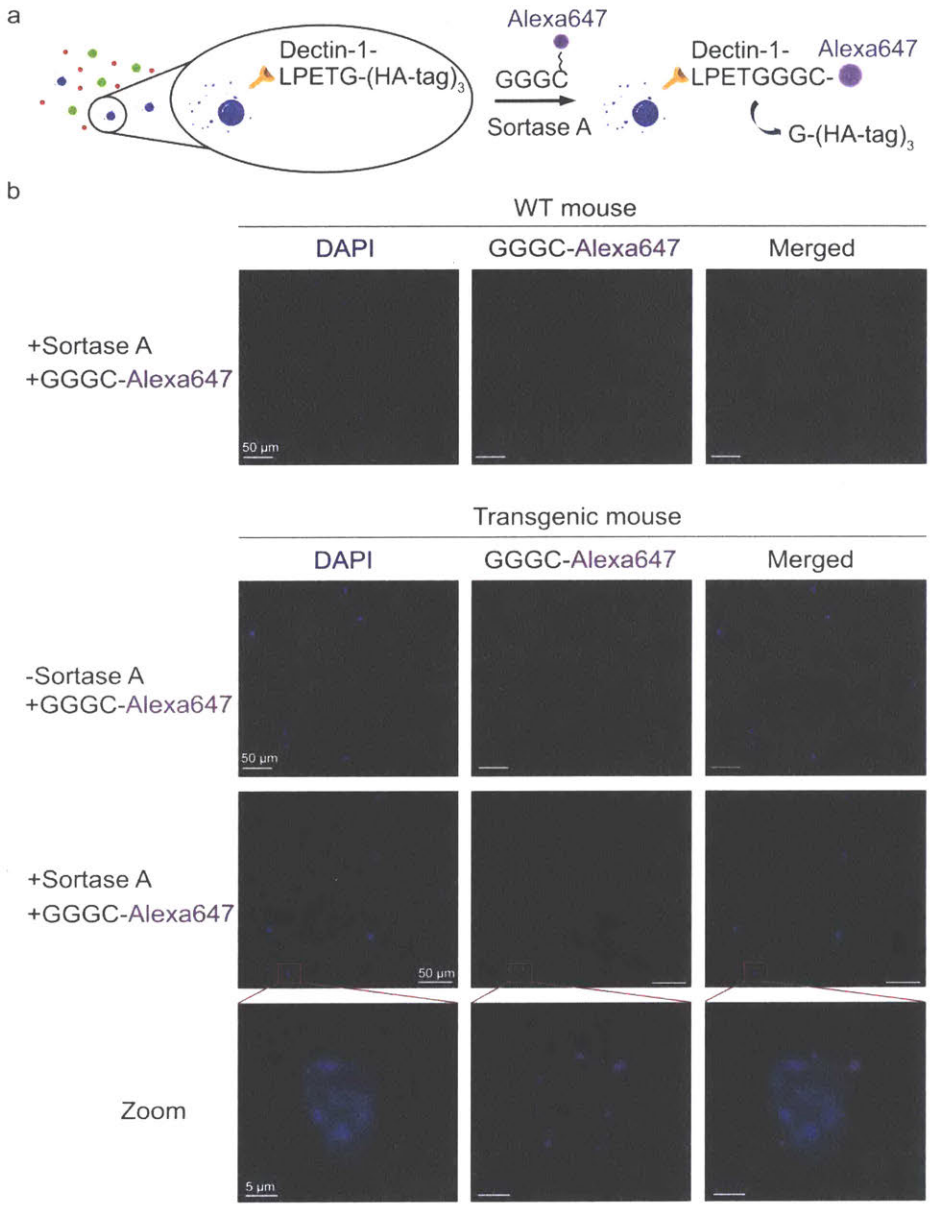

Figure 2.3.9 Confirmation of sortase-labeled cells from 30 μL of whole blood. (A) Sortase-mediated labeling of cells expressing dectin-1-LPETG-$(HA\text{-}tag)_3$. (B) Confocal microscopy images of dectin-1-LPETG-$(HA\text{-}tag)_3$ cells from transgenic mice with or without sortase-mediated labeling. Sortase-labeled cells with dectin-1-LPETGGGC-Alexa647 were captured on VHH DC13-modified substrates. Blood sample from wild-type (WT) mouse served as control.

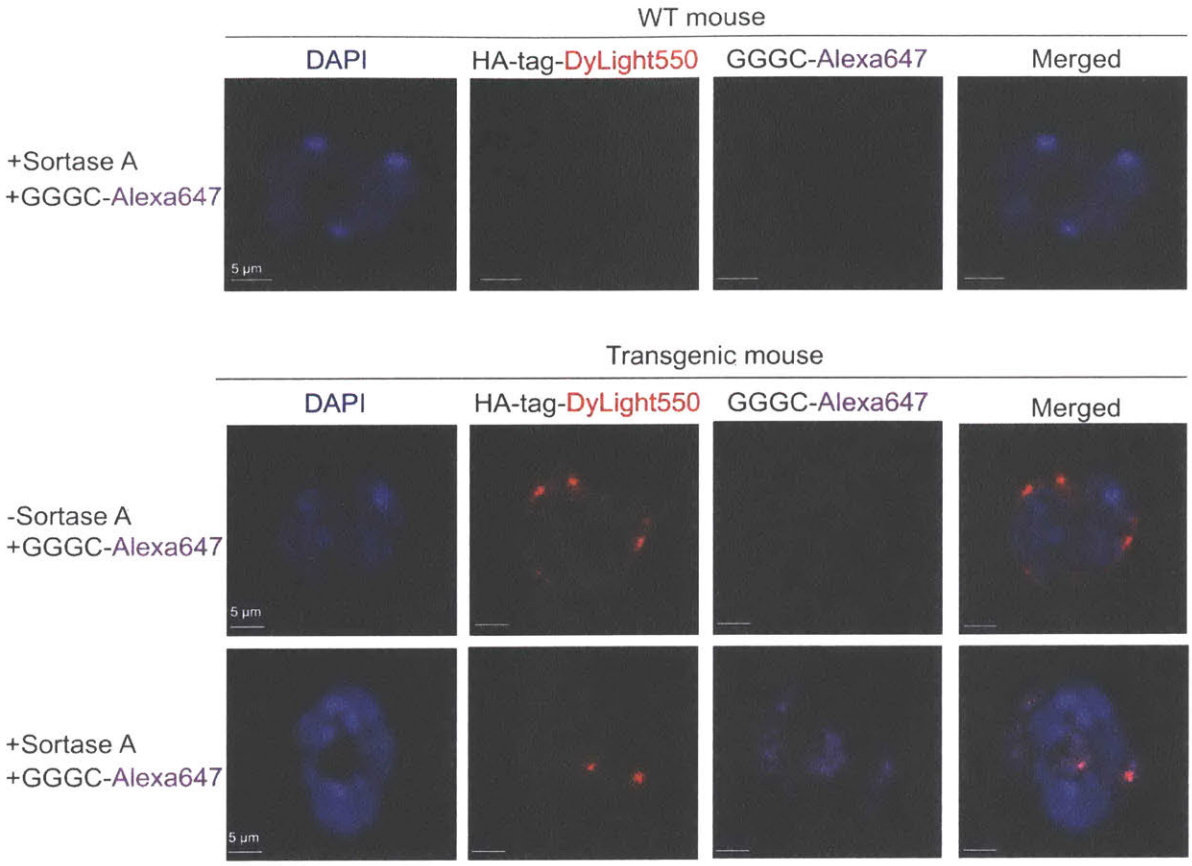

Figure 2.3.10 Confirmation of sortase-mediated transpeptidation reaction from captured cells. Fresh blood sample from wild type or transgenic mice were incubated with or without 50 μM sortase A and 500 μM GGGC-Alexa647 peptide, then loaded into the VHH's-functionalized flow system. Captured cells were stained with DyLight550-conjugated anti-mouse HA-tag and DAPI and visualized by confocal microscopy. Confocal microscopy shows cells with sortase-mediated labeling of dectin-1 with lower HA-tag signal when compared to cells without sortase-mediated transpeptidation reaction or wild-type control (WT).

2.3.3.4 Capture of labeled cells binding to *Candida albicans*

To assess the potential of our device to capture labeled cells exposed to a fungal challenge, fresh blood from transgenic mice was first incubated with *Candida albicans* for 30 min at 37°C. A strain of *Candida* engineered to express blue fluorescent protein (*Candida*-BFP) was used. After incubation, labeled cells were loaded into the VHH-functionalized chamber. The captured cells were then fixed and stained using Alexa647-conjugated anti-CD11b. Merged confocal images were used to analyze the percentage of $CD11b^+$ cells that bound *Candida albicans*, as shown in Figure 4a. Confocal microscopy images showed that all captured $CD11b^+$ cells were in the process of engulfing *Candida albicans*. The process of *Candida albicans* phagocytosis is not limited to the small percentage of dectin-1 positive cells detected using sortase-labeling (**Figure 2.3.10B**). Yeast recognition and phagocytosis in dectin-1 deficient cells can occur through the interaction of the yeast with other receptors, such as mannose or C3 receptors [37-39].

We next mixed a blood sample pre-incubated with *Candida albicans*, with sortase and GGGC-Alexa647 peptide to label dectin-1 positive cells with the fluorophore. The mixture was then loaded into two VHH-functionalized flow cells and visualized by confocal microscopy. Confocal microscopy images revealed that Alexa647 positive cells in the process of engulfing *Candida albicans* had been captured in the VHH-functionalized flow cell. The surface of these cells exhibited red fluorescence from the Alexa647 fluorophore, while control cells incubated without sortase did not show fluorescence (**Figure 2.3.11B**). The VHH-functionalized flow system thus provides a convenient and reliable method to

directly measure and track pathogen-exposed effector cells in the blood without any immunofluorescence staining.

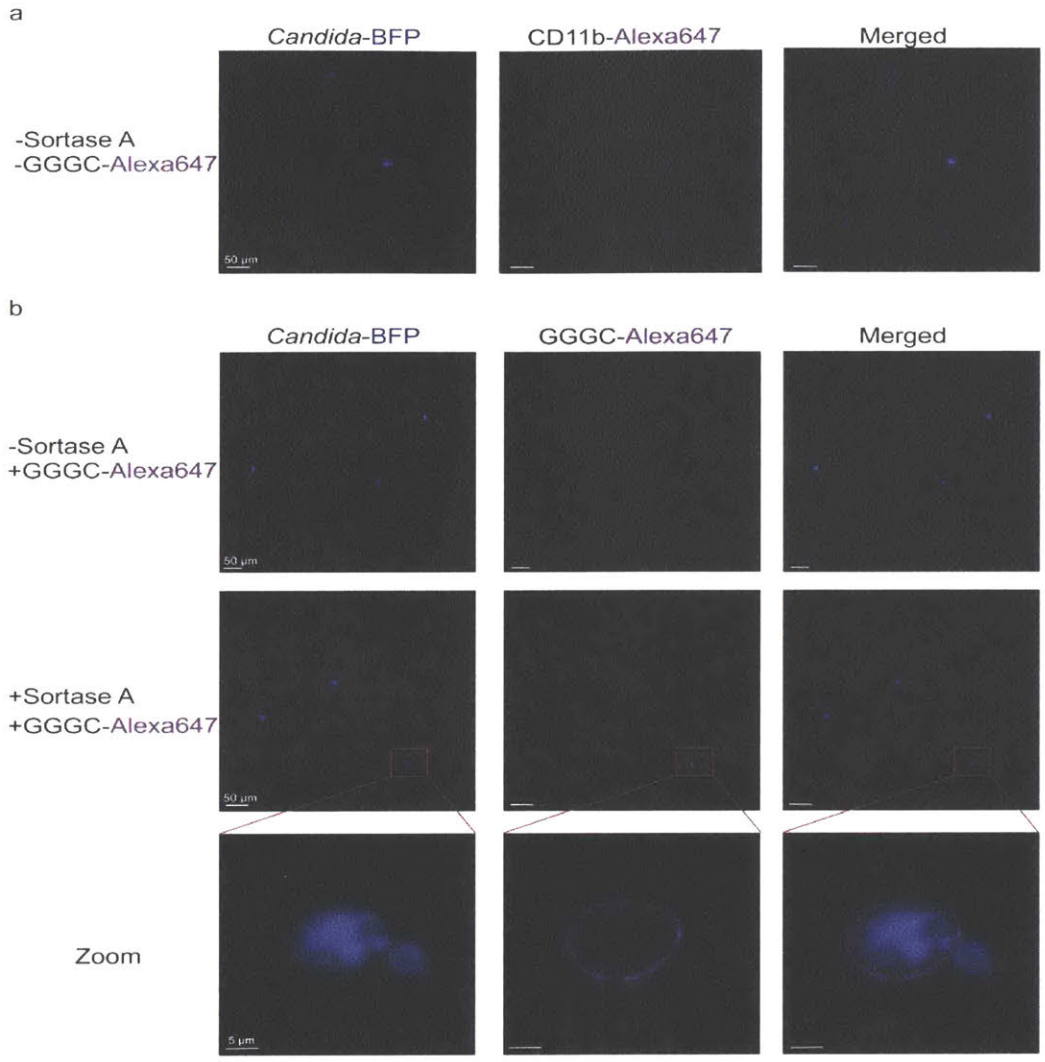

Figure 2.3.11 VHH7-modified nanosubstrates allow capture of IgG+ cells from transgenic mice. We have demonstrated that VHH7-modified substrate captured Class II MHC-eGFP$^+$ cells from Class II MHC-eGFP knock-in mice, and most of the captured Class II MHC-eGFP$^+$ cells can be stained with anti-IgG antibody and thus identifies them as B cells1. Cells from transgenic mice can be captured on VHH7-modified substrates and stained with anti-IgG antibody, confirming that most B cells can be depleted by first passing through an additional VHH7 coated surface.

2.3.4 Conclusions

We have shown an efficient site-specific labeling of cell surface receptors on intact cells using sortase. VHH-immobilized GO flow efficiently captures labeled leukocytes from a small amount of blood, allowing the detection and identification of cells exposed to a fungal challenge in a timely manner. This method can be potentially applied to studies of immune homeostasis, leukocytes trafficking and fungal recognition from whole blood samples. Finally, the implementation of VHH-based sensing system gives the advantage of small sample volume, rapid processing time, stability and low cost. This method holds promise for the isolation, capture, labeling, identification and analysis of other cell types such as different leukocytes in a minimally invasive detection and diagnostics system.

2.3.5 References

1. Bellucci, J. J.; Bhattacharyya, J.; Chilkoti, A., A noncanonical function of sortase enables site-specific conjugation of small molecules to lysine residues in proteins. *Angewandte Chemie* **2015,** *54* (2), 441-5.

2. Kim, W.; Haller, C.; Dai, E.; Wang, X.; Hagemeyer, C. E.; Liu, D. R.; Peter, K.; Chaikof, E. L., Targeted antithrombotic protein micelles. *Angewandte Chemie* **2015,** *54* (5), 1461-5.

3. Policarpo, R. L.; Kang, H.; Liao, X.; Rabideau, A. E.; Simon, M. D.; Pentelute, B. L., Flow-based enzymatic ligation by sortase A. *Angewandte Chemie* **2014,** *53* (35), 9203-8.

4. Shi, J.; Kundrat, L.; Pishesha, N.; Bilate, A.; Theile, C.; Maruyama, T.; Dougan, S. K.; Ploegh, H. L.; Lodish, H. F., Engineered red blood cells as carriers for systemic delivery of a wide array of functional probes. *Proceedings of the National Academy of Sciences of the United States of America* **2014,** *111* (28), 10131-6.

5. Li, Z.; Theile, C. S.; Chen, G. Y.; Bilate, A. M.; Duarte, J. N.; Avalos, A. M.; Fang, T.; Barberena, R.; Sato, S.; Ploegh, H. L., Fluorophore-Conjugated Holliday Junctions for Generating Super-Bright Antibodies and Antibody Fragments. *Angew Chem Int Ed Engl* **2015,** *54* (40), 11706-10.

6. de Vries, E. F.; Roca, M.; Jamar, F.; Israel, O.; Signore, A., Guidelines for the labelling of leucocytes with (99m)Tc-HMPAO. Inflammation/Infection Taskgroup of the European Association of Nuclear Medicine. *European journal of nuclear medicine and molecular imaging* **2010,** *37* (4), 842-8.

7. Pillay, J.; den Braber, I.; Vrisekoop, N.; Kwast, L. M.; de Boer, R. J.; Borghans, J. A.; Tesselaar, K.; Koenderman, L., In vivo labeling with 2H2O reveals a human neutrophil lifespan of 5.4 days. *Blood* **2010,** *116* (4), 625-7.

8. Salmi, M.; Jalkanen, S., Cell-surface enzymes in control of leukocyte trafficking. *Nature reviews. Immunology* **2005,** *5* (10), 760-71.

9. Kolaczkowska, E.; Kubes, P., Neutrophil recruitment and function in health and inflammation. *Nature reviews. Immunology* **2013,** *13* (3), 159-75.

10. Agrawal, N.; Toner, M.; Irimia, D., Neutrophil migration assay from a drop of blood. *Lab on a chip* **2008,** *8* (12), 2054-61.

11. Hume, D. A., Macrophages as APC and the dendritic cell myth. *J Immunol* **2008,** *181* (9), 5829-35.

12. Lai, L.; Alaverdi, N.; Maltais, L.; Morse, H. C., 3rd, Mouse cell surface antigens: nomenclature and immunophenotyping. *J Immunol* **1998,** *160* (8), 3861-8.

13. Chen, Z.; Hong, G.; Wang, H.; Welsher, K.; Tabakman, S. M.; Sherlock, S. P.; Robinson, J. T.; Liang, Y.; Dai, H., Graphite-coated magnetic nanoparticle microarray for few-cells enrichment and detection. *ACS Nano* **2012,** *6* (2), 1094-101.

14. Li, W.; Wang, J.; Ren, J.; Qu, X., 3D graphene oxide-polymer hydrogel: near-infrared light-triggered active scaffold for reversible cell capture and on-demand release. *Adv Mater* **2013,** *25* (46), 6737-43.

15. Yoon, H. J.; Kim, T. H.; Zhang, Z.; Azizi, E.; Pham, T. M.; Paoletti, C.; Lin, J.; Ramnath, N.; Wicha, M. S.; Hayes, D. F.; Simeone, D. M.; Nagrath, S., Sensitive capture of circulating tumour cells by functionalized graphene oxide nanosheets. *Nat Nanotechnol* **2013,** *8* (10), 735-41.

16. Jung, J. H.; Cheon, D. S.; Liu, F.; Lee, K. B.; Seo, T. S., A graphene oxide based immuno-biosensor for pathogen detection. *Angew Chem Int Ed Engl* **2010,** *49* (33), 5708-11.

17. Trilling, A. K.; Harmsen, M. M.; Ruigrok, V. J.; Zuilhof, H.; Beekwilder, J., The effect of uniform capture molecule orientation on biosensor sensitivity: dependence on analyte properties. *Biosens Bioelectron* **2013,** *40* (1), 219-26.

18. Trilling, A. K.; Hesselink, T.; van Houwelingen, A.; Cordewener, J. H.; Jongsma, M. A.; Schoffelen, S.; van Hest, J. C.; Zuilhof, H.; Beekwilder, J., Orientation of llama antibodies strongly increases sensitivity of biosensors. *Biosens Bioelectron* **2014,** *60*, 130-6.

19. Muyldermans, S., Nanobodies: natural single-domain antibodies. *Annu Rev Biochem* **2013,** *82*, 775-97.

20. Siontorou, C. G., Nanobodies as novel agents for disease diagnosis and therapy. *Int J Nanomedicine* **2013,** *8*, 4215-27.

21. De Meyer, T.; Muyldermans, S.; Depicker, A., Nanobody-based products as research and diagnostic tools. *Trends Biotechnol* **2014,** *32* (5), 263-70.

22. Chen, G. Y.; Li, Z.; Theile, C. S.; Bardhan, N. M.; Kumar, P. V.; Duarte, J. N.; Maruyama, T.; Rashidfarrokh, A.; Belcher, A. M.; Ploegh, H. L., Graphene Oxide Nanosheets Modified with Single-Domain Antibodies for Rapid and Efficient Capture of Cells. *Chemistry* **2015**.

23. Tafesse, F. G.; Rashidfarrokhi, A.; Schmidt, F. I.; Freinkman, E.; Dougan, S.; Dougan, M.; Esteban, A.; Maruyama, T.; Strijbis, K.; Ploegh, H. L., Disruption of Sphingolipid Biosynthesis Blocks Phagocytosis of Candida albicans. *PLoS pathogens* **2015,** *11* (10), e1005188.

24. Strijbis, K.; Tafesse, F. G.; Fairn, G. D.; Witte, M. D.; Dougan, S. K.; Watson, N.; Spooner, E.; Esteban, A.; Vyas, V. K.; Fink, G. R.; Grinstein, S.; Ploegh, H. L., Bruton's Tyrosine Kinase (BTK) and Vav1 contribute to Dectin1-dependent phagocytosis of Candida albicans in macrophages. *PLoS pathogens* **2013,** *9* (6), e1003446.

25. Beard, C.; Hochedlinger, K.; Plath, K.; Wutz, A.; Jaenisch, R., Efficient method to generate single-copy transgenic mice by site-specific integration in embryonic stem cells. *Genesis* **2006,** *44* (1), 23-8.

26. Saijo, S.; Fujikado, N.; Furuta, T.; Chung, S. H.; Kotaki, H.; Seki, K.; Sudo, K.; Akira, S.; Adachi, Y.; Ohno, N.; Kinjo, T.; Nakamura, K.; Kawakami, K.; Iwakura, Y., Dectin-1 is required for host defense against Pneumocystis carinii but not against Candida albicans. *Nature immunology* **2007,** *8* (1), 39-46.

27. Chen, G. Y.; Pang, D. W.; Hwang, S. M.; Tuan, H. Y.; Hu, Y. C., A graphene-based platform for induced pluripotent stem cells culture and differentiation. *Biomaterials* **2012,** *33* (2), 418-27.

28. Witte, M. D.; Cragnolini, J. J.; Dougan, S. K.; Yoder, N. C.; Popp, M. W.; Ploegh, H. L., Preparation of unnatural N-to-N and C-to-C protein fusions. *Proc Natl Acad Sci U S A* **2012,** *109* (30), 11993-8.

29. Li, Y.; Kurlander, R. J., Comparison of anti-CD3 and anti-CD28-coated beads with soluble anti-CD3 for expanding human T cells: differing impact on CD8 T cell phenotype and responsiveness to restimulation. *J Transl Med* **2010,** *8*, 104.

30. Zhang, X.; Goncalves, R.; Mosser, D. M., The isolation and characterization of murine macrophages. *Curr Protoc Immunol* **2008,** *Chapter 14*, Unit 14 1.

31. Branzk, N.; Lubojemska, A.; Hardison, S. E.; Wang, Q.; Gutierrez, M. G.; Brown, G. D.; Papayannopoulos, V., Neutrophils sense microbe size and selectively release neutrophil extracellular traps in response to large pathogens. *Nature immunology* **2014,** *15* (11), 1017-25.

32. Esteban, A.; Popp, M. W.; Vyas, V. K.; Strijbis, K.; Ploegh, H. L.; Fink, G. R., Fungal recognition is mediated by the association of dectin-1 and galectin-3 in macrophages. *Proceedings of the National Academy of Sciences of the United States of America* **2011,** *108* (34), 14270-5.

33. Kirak, O.; Frickel, E. M.; Grotenbreg, G. M.; Suh, H.; Jaenisch, R.; Ploegh, H. L., Transnuclear mice with predefined T cell receptor specificities against Toxoplasma gondii obtained via SCNT. *Science* **2010,** *328* (5975), 243-8.

34. Popp, M. W.; Antos, J. M.; Grotenbreg, G. M.; Spooner, E.; Ploegh, H. L., Sortagging: a versatile method for protein labeling. *Nat Chem Biol* **2007,** *3* (11), 707-8.

35. Tsukiji, S.; Nagamune, T., Sortase-mediated ligation: a gift from Gram-positive bacteria to protein engineering. *Chembiochem* **2009,** *10* (5), 787-98.

36. Popp, M. W.; Ploegh, H. L., Making and breaking peptide bonds: protein engineering using sortase. *Angew Chem Int Ed Engl* **2011,** *50* (22), 5024-32.

37. Li, X.; Utomo, A.; Cullere, X.; Choi, M. M.; Milner, D. A., Jr.; Venkatesh, D.; Yun, S. H.; Mayadas, T. N., The beta-glucan receptor Dectin-1 activates the integrin Mac-1 in neutrophils via Vav protein signaling to promote Candida albicans clearance. *Cell host & microbe* **2011,** *10* (6), 603-15.

38. McDonald, J. U.; Rosas, M.; Brown, G. D.; Jones, S. A.; Taylor, P. R., Differential dependencies of monocytes and neutrophils on dectin-1, dectin-2 and complement for the recognition of fungal particles in inflammation. *PloS one* **2012,** *7* (9), e45781.

39. van de Veerdonk, F. L.; Marijnissen, R. J.; Kullberg, B. J.; Koenen, H. J.; Cheng, S. C.; Joosten, I.; van den Berg, W. B.; Williams, D. L.; van der Meer, J. W.; Joosten, L. A.; Netea, M. G., The macrophage mannose receptor induces IL-17 in response to Candida albicans. *Cell host & microbe* **2009,** *5* (4), 329-40.

Noninvasive Immuno-PET Imaging of $CD8^+$ T cell Behavior in Influenza A Virus-infected Mice

3.1 Introduction

Influenza A virus (IAV) is a segmented, negative sense, single-stranded RNA virus of the family *Orthomyxoviridae*. IAV is a human pathogen that can cause serious global, seasonal epidemics, as does the related influenza B virus. Interactions between the IAV hemagglutinin (HA) glycoprotein and host cell surface sialic acids mediate attachment to cells prior to endocytosis of the virus. Once localized in the endosome, the resident low pH induces a conformational change in HA that enables fusion of the viral envelope with endosomal membranes[1-2]. Following membrane fusion, the viral capsid uncoats and ribonucleoprotein complexes are released into the cytosol. Replication and transcription of the viral genome then take place in the nucleus to produce new virions, which bud from the cell assisted by the neuraminidase (NA) glycoprotein [3-5].

Viral replication occurs throughout the upper and lower respiratory tract, with nascent virions spreading from the site of infection to the lower respiratory tract. IAV infection causes a range of clinical manifestations, from mild self-limiting respiratory tract infections, to progressive and sometimes lethal pneumonia[6-8]. During the initial stages of infection, IAV infects epithelial cells that line the bronchotracheal system, alveolar epithelial cells, airway macrophages, and dendritic cells[9-10]. IAV infection elicits clinically significant pathology in the respiratory tract, including mucosal inflammation and edema of the larynx, trachea, and bronchi. Serious infection is characterized by interstitial pneumonitis with hyperemia and broadening of the alveolar walls, as well as by leukocyte infiltration, capillary dilation, and thrombosis. IAV infection causes cellular damage by shutting off cell protein synthesis and inducing apoptosis. Complete repair of epithelial damage is thought to take up to one month[11-12].

The respiratory tract has multiple protective barriers that guard against initial IAV infection. Upon detection of IAV infection, the host immune system defends against and clears the viral infection using both innate and adaptive immune components. The rapid induction of innate defense plays a critical role in early protection, limiting viral spread to host tissues as adaptive

immunity develops. Early stages of innate immunity include the rapid production of type I interferon, cytokines, and chemokines through activation of pattern recognition receptors. This leads to airway recruitment of inflammatory cells, including macrophages, neutrophils, and lymphocytes. These cells contribute to innate immunity by clearing virus through phagocytosis or lysis of infected cells, production of chemokines and cytokines, and/or stimulating the adaptive immune response. The recruitment of virus-specific T lymphocytes and neutralizing antibodies secreted by B cells then follow these innate immune responses. $CD8^+$ cytotoxic T lymphocyte (CTL)-mediated immunity plays a key role in the clearance of virus-infected cells through cytolysis [13-14] when neutralizing antibodies are absent during the early stage of infection. CTL infiltration into the airways is also associated with extensive secretion of proinflammatory cytokines and severe tissue damage, which results in immunopathology[15].

In this study, we used single domain antibody fragments (VHHs) derived from heavy chain-only antibodies to study the time course of $CD8^+$ T cell recruitment to the site of infection, using mouse-adapted IAV, as well as to identify the location of $CD8^+$ T cells after adoptive transfer using non-invasive imaging methods. Prior studies have relied mostly on invasive techniques, such as organ excision, followed by flow cytometry to quantify the percentage of $CD8^+$ T cells in a specific location. While such invasive methods provide insight to the local distribution of $CD8^+$ T cells, it does not provide longitudinal information about the total population of $CD8^+$ T cells in the body in terms of numbers and distribution. Here we apply a method by which we can noninvasively monitor the total population of $CD8^+$ T cells over the entire course of an IAV infection. Furthermore, we can visualize the distribution of adoptively transferred $CD8^+$ T cells in uninfected and IAV-infected mice over a 24-hour time period. This approach provides a new means of tracking a CD8 T cell response in a living animal.

3.2 Result

3.2.1 Scheme of $CD8^+$ CTL Immunity and VHH Construct Design

Influenza A virus-specific $CD8^+$ CTLs play a critical role in eradicating IAV-infected host cells in the lung through antigen-specific cytotoxicity and cytokine/chemokine production. Unlike antibody and B cell memory-based protection, T cell-based immunity requires the presence of memory T cells at the site of infection. When mice are infected with IAV, lung-resident DCs are activated by infection, by acquisition of debris from dying cells and in response to innate cytokines. DCs then migrate from the inflamed lung into the lung draining lymph nodes (LNs) carrying the newly acquired viral antigen(s), processed to yield peptide-MHC complexes (**Figure 3.1A**). Naïve antigen-specific T cells in the LNs recognize these complexes, clonally expand and then differentiate into IAV antigen-specific $CD8^+$ and $CD4^+$ (mainly Th1) effector T cells (ref). Secondary lymphoid organs, such as LNs and spleen, provide the spatial organization and appropriate chemokine environment to prime the anti-viral immune response by bringing together Th1 and naïve $CD8^+$ cells during the generation of flu-specific CD8 CTL (**Figure 3.1A**).

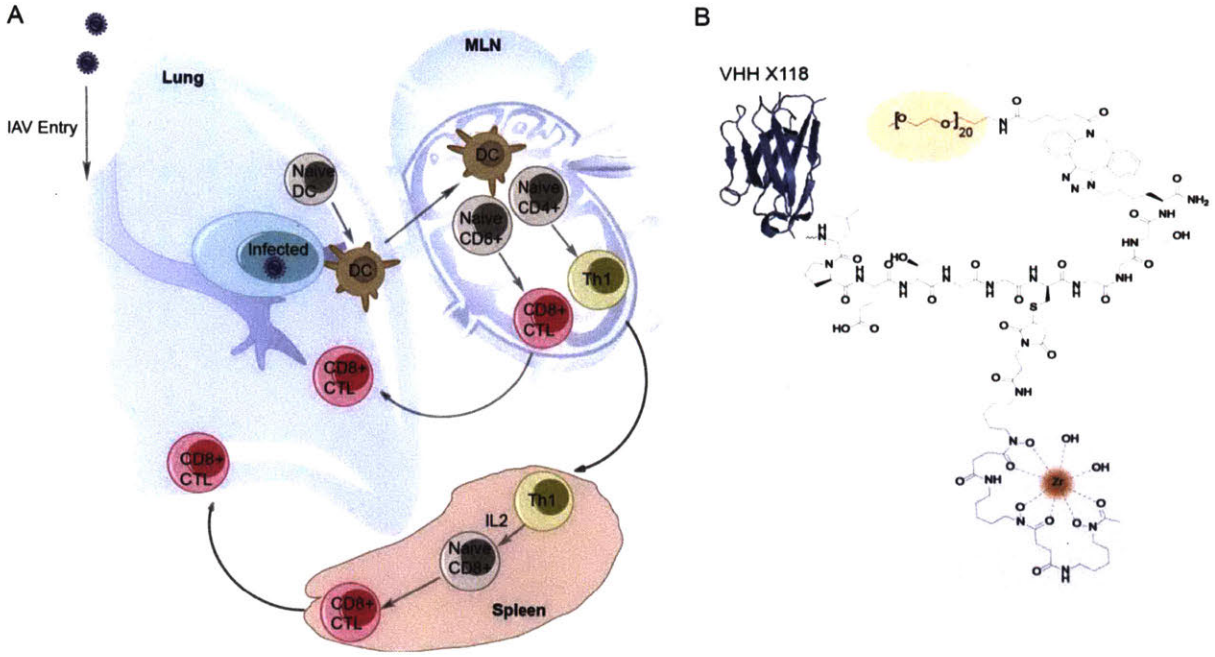

Figure 3.1 Scheme of $CD8^+$ CTL Immunity and VHH Construct Design

(A) Schematic depicting $CD8^+$ CTL maturation in the context of IAV infection.

(B) VHH-X118 construct used to track $CD8^+$ T cells in vivo. Shown is a representative VHH structure covalently bound by a modifiable peptide probe. The cysteine thiol was reacted with maleimide-desferrioxamine (grey), which is shown chelating ^{89}Zr (highlighted in red). The azide-containing lysine is covalently modified with a PEG_{20} substrate (peach) for improved circulation.

In order to follow $CD8^+$ T cells noninvasively and in real time in the course of IAV infection, we used a VHH specific to CD8 alpha, VHH-X118.[16] We generated two versions of ^{89}Zr-labeled VHH-X118, both arrived at via modification of the C-terminal sortase recognition motif (LPETG) to incorporate a peptide probe containing an N-terminal GGG sequence to serve as a nucleophile in a sortase A mediated transpeptidation reaction. By reacting the cysteine thiol with maleimido-desferrioxamine (DFO) we installed ^{89}Zr for PET imaging. We also generated a PEGylated version of ^{89}Zr-labeled VHH-X118 by using an azide-substituted lysine in the course of synthesis to enable the addition of polyethylene glycol (PEG) moieties for in vivo injections to reduce non-specific retention in the kidneys (**Figure 3.1B**).[16] The construct used for in vitro labeling of $CD8^+$ T cells prior to the adoptive transfer experiments described below did not include a PEG moiety.

3.2.2 $CD8^+$ T Cells Transiently Accumulate in the Lung and MLN of IAV Infected Mice, Corresponding with Morbidity

To establish the distribution of CD8 T cells during IAV infection in mice, we acquired $CD8^+$ PET images using ^{89}Zr labeled VHH-X118 and tracked weight loss after intranasal inoculation of C57BL/6 mice ($n \geq 3$ for each group) with a sub-lethal dose (3×10^4 IU) of influenza A/WSN/33 virus (H1N1) **(Figure 3.2)**.

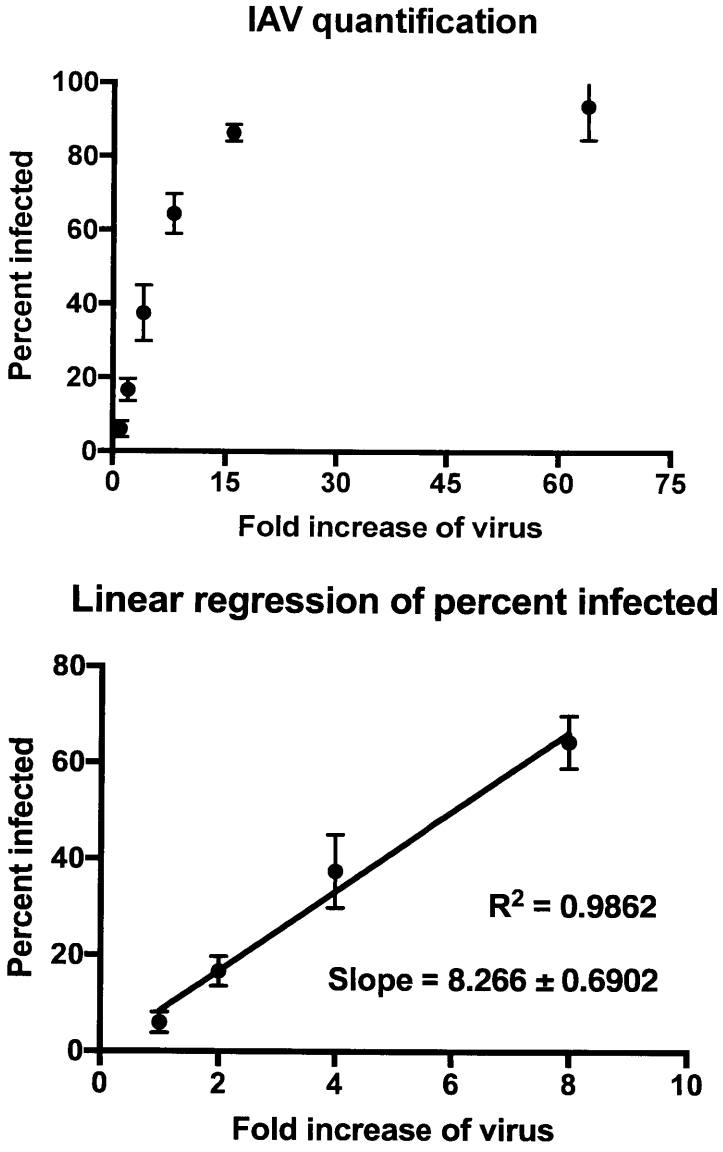

Figure 3.2 (Top) Fluorescence was quantified using a BD Accuri C6 Plus. The NP-positive population was determined by comparing with the uninfected control population. Data were processed using the FlowJo software package. (Bottom) A linear regression model was applied to the linear portion of these data

In uninfected mice, $CD8^+$ T cells were distributed in the cervical, axillary and brachial (lung draining), mediastinal (lung draining), popliteal, renal, iliac, and inguinal lymph nodes, as well as in the spleen, consistent with previous observations in a tumor model[16]. PET signals in the organs of elimination (kidneys, liver, and bladder) and the site of injection (retro-orbital plexus) are a non-specific and common occurrence. During the first week of IAV infection mice lost weight, paralleled by increases in PET signal in the mediastinal lymph node (MLN) and lung. Attribution of PET signals to particular anatomical structures were confirmed by imaging of a dissected organs, including MLN, lung, heart, and thymus (**Figure 3.3**).

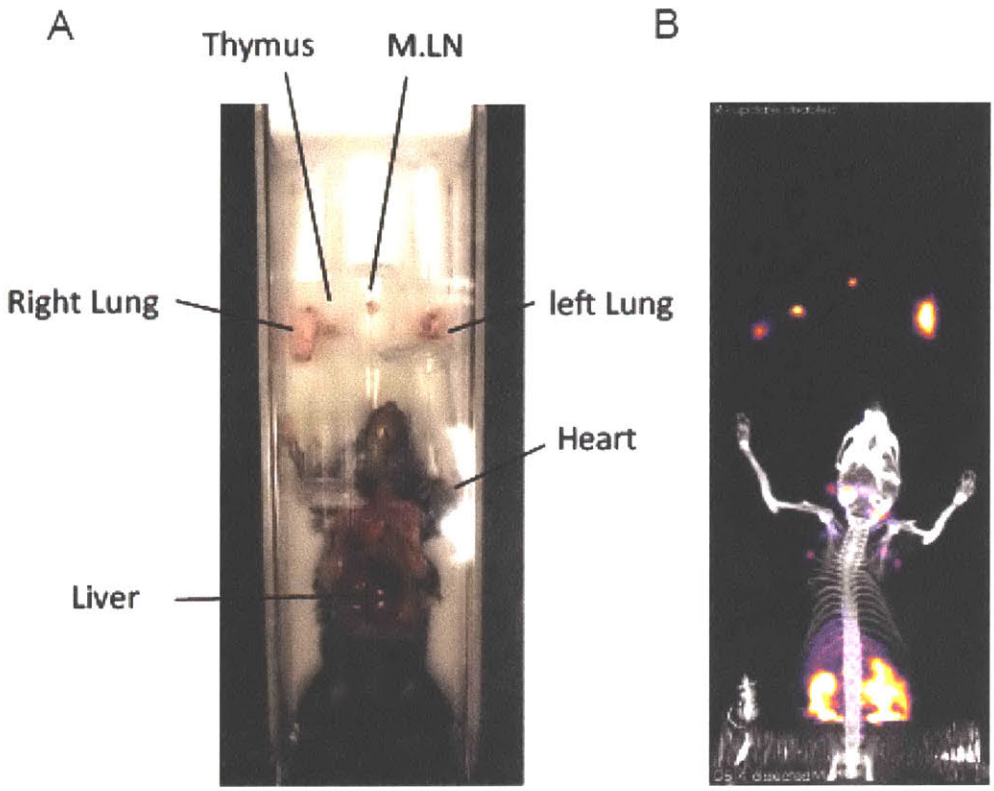

Figure 3.3 (A) Attribution of PET signals to particular anatomical structures were confirmed by imaging of a dissected organs, including MLN, lung, heart, and thymus. Dissected organs were saved into separate 1.5ml tubes. (B) PET image was acquired with the body facing up as well as organs, including MLN, lung, heart, and thymus.

As shown in **Figure 3.4**, At 4 dpi. mice showed a striking increase in CD8 T cells in the area corresponding to the MLN, as inferred from the PET signal, and in the draining lymph nodes. At 6 dpi, at the peak of infection as determined by weight loss, a diffuse pattern of $CD8^+$ signal was present in the lung, likely caused by $CD8^+$ T cells migrating towards particular foci of infection. This signal became more concentrated and localized in specific regions of the lungs over the course of the infection, starting at 9 dpi and finally decreased around 18 dpi when mice were in the recovery phase, to disappear completely by day 21 post-infection.

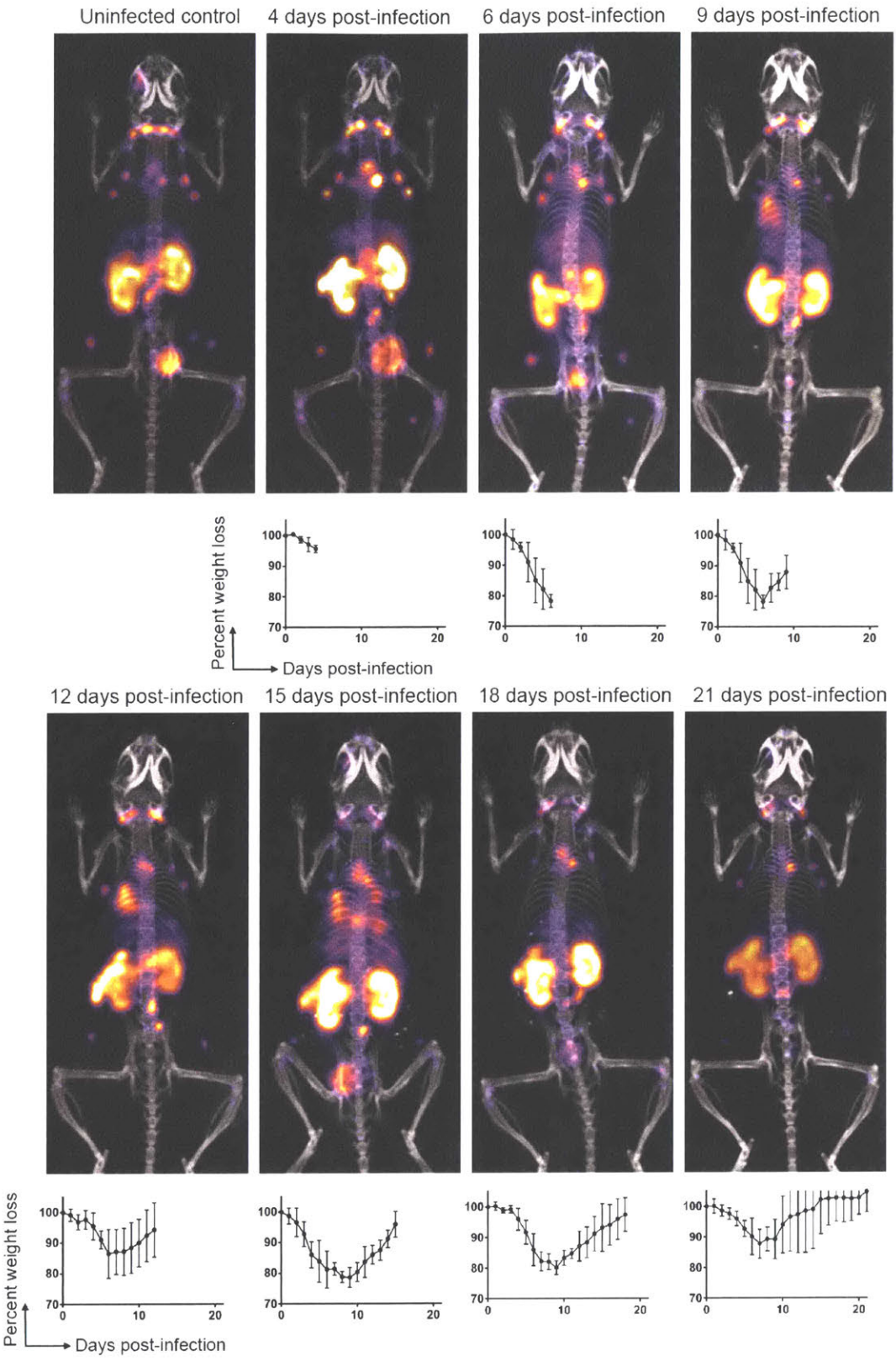
Uninfected control
4 days post-infection
6 days post-infection
9 days post-infection
Percent weight loss
100
90
80
70
0
10
20
Days post-infection
12 days post-infection
15 days post-infection
18 days post-infection
21 days post-infection
Percent weight loss
Days post-infection

Figure 3.4 $CD8^+$ T Cells Transiently Accumulate in the Lung and MLN of IAV Infected Mice, Corresponding with Morbidity

Representative (n≥3) immuno-PET images of IAV WSN/33 infected mice (facing down) injected with ^{89}Zr-labeled VHH-X118-PEG_{20} on the day indicated. Below each image is a graph plotting percent weight loss over time. PET signal increases in the MLN of mice 4 dpi and in the lung 6 dpi. Signal localizes in specific areas of the lung until infection is resolved. MLN signal remains elevated and lung signal gradually decrease as the mice recover from infection.

3.3.3 Lung-Infiltrating Cells Are Predominantly $CD8^+$ T_{EFF}/ T_{EM} Cells

To characterize the infiltrating T cell population in infected and uninfected mice, we performed cytofluorimetry on cells isolated from lung and MLN (shown in **Figure 3.5**). The ratio of infiltrating $CD4^+$ versus $CD8^+$ T cells was determined by gating on CD3+CD45+ population (Figure 4A). The lungs of infected mice contained far greater numbers of infiltrating lymphocytes. We saw a significant increase in the $CD8^+/CD4^+$ ratio in the lung for mice 9 dpi. (Figure 4C). To establish the percentage of $CD44^+CD62L^+(T_{CM})$ and $CD44^+CD62L^-(T_{EFF/}\ T_{EM})$ population, we gated on either the $CD8^+$ or $CD4^+$ T cell population (Figure 4B). For both $CD8^+$ and $CD4^+$ infiltrating T cells in the lung, the majority of the infiltrating population was $CD44^+CD62L^-$ $(T_{EFF/}\ T_{EM})$. No significant increase in $CD8^+$ $CD44^+CD62L^+(T_{CM})$ was detected in the lungs of the infected animals.

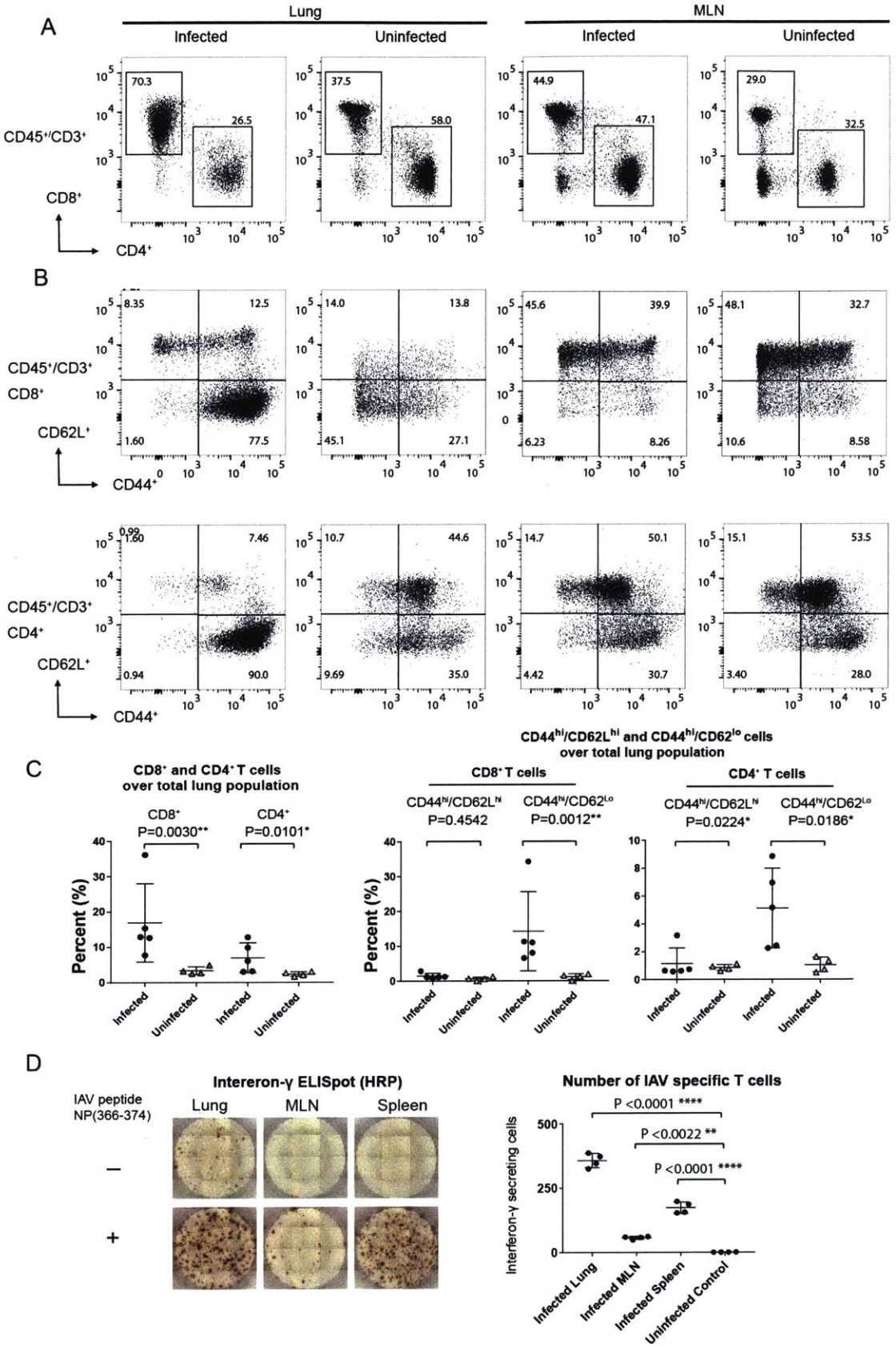
A
Lung
MLN
Infected
Uninfected
Infected
Uninfected
CD45+/CD3+
CD8+
CD4+
70.3
26.5
37.5
58.0
44.9
47.1
29.0
32.5
B
CD45+/CD3+
CD8+
CD62L+
CD44+
8.35
12.5
1.60
77.5
14.0
13.8
45.1
27.1
45.6
39.9
6.23
8.26
48.1
32.7
10.6
8.58
CD45+/CD3+
CD4+
CD62L+
CD44+
0.99
1.60
7.46
0.94
90.0
10.7
44.6
9.69
35.0
14.7
50.1
4.42
30.7
15.1
53.5
3.40
28.0
C
CD8+ and CD4+ T cells over total lung population
CD8+
P=0.0030**
CD4+
P=0.0101*
Percent (%)
Infected
Uninfected
Infected
Uninfected
CD44hi/CD62Lhi and CD44hi/CD62lo cells over total lung population
CD8+ T cells
CD44hi/CD62Lhi
P=0.4542
CD44hi/CD62Lo
P=0.0012**
CD4+ T cells
CD44hi/CD62Lhi
P=0.0224*
CD44hi/CD62Lo
P=0.0186*
D
Intereron-γ ELISpot (HRP)
IAV peptide NP(366-374)
Lung
MLN
Spleen
–
+
Number of IAV specific T cells
P <0.0001 ****
P <0.0022 **
P <0.0001 ****
Interferon-γ secreting cells
Infected Lung
Infected MLN
Infected Spleen
Uninfected Control

Figure 3.5 Lung-Infiltrating Cells Are Predominantly CD8+ TEFF/TEM Cells, a Significant Amount of Which are IAV Specific.

(A)The infiltrating T cells were gated on CD45+/CD3+ and the ratio of CD4+ and CD8+ was determined. An increased ratio of CD8+/CD4+ were found in infected mice.

(B) CD8+ and CD4+ TEFF/TEM(CD44hiCD62Llo) and Tcm (CD44hiCD62Lhi) were gated on CD45+/CD3+/CD4+/CD44/CD62L and CD45+/CD3+/CD8+/CD44/CD62L.

(C) Data from (A) and (B) was statistically analyzed. Both CD8+ and CD4+ TEFF/TEM were found in lung-infiltrating cells with the CD8+ TEFF/TEM as the predominant population.

(D) ELIspot assays showed IAV specific T cell responses in lungs, MLN, and spleen. The representative ELIspot wells are shown in the left panel and the statistical analysis of lung, MLN and spleen IAV specific T cells are shown in the right panel.

3.3.4 Lung-Infiltrating Cells Contain IAV Specific T Cells.

We next established the presence of IAV-specific T cell responses in lung, MLN, and spleen using an IFN-γ ELISpot assay (**Figure 3.5D**) in response to inclusion to a peptide corresponding to the immunodominant H-2D^b-restricted IAV NP epitope, ASNENMETM. As expected, we saw a significant increase in the number of IAV-specific CD8 T cells in the lung, MLN, and spleen samples. We detected IFN-γ-producing cells in the media-only controls in the lung from infected animals, presumably due to the persistence of antigen and/or previously activated IFNγ-producing T cells.

3.3.5 Distribution of Adoptively Transferred CD8$^+$ T Cells Relies on the Site of T Cell Maturation and the Local Inflammatory Environment.

Adoptive transfer of IAV-specific CD8$^+$ T cells showed efficient IAV clearance in a B cell deficient mouse model[17]. In such settings, the exact distribution of donor CD8$^+$T cells remains unclear. We approached the question using adoptive transfer of ^{89}Zr labeled CD8$^+$ T cells to trace their distribution at 1 hour and 24 hours post-transfer using whole body immuno-PET imaging (**Figure 3.6**). T cells were harvested and purified from the lungs of IAV-infected mice 9 dpi, with additional negative selection steps to remove epithelial and endothelial cells (see methods). We likewise harvested splenocytes from uninfected mice as described[18] and purified CD8 T cells from them. These naïve T cells were then activated on plate-bound anti-CD3 and anti-CD28 supplemented with IL-2. CD8$^+$ T cells from IAV-infected mice or activated CD8$^+$ T cells from control mice were labeled with ^{89}Zr-VHH X118. Labeled cells were adoptively transferred into either IAV-infected (4 dpi) or uninfected control mice via retro-orbital injection. PET images were acquired at 1-hour and 24-hours post-transfer.

Mature donor CD8$^+$ T cells from IAV-infected mice initially homed to the lungs, liver, and spleen in both 4 dpi and uninfected recipients imaged 1-hour post-adoptive transfer. After 24 hours, CD8$^+$ T cells from IAV-infected mice migrated to the MLN and spleen in addition to lungs and liver in 4 dpi recipient mice. However, CD8$^+$ T cells from IAV-infected animals did not migrate from the lungs, liver, and spleen when transferred into uninfected mice, and no significant change in CD8+ T cell distribution was noted from 1 to 24 hours post-adoptive transfer.

Control CD8$^+$ T cells activated ex vivo initially localized to the lungs and spleen in IAV-infected (4 dpi) recipient mice. After 24 hours, CD8$^+$ T cells disappeared from the lungs, accompanied by an apparent increase in the number of CD8+ T cells in the spleen. Activated CD8$^+$ T cells generated from control splenocytes transferred into naïve mice localized mostly to the spleen and remained there after 24 hours.

$CD8^+$ T cells obtained from IAV-infected mice (9 dpi) localized to the lung and spleen of both infected and uninfected mice, but persisted only in the lung of infected mice. In contrast, control $CD8^+$ activated T cells transiently localized to the lung of IAV-infected recipient mice, and did not populate the lung of uninfected recipients. Control activated $CD8^+$ T cells initially migrated to the lung of infected mice presumably because of pro-inflammatory signals that resulted from infection, though this was seemingly insufficient for them to remain there.

A

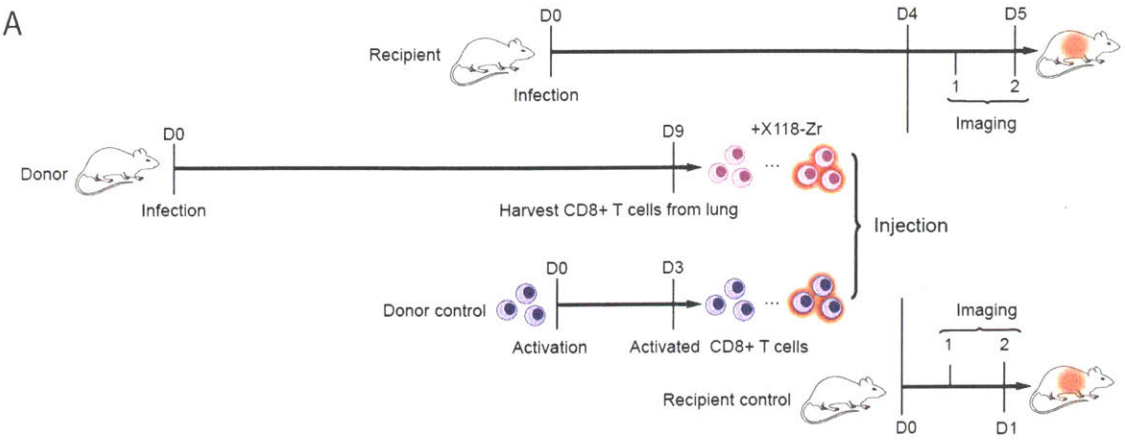
Recipient
D0
Infection
D4
D5
1
2
Imaging
Donor
D0
Infection
D9
+X118-Zr
Harvest CD8+ T cells from lung
Injection
Donor control
D0
Activation
D3
Activated CD8+ T cells
Imaging
1
2
Recipient control
D0
D1

B

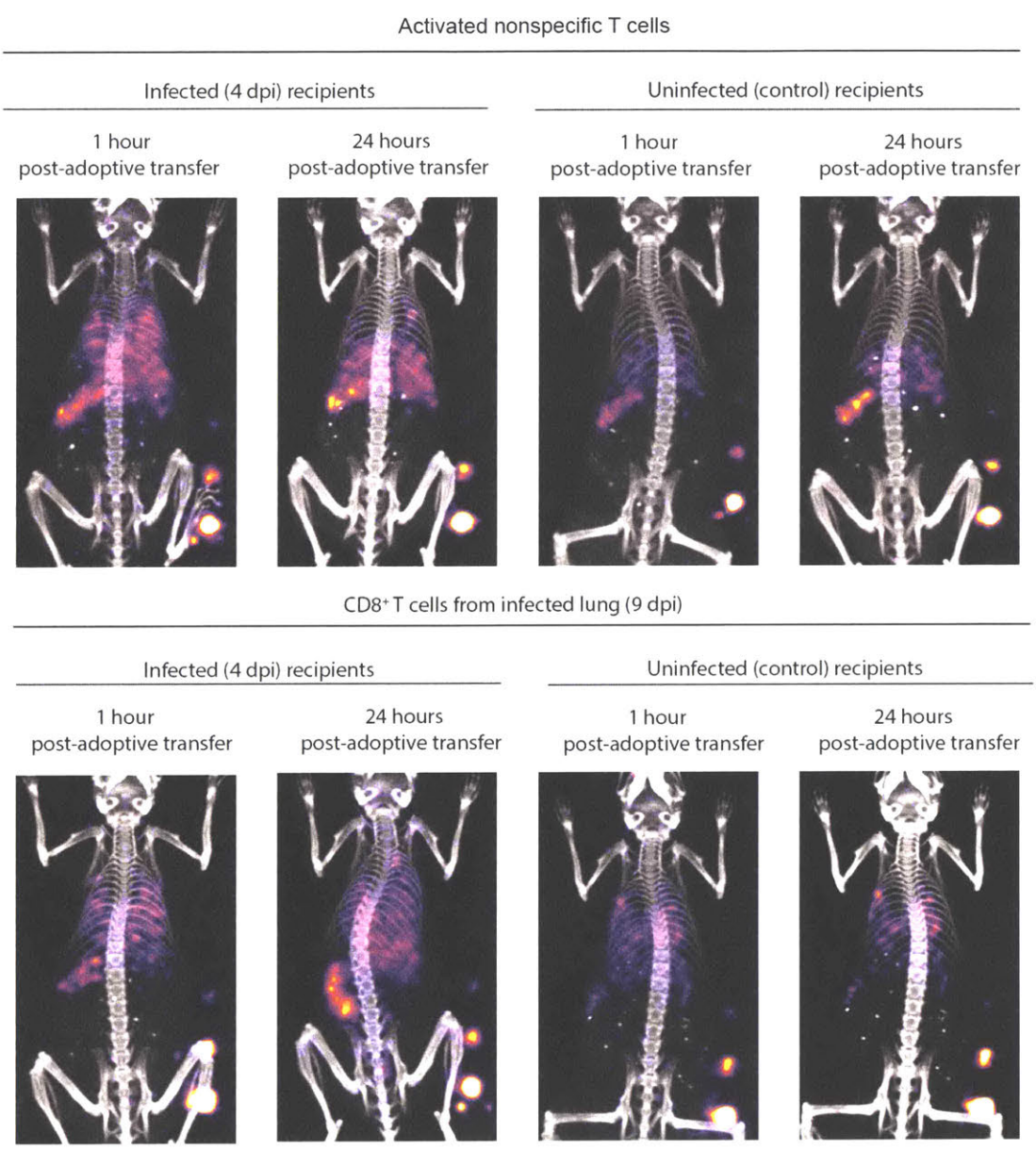
Activated nonspecific T cells
Infected (4 dpi) recipients
Uninfected (control) recipients
1 hour post-adoptive transfer
24 hours post-adoptive transfer
1 hour post-adoptive transfer
24 hours post-adoptive transfer
CD8+ T cells from infected lung (9 dpi)
Infected (4 dpi) recipients
Uninfected (control) recipients
1 hour post-adoptive transfer
24 hours post-adoptive transfer
1 hour post-adoptive transfer
24 hours post-adoptive transfer

Figure 3.6 Distribution of Adoptively Transferred $CD8^+$ T Cells Relies on Site of T Cell Maturation and Local Inflammatory Environment

(A) Schematic depicting the design of the adoptive transfer experiments. Donor mice were infected with IAV WSN/33 and $CD8^+$ T cells were harvested from the lungs. Cells were ex vivo labeled with VHH-X118-89Zr and injected into day 4 infected or uninfected mice. As a control, naïve splenocytes from uninfected mice were ex vivo activated and injected into day 4 infected and uninfected mice. Additionally, naïve T cells were isolated from the spleen of uninfected mice and ex vivo activated, followed by transfer to day 4 infected and uninfected mice. All mice were imaged 1 hour and 24 hours post-adoptive transfer.

(B) $CD8^+$ T cells ex vivo activated from the spleen of uninfected mice initially localize to the lungs of day 4 infected mice, though they do not remain there. These cells do not localize to the lungs of uninfected mice (top panels). $CD8^+$ T cells from day 9 infected mice localize to and remain in the lung of day 4 infected and uninfected mice (bottom panels). A standard with set amounts of radioactivity in 2-fold dilutions starting at 0.4 μCi is on the lower right side of each image.

3.3.6 Transcript assembly and quantification by RNA-Seq for future directions

To understand the mechanistic basis for the differences in $CD8^+$ T cell localization we used RNA-seq on cells obtained from mice 9 days post-infection. $CD8^+$ T cells from 45.2 C57/B6 were sorted and transferred into 45.1 $CD8^+$ T cells. 24 hours after the adoptive transfer, $CD45.2^+/CD8^+$ T cells were sorted from MLN, lung, and spleen of the recipient mice.

Transcript assembly and quantification will be performed in the future using RNA-seq. A proposed model is shown in **Figure 3.7**

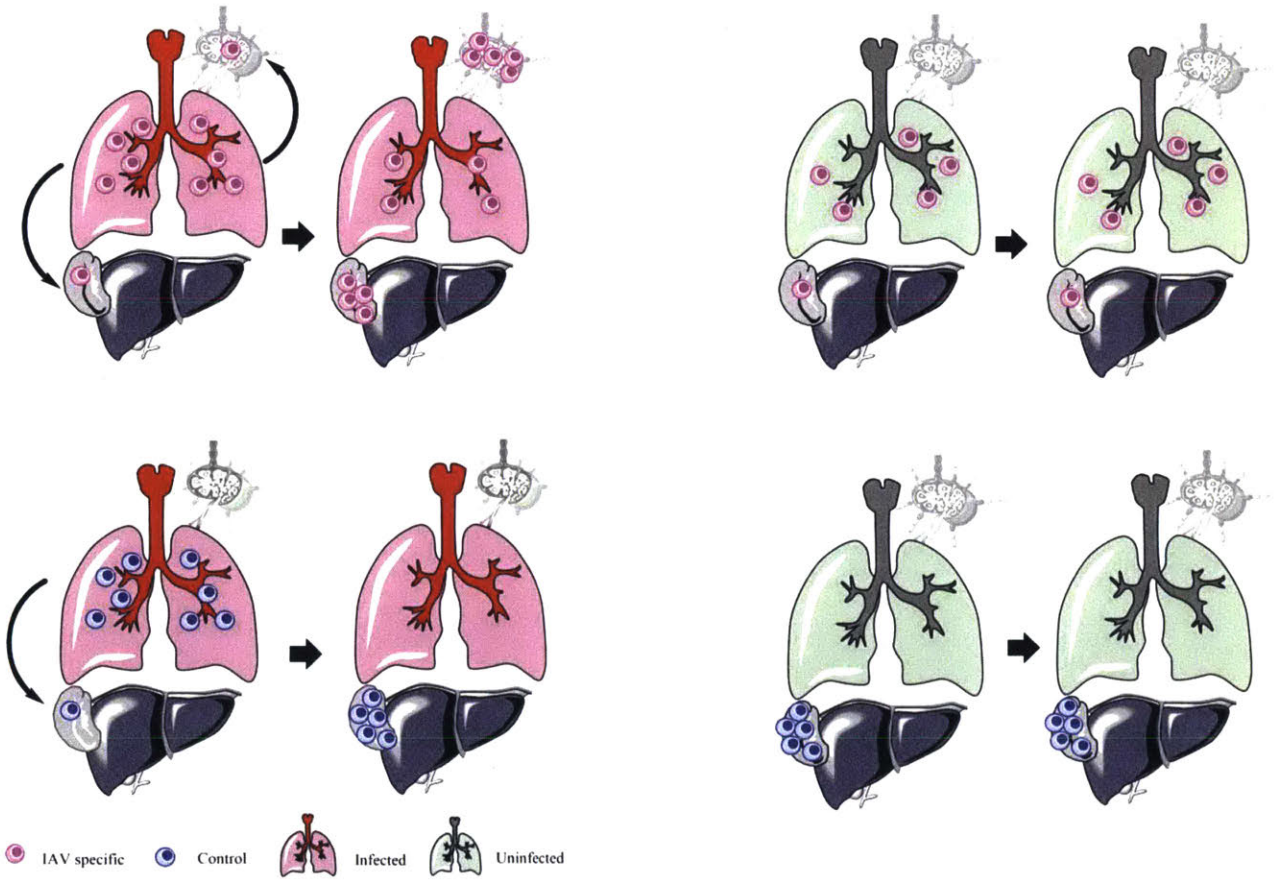

Figure 3.7 A Proposed Model Summarized the Distribution of Adoptively Transferred $CD8^+$ T Cells Relies on Site of T Cell Maturation and Local Inflammatory Environment

3.3 Experimental Section

3.3.1 Synthesis of Peptide Probes for Sortase Reactions

Peptide GGGCGGSK(azide) with N terminal amine and C terminal CONH2 was synthesized following standard solid phase synthesis protocols[19]. All Fmoc amino acids were purchased from Chempep, Inc. Fmoc-Lys(azide)-OH was used as building block to provide the bioorthogonal moiety. The peptide was purified by reverse phase HPLC and was confirmed by LCMS prior to maleimido-DFO coupling on the cysteine side chain. The peptide was further purified by reverse phase HPLC and its identity was confirmed again by LCMS.

3.3.2 C-Terminal Sortagging and PEGylation

Ca^{2+} independent heptamutant Sortase A derived from *S. aureus* (10 μM final concentration, 10× stock in 50 mM Tris, pH 7.4, 150 mM NaCl) and probe (1 mM final concentration, 50× stock) were added to VHH-X118 (200 μM final concentration) in PBS. The resulting mixture was incubated at 4 °C overnight. 0.5 ml Ni-NTA was added to the reaction mixture and incubated for 20 min to remove sortase and unreacted VHHs. The mixture was centrifuged and the supernatant was collected and purified by size exclusion chromatography (Superdex 75- GE Life Sciences), and analyzed by SDS-PAGE and LC/MS. PEGylated VHH-X118 was generated by reacting the bio-orthogonal azide group with dibenzocyclooctyne DBCO-$(PEG)_{10}$ overnight. The end product was analyzed by SDS-PAGE to confirm efficiency of coupling.

3.3.3 Virus Quantification

IAV was quantified by flow cytometry, using a method adapted from Schmidt *et al.* 2016. Briefly, confluent MDCK cells were infected in triplicate with 2-fold serial dilutions of IAV WSN/33 (in DMEM, 0.2% BSA) for 1 hour. The inoculum was removed and replaced with DMEM, 0.2%

(w/v) BSA for 5 hours. Cells were washed with PBS, trypsinized, and fixed with 4% formaldehyde/PBS. Cells were stained with 1 μg/mL VHH62 (anti-IAV NP)-Alexa Fluor 647 under permeabilizing conditions. Fluorescence was quantified using a BD Accuri C6 Plus. The NP-positive population was determined by comparison with an uninfected control population. Data were processed using the FlowJo software package. A linear regression model was applied. The slope of the line of best fit was used to determine the percentage of cells infected, which was multiplied by the number of cells per well to yield the number of viral particles per well.

3.3.4 Infection of mice with IAV

Age-matched, 6-week old,female C57BL/6J mice ($n \geq 3$ in each group) were purchased from the Jackson Laboratory. Mice were anesthetized with isoflurane and infected intranasally with 40,000 infectious units of IAV WSN/33 diluted in PBS. Control mice were inoculated intranasally with an equal volume of PBS. Infection was tracked by monitoring daily weight loss. Mice were euthanized with CO_2 when weight loss exceeded 25% of initial body weight and/or animals displayed signs of severe distress, or if no weight was recovered 9 days post-infection.

3.3.5 Immuno-PET imaging

PET-CT procedures have been described in detail previously.[16] Briefly, mice were anesthetized using 2% isoflurane in O_2 at a flow rate of about 1 liter per minute. Mice were imaged with a G8 PET-CT small-animal scanner (PerkinElmer). Each PET acquisition took 20 minutes, followed by about 2 minutes of CT acquisition. As a standard for absolute intensity, a fixed quantity of radioactivity was imaged using 5-fold serial dilutions of radioisotope in PCR strip tubes.

3.3.6 PET Quantification

We processed and quantified PET images using VivoQuant software. The CT scan was used as a guide to generate 3D regions of interest (ROIs) to represent regions corresponding to the lungs and MLN/thymus. ROIs were drawn for each image corresponding to the absence of CT signal in the ribcage, surrounding the heart as a means of identifying pulmonary space. An additional ROI was drawn in the muscle of the hind leg of each mouse, avoiding bones and LNs, which was subtracted as background. Once all ROIs were generated, statistical information for each ROI containing mean PET signal, was exported and processed. Level of significance was determined using a Student's t-test.

3.3.7 T Cell Purification

Dynabeads Untouched Mouse T Cells Kit was used for T cell isolation from spleen. Two additional antibodies, anti-CD326 for epithelial cells and anti CD31 for endothelial cells, were included as well for isolation of T cells from the lungs. We followed the suppliers' recommended incubation and purification procedures.

3.3.8 Flow Cytometry

All data were acquired on a Fortessa instrument (BD Bioscience) and analyzed using FLowjo software (Tree Star). Cells obtained from the lungs and MLN of CD45.2 C57/B6 mice were used for flow cytometry. Cells were suspended in PBS (137mM NaCl, 2.7mM KCl, 10mM Na2HPO4, 1.8mM KH2PO4) with 2% (v/v) fetal bovine serum and passed through 40-μm cell strainers to obtain single-cell suspensions prior to antibody staining (30min at 4°C). All antibodies were obtained from BioLegend (San Diego, CA). For statistical analysis we applied Student's t-test.

3.3.9 ELISpot Assay

96-well ELISpot plates (BD ELISPOT Mouse IFN-γ ELISPOT Set, BD Biosciences, San Jose, CA) were coated with an IFN-γ capture antibody (BD Biosciences) in PBS overnight at 4°C, following by incubation with complete RPMI medium for 2 hours at room temperature (RT). Single cell suspensions from selected organs of IAV-infected and uninfected mice were prepared. Red blood cells were removed by hypotonic lysis. Quadruplicate ELISpot wells containing mononulcear cells, were supplemented with the IAV peptide NP (366-374; ASNENMETM) Strain (2 μg/mL), to serve as a H2-D^b-restricted epitope from the Influenza A/PR/8/34 nucleoprotein. As controls medium without added IAV peptide was used. ELISpot plates were incubated overnight at 37°C for 18 hours., washed and incubated with a biotinylated IFN-γ detection antibody (BD Biosciences) for 2 hours, followed by incubation with a streptavidin-horse radish peroxidase (HRP) conjugate (BD Biosciences) for 1 hour at RT. ELISpot plates were developed with 3-amino-9-ethyl-carbazole substrate (BD ELISPOT AEC Substrate Set) and dried. Spots were counted using the KS ELISpot analysis system (Carl Zeiss, Thornwood, NY).

3.3.9 T Cell Activation

Splenocytes from C57Bl/6 mice were cultured in plates pre-coated with anti-CD3 (5 μg/ml24 and anti-CD28 (1 μg/ml) antibodies in complete RPMI1640 medium supplemented with 250 ng/ml of IL-2 (methods). Following activation, for 18 hours, cells were transferred to fresh dishes without anti-CD3 and anti-CD28 in complete RPMI1640 supplemented with 250 ng/ml of IL-2, followed by two additional days of culture. Cells were washed three times with PBS and cell numbers were determined prior to adoptive transfer experiments.

3.3.10 Adoptive Transfer

Cells were labeled with ^{89}Zr-VHH-X118 in PBS at 4 °C for 20min with constant agitation. Cells were then washed three times with PBS to remove unbound VHH. Labeled cells ($6x10^6$) were then transferred into the retro-orbital plexus of each mouse.

3.4 References

1. Saito, T., [Review on replication cycle of influenza virus]. *Nihon Rinsho* **2006,** *64* (10), 1803-7.

2. Edinger, T. O.; Pohl, M. O.; Stertz, S., Entry of influenza A virus: host factors and antiviral targets. *J Gen Virol* **2014,** *95* (Pt 2), 263-77.

3. Knipe, D. M.; Howley, P. M., *Fields virology*. 6th ed.; Wolters Kluwer/Lippincott Williams & Wilkins Health: Philadelphia, PA, 2013; p 2 volumes.

4. Review of global influenza activity, October 2016-October 2017. *Wkly Epidemiol Rec* **2017,** *92* (50), 761-79.

5. Chong, P. P.; Handler, L.; Weber, D. J., A Systematic Review of Safety and Immunogenicity of Influenza Vaccination Strategies in Solid Organ Transplant Recipients. *Clin Infect Dis* **2017**.

6. Londrigan, S. L.; Tate, M. D.; Brooks, A. G.; Reading, P. C., Cell-surface receptors on macrophages and dendritic cells for attachment and entry of influenza virus. *J Leukoc Biol* **2012,** *92* (1), 97-106.

7. Luo, M., Influenza virus entry. *Adv Exp Med Biol* **2012,** *726*, 201-21.

8. Mei, R.; Raschi, E.; Poluzzi, E.; Diemberger, I.; De Ponti, F., Recurrence of pericarditis after influenza vaccination: a case report and review of the literature. *BMC Pharmacol Toxicol* **2018,** *19* (1), 20.

9. Kan, T.; Zhang, J., Factors influencing seasonal influenza vaccination behaviour among elderly people: a systematic review. *Public Health* **2018,** *156*, 67-78.

10. Moolasart, V.; Chottanapund, S.; Ausavapipit, J.; Samadchai, S.; Likanonsakul, S.; Uttayamakul, S.; Srisopha, S.; Changsom, D.; Lerdsamran, H.; Puthavathana, P., Influenza A Virus Infection and Nucleotide Sequencing in HIV-Infected Children: A Case Report and Review of Literature. *Glob Pediatr Health* **2017,** *4*, 2333794X17719203.

11. Sarkanen, T. O.; Alakuijala, A. P. E.; Dauvilliers, Y. A.; Partinen, M. M., Incidence of narcolepsy after H1N1 influenza and vaccinations: Systematic review and meta-analysis. *Sleep Med Rev* **2018,** *38*, 177-186.

12. Sparrow, E.; Friede, M.; Sheikh, M.; Torvaldsen, S.; Newall, A. T., Passive immunization for influenza through antibody therapies, a review of the pipeline, challenges and potential applications. *Vaccine* **2016,** *34* (45), 5442-5448.

13. Doherty, P. C.; Turner, S. J.; Webby, R. G.; Thomas, P. G., Influenza and the challenge for immunology. *Nat Immunol* **2006,** *7* (5), 449-55.

14. Lei, W. T.; Shih, P. C.; Liu, S. J.; Lin, C. Y.; Yeh, T. L., Effect of Probiotics and Prebiotics on Immune Response to Influenza Vaccination in Adults: A Systematic Review and Meta-Analysis of Randomized Controlled Trials. *Nutrients* **2017,** *9* (11).

15. Stech, J.; Beer, M.; Vahlenkamp, T.; Harder, T., [The pandemic influenza virus H1N1/2009: a review of the molecular biology, phylogeny, history of reassortments, and parameters of host switching]. *Bundesgesundheitsblatt Gesundheitsforschung Gesundheitsschutz* **2010,** *53* (12), 1231-7.

16. Rashidian, M.; Ingram, J. R.; Dougan, M.; Dongre, A.; Whang, K. A.; LeGall, C.; Cragnolini, J. J.; Bierie, B.; Gostissa, M.; Gorman, J.; Grotenbreg, G. M.; Bhan, A.; Weinberg, R. A.; Ploegh, H. L., Predicting the response to CTLA-4 blockade by longitudinal noninvasive monitoring of CD8 T cells. *J Exp Med* **2017,** *214* (8), 2243-2255.

17. Duan, S.; Thomas, P. G., Balancing Immune Protection and Immune Pathology by CD8(+) T-Cell Responses to Influenza Infection. *Front Immunol* **2016,** *7*, 25.

18. Renegar, K. B., Influenza virus infections and immunity: a review of human and animal models. *Lab Anim Sci* **1992,** *42* (3), 222-32.

19. Li, Z.; Theile, C. S.; Chen, G. Y.; Bilate, A. M.; Duarte, J. N.; Avalos, A. M.; Fang, T.; Barberena, R.; Sato, S.; Ploegh, H. L., Fluorophore-Conjugated Holliday Junctions for Generating Super-Bright Antibodies and Antibody Fragments. *Angew Chem Int Ed Engl* **2015,** *54* (40), 11706-10.